## ABSTRACT

MYERS, AMANDA CATON. Textile Considerations for Wearable Thermal Energy Harvesting: Knit Structures and Body Mapping. (Under the direction of Dr. Jesse S. Jur and Dr. Lawrence Silverberg).

To improve thermal energy harvesting from the body, a complex set of microclimates, components, and functions must be considered in relation to each other. While much literature on energy harvesting improvements highlights the importance of device and material optimization, little focus has been geared towards improving the collective textile-electronic as a whole. The objective of this work is to integrate thermal energy harvesters into a knit textile and to generate a power generation map for locations and scenarios from thermal energy harvesting on the body. A test method for evaluating the performance of a TEG in a wearable form is developed and demonstrated using both in-lab and out-of-lab procedures. The fabrication procedure of an energy harvesting wearable device demonstrates a method of integrating rigid devices into a flexible substrate. The wearable device is used in a human trial, which covered a series of activities in different environmental conditions. The outcomes of these trials demonstrate the significant effect of movement, or convection, on thermal energy harvesting. Finite-element simulations explored how convection and conduction change the heat flux through the textile and the thermoelectric generator (TEG). This research also identifies which knit properties improve thermal energy harvesting by modifying the environment immediately surrounding the TEG through finite element simulations. These simulations provide guidance on critical design considerations for integrating wearable technology with knit textiles. Textile swatches were knit and characterized accordingly for validation of the simulation results. The research shows the significant effect of stitch density on air permeability of the textile and corresponding heat flow induced by convection. These

results have led to the design of a knitted shirt with structured stitches that promote energy harvesting. The shirt is used in a human trial, which covered a series of activities in different environmental conditions. The results of these trials confirm the influence of convection on thermal energy harvesting in addition to mapping energy harvesting levels over the torso. Preliminary results show that the best locations for thermal energy harvesting are at the extremities rather than the core of the body. TEGs placed on the back, torso, and side of the body showed the lowest power values for all activities performed in the trial. The results of this work quantify how smart garment design should include consideration of the use case scenario and where thermal energy harvesters are located. As wearable technology advances, this work can be referenced as a foundation for investigating textile design based on human factors and device functionality.

# Textile Considerations for Wearable Thermal Energy Harvesting: Knit Structures and Body Mapping

by
Amanda Caton Myers

A dissertation submitted to the Graduate Faculty of
North Carolina State University
in partial fulfillment of the
requirements for the degree of
Doctor of Philosophy

Mechanical Engineering

Raleigh, North Carolina

2017

APPROVED BY:

| | |
|---|---|
| _____ | _____ |
| Dr. Jesse S. Jur<br>Committee Co-Chair | Dr. Larry Silverberg<br>Committee Co-Chair |
| _____ | _____ |
| Dr. Brendan O'Connor | Dr. Scott Ferguson |

_____
Dr. Veena Misra

## DEDICATION

*For Papaw*

## BIOGRAPHY

Amanda was born and raised in Little Rock, AR where she graduated with honors from Little Rock Central High School in 2008. She received a full scholarship to Mississippi State University and began studying mechanical engineering in the fall of 2008. Amanda graduated magna cum laude and received a BS in mechanical engineering in 2012. During this time, she worked with the Advanced Combustion Engines laboratory on optimizing dual-fuel injection and piston bowl design for diesel engines. She also worked with the Industrial Assessment Center in evaluating energy expenditures from manufacturing facilities in the area. In the summer of 2011, she worked at Argonne National Laboratory as a summer undergraduate intern. She performed a life cycle analysis on the manufacturing process of turning lignocellulosic biomasses into ethanol for fuel. The work was later integrated into the GREET analysis system developed at the laboratory.

Amanda pursued a direct to Ph.D. program at North Carolina State University in mechanical engineering starting in August 2012. She initially worked in Dr. Yong Zhu's lab on applications of silver nanowire/PDMS composites. After completing the requirements for her M.S., Amanda moved to work in the Nano-Extended Research lab under the mentorship of Dr. Jesse S. Jur.

## ACKNOWLEDGMENTS

This work would not have been possible without the help of a small army. Many thanks to Steve for supporting me, loving me and letting me bounce all my crazy ideas off him. My dogs, Indy and Luna for their love and happiness that encouraged me even on the worst of days. My family, Mom, Dad, William, Andrew, and Catherine for their never-ending support. Aunt Christy and Uncle Jimmy for feeding me at holidays and making sure none of my holidays were spent away from my family. To Lisa, thank you for befriending me and giving me a reason to call Raleigh home. To all my friends, thank you for understanding when I opted out of fun things to go work.

I'd like to thank the ASSIST Center for providing funding for this research and a sense of community that is rare in graduate school. Veena, Mehmet, Rajinder, Elena, Tom, Casey, Roy, Jason and so many others that provided valuable feedback throughout this process. All the students from the center, Francisco, Michael (both of them), Shake, Leah, Tim, Saba, James, Lauren, Namita, Murat, Jose, Rita, Fabian…….and everyone else for great times and memories.

To the next lab, Raj, Allison, Jack, Hasan, Wade, Braden, Nate, Alexa, Cemile, Ryan, Nasim, Halil, Kelly, Raju, Brian, Rachel and Fernanda, for beers and brainstorming, friendship, and being great people to work with! Also thank you to my first group members, Russ, Shanshan, Jimi, Zheng, Felipe, Chengjun, Guangming, and Jianxun for your advice and friendship.

To my committee, Dr. Silverberg, Dr. O'Connor, Dr. Ferguson, and Dr. Misra for your feedback and guidance. My first advisor, Dr. Zhu, for teaching me what good research entails

and how to ask the right questions. Also, to my advisor Dr. Jur for all the support, feedback, and mentorship you've offered in the years I've been at NC State.

Finally, to Nana, Papaw, Grandpa Gudaitis and Grandma Gudaitis, thank you for inspiring me to work hard and go to graduate school in the first place.

Thank you.

## TABLE OF CONTENTS

## LIST OF TABLES

## LIST OF FIGURES

# CHAPTER 1: Introduction

Recent advances in low power electronics, including semiconductor, on-chip designs, and radios are enabling opportunities in wearable devices that utilize sources of energy that minimize the use of a battery. In wearable devices, batteries add both bulk and weight to a device reducing its perceived comfort [1]–[4] , as well as require plug-in recharging that can seem burdening to the user. While low power electronics enable strategies in reducing the battery size or improving the operating lifetime between battery charges, the ability to use energy harvesting directly from the body has been suggested as an alternate source of power. Studies exploring mechanical and thermal energy harvesting have shown promise in guiding energy harvesting materials design, but have been limited to benchtop and short term use case studies [5]–[8]. The energy harvesting packaging design for on-body use has a number of complex design criteria that define the device comfort and performance. For example, the on-body location of the device is subject to form factor, flexibility, and materials that need to be considered with respect to influencing user comfort. The device performance is highly dependent on human use and activity factors that are even more influential to the performance of the energy harvester [9]–[11]. For a thermal energy generator (TEG), significant human factors include the temperature difference between the surface of the skin and ambient air, air velocity over the TEG, and the metabolic rate of the user, resulting in a complex combinatorial effect on the energy harvesting ability of the TEG. The influence of these variables are dependent on the harvester's location on the body and the user’s metabolic rate, or activity level.

This work explores testing strategies for determining the effect of human factors related to thermal energy harvesting, including environmental influences and position, or location, of energy harvesting on the body, whereby enabling future strategic design of the materials surrounding the energy harvesting for improving performance. We begin by discussing state of the art of energy harvesting technology, smart textiles, and wearable technology in Chapter 2. Then, a proof of concept human trial study is discussed in Chapter 3, which yields preliminary data for further experiments. A circuit, the energy harvesting subsystem (EHSS), is designed and used in these trials to monitor environmental conditions each person was exposed to during the procedure. The data gathered in this study is used to define a model of the effect of knit structure and tightness factor on the power output of the TEG covered in Chapter 4. The results of the modelling are used to design a knit shirt with strategic knit structure placement to improve thermal energy harvesting. This shirt is worn during a continuation of the initial human trial study the results of which are covered in Chapter 5 as well as the development of a new energy harvesting subsystem circuit. This circuit improved on the first EHSS in that it consumed a smaller footprint which enabled several systems to be used simultaneously. Chapter 6 recaps the results and draws overall conclusions from all the studies including directives for wearable technology design from a textile perspective. Directions for future studies in each aspect of this project are also covered in Chapter 6, as well as possible outcomes of these studies and applications to industry and consumer products.

Included in this dissertation are papers not relevant to the dissertation topic. They are included in this work because they were published during my tenure at North Carolina State University. Appendix A contains these two papers, one describing a silver nanowire electrode for

bioelectric (electrocardiogram and electromyogram) signal recording and the other describing a silver nanowire impedance-based hydration sensor and corresponding multi-modal sensor. Details on the design and implementation of the energy harvesting circuit used in the human trials as approved by NC State's Internal Review Board (IRB) are found in Appendix B.

# CHAPTER 2: Literature Review

## 2.1 Energy Harvesting

### *2.1.1 Wearable Energy Harvesting*

In today's consumer electronics market, interest in wearable electronics is rapidly increasing. The smart textiles market is forecasted to grow to USD 4.72 billion by 2020 [12] and the wearable technology market is expected to grow to USD 34 billion by 2020 [13]. The ability to operate these smart devices continuously for extended periods is vital to the market's success. To facilitate continuous operation, electronics researchers are developing ultra-low power electronics, improved battery energy density, and innovative packaging methods. However, battery technology is not expected to improve significantly over the next few years. Additionally, batteries have a large footprint, are considerably heavier than textiles, require replacement or re-charging, and are challenged by the day to day operation of textiles (i.e. washing) [14]. Rigid components and stiff interconnects are other challenges encountered in developing wearable devices. Therefore, textile researchers are creating flexible, textile-based sensors, actuators, and energy harvesters. Still, many of these advancements do not yet reach wearable technology performance requirements. Both collaborations between the electronics and textile fields and detailed studies of electronic-textile interfaces are necessary for creating comfortable and high performing wearable devices.

Energy harvesting, also referred to as energy scavenging, offers an opportunity to unequivocally eliminate batteries as a power source. Methods of energy harvesting include piezoelectric, thermoelectric, triboelectric, photovoltaic, and radio frequency (RF) power

harvesting. The human body is source for piezoelectric, thermoelectric, and triboelectric energy harvesting methods. Table 1 summarizes energy harvesting power values from both human and industrial sources as reported in literature for perspective. This review will only focus on energy harvesting from the human body, as industrial energy harvesting is not relevant to the discussion topic.

According to Starner and Paradiso [15], [16], the body is capable of producing up to 4.8 W of power, a value that can vary based on the human's physiology and activity level. Thermal energy harvesting serves wearable applications well as the user does not need to actively input effort into generating power i.e. walking or moving for kinetic energy harvesting. The amount of heat generation from the body is related to metabolic activity, measured in METs, Metabolic Equivalent of Tasks). Metabolic heat generated from activity may be measured by oxygen uptake rate. The created energy is then released in several ways: i) metabolic heat transferred through the skin surface ii) heat of vaporization and convection from respiration and iii) external work. [9], [11] Metabolic rates range from 0.7 – 12 MET for an average adult with a skin surface area of 1.8 $m^2$ [11], [17] which equates to 40 – 700 $W/m^2$. Not all of this energy contributes to energy harvesting as approximately 7% is lost through respiration and even more is lost via external work efficiency [9]. Additionally, as activity intensity increases, so does the production of sweat which alters the thermal resistance of the skin.

**Table 2.1** A summary of energy harvested from various sources as reported in literature. Thermal, solar, radio frequency, and kinetic energy harvesting methods are included as well as the power input to the harvesting device.

| Source | *Source Power* | *Harvested Power* |
|---|---|---|
| Ambient light | | |
| Indoor | 0.1 mW/cm$^2$ [16], [18]<br>3.5 – 20 W/m$^2$ [19] | 10 µW/cm$^2$ [18]<br>100 µW/cm$^2$ [16], [20] |
| Outdoor | 100 mW/cm$^2$ [18]<br>100 – 1000 W/m$^2$ [20] | 10 mW/cm$^2$ [18], [20]<br>100 mW/cm$^2$ [16] |
| Not specified | 15 mW/cm$^3$ [21] | |
| Vibration/kinetic | | |
| Human | 0.5 m@ 1 Hz 1 m/s$^2$ @ 50 Hz [18] | 4 µW/cm$^2$ [18]<br>4 µW/cm$^3$ [22] |
| Industrial | 1 m @ 5 Hz 10 m/s$^2$ @ 1 kHz [18] | 100 µW/cm$^2$ [18]<br>800 µW/cm$^3$ [22] |
| Not specified | 330 µW/cm$^3$ [21]<br>116 µW/cm$^3$ [21] | 10 µW @ 64 Hz [19] |
| Thermal energy | | |
| Human | 20 mW/cm$^2$ [18] | 30 µW/cm$^2$ [18]<br>100 µW/cm$^2$ [20] |
| Industrial | 100 mW/cm$^2$ [18] | 1 – 10 mW/cm$^2$ [18]<br>3.5 mW/cm$^2$ [20] |
| Not specified | 40 µW/cm$^3$ [21] | 60 µW/cm$^2$ [16] |
| RF | | |
| Cell phone | 0.3 µW/cm$^2$ [18] | 0.1 µW/cm$^2$ [18] |
| Not specified | 0.26 µW/cm$^2$ [16] | |

The focus of on-body energy harvesting is of particular interest due to the sensing and wearability limitations that batteries impose. Currently, batteries are the heaviest and bulkiest of any wearable components. Eliminating the use of battery power makes the long term adoption of wearables more feasible due to improved ease of use and continuous sensing reliability [23]. Solar, kinetic, and thermal energy harvesting are some current variations of energy harvesting that can be adapted to wearables. A study performed by Starner and Paradiso

[15] defined a range of power that can be harvested from the body using various techniques. Notably, the largest amount of energy harvesting potential is found in human motion or kinetic energy harvesting with piezoelectric materials. However, the energy harvesting potential drops significantly when movement ceases, yielding an unsteady supply of power to a wearable sensor or gadget [14], [24]–[27]. A similar issue arises with the use of solar energy harvesting when the energy harvester is not exposed to a constant source of light [25]. Thermal energy harvesting offers the most consistent supply of energy for wearable energy harvesting purposes[28], [29]. However, limited temperature differentials between the body and microclimate surrounding it reduce the amount of power that can be produced. The use of heat spreaders and heat sinks have been used [14], [24], [30]–[33] to aid in maintaining a consistent temperature gradient, but they are rigid and bulky and reduce the comfort of the wearer.

The type of energy harvesting determines how efficiently the device generates power at a specific location. For example, a flexible solar panel integrated into a hat will generate much more power than a piezoelectric harvester in the same location. In addition to type of energy harvesting, the on-body location of the wearable imposes design constraints such as form factor, flexibility, and material usage. It is crucial to consider the body location of a wearable when designing a novel body-powered sensor or device.

In addition to the location of the energy harvester on the body, other variables will influence the response of the energy harvester. For a thermal energy generator, TEG, temperature difference between the surface of the skin and ambient air, air velocity over the TEG, conditions of the ambient air such as humidity, and other variables could all have an effect on the energy harvesting ability of the TEG regardless of the harvester's location on the body.

Additionally, the variables may have different effects on the TEG based on the location of the TEG.

### *2.1.2 Thermoelectric Energy Harvesting*

A thermoelectric device, seen in Figure 1, takes advantage of the dry heat rejected from the body via the Seebeck effect to passively generate power. While many of the current devices are utilized for harvesting waste heat from manufacturing, there is an opportunity for these devices to be integrated into clothing for power generation from the body. By integrating a thermoelectric generator (TEG) into a textile, one can generate reliable power from the human body; however, the amount of power a wearable TEG can produce is directly correlated to the difference in hot and cold temperatures and the activity of the user [14], [28], [30], [31], [34]. For wearable applications, there is a small temperature difference across the human microclimate (skin-textile-air system) so a TEG cannot generate much energy. The body, however, continuously generates heat. This, coupled with changing environments and scenarios, provide the TEG with a steady tempearture gradient.

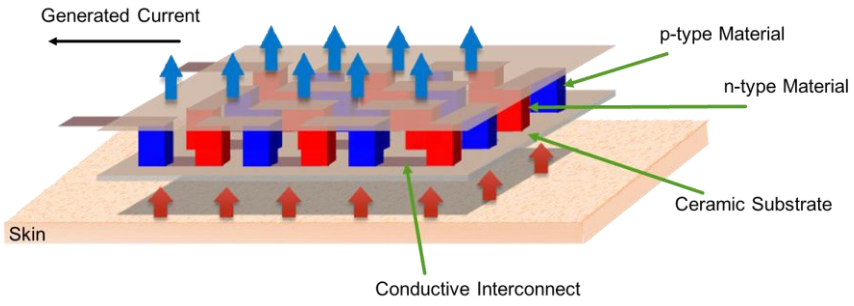


**Figure 2.1** Schematic of a thermal energy-harvesting device with the human body as a heat source.

Commercially available thermoelectric (TE) devices have a high fill factor of legs per unit area. This is maximize the cooling power of the TE device. Suarez et al. [8] showed that the fill factor is a critical variable in determining energy harvesting performance. For wearable energy harvesting, they recommend a maximum fill factor of approximately 20%. Not only does this improve TEG efficiency, but it also enables the possibility of flexible TEGs. Suarez et al. [35] went on to fabricate a flexible TEG using rigid legs embedded in a polymer substrate. The legs were connected using a eutectic gallium indium (EGaIn) liquid metal, so the device is fully flexible. When applied to the distal side of the wrist, the TEG produced 3.5 mV open circuit voltage at room temperature. The group intends to improve efficiency by modifying the polymer filler material and by adding heat spreaders on top of and below the TEG.

Many researchers focus on improving the TEG itself by manipulating the thermoelectric materials or form factor of the device. While this is a critical approach to improving TEG energy harvesting, it does not address two limiting factors i) the thermal resistance and ii) the cooling sensation from a TEG. An ideal TEG has a low thermal resistance on its surfaces to collect and reject heat, and a high thermal resistance on its 'legs' to generate the most current possible. This low thermal resistance requirement also applies to the materials surrounding the TEG i.e. the textile above and below the TEG. When heat flow through the TEG reaches 15 – 25 $mW/cm^2$, the person wearing the TEG may begin to feel a cooling sensation that can lead to discomfort. This approaches the maximum heat flow from the distal forearm, 30 $mW/cm^2$ [14]. It should be noted that these values vary from person-to-person depending on the position of the TEG on the body, personal sensitivities to the environment, and the local thermal resistance of the body. The ideal energy harvesting conditions occur when heat flow into the

textile (from the body via radiation and conduction) is equivalent (or slightly less than) to the heat flow leaving the TEG via convection [24].

Thermal energy harvesting offers a consistent supply of energy for wearable energy harvesting purposes [27]–[30], [36], [37]. Of particular note is the work conducted by Leonov et al. [24], [28], [30], [31] that have demonstrated TEG performance in watch and shirt platforms. Their research demonstrated that the key challenge of thermal energy harvesting from the body is the temperature differential between the body and microclimate surrounding the device that ultimately limits the energy that can be harvested. The most common approach to improve thermal energy harvesting is to include a heat spreader and/or a heat sink to improve power output and maintain a temperature gradient across wearable TEGs. The improved power generation comes at the expense the perceived comfort of the device due to the rigidity and bulkiness of the heat sink. Settaluri et al. [38] characterized and optimized a heat sink and heat spreader system for use with a wearable TEG wristband, acquiring a power density of 28.5 $\mu W/cm^2$. Another method of harvesting body heat is the fabrication of flexible and fiber-based TEGs [8], [39]–[41] which improves the TEG-to-skin contact and will be discussed in detail later in this chapter.

Flexible TEGs are appealing due to the ability to maintain conformal contact on a wide variety of heat source geometries. This reduces thermal contact resistance and improves energy harvesting. Delaizir et al. [42] fabricated a flexible TEG by following a one-step Spark Plasma Sintering method. For flexibility, Kapton polymer was used as the substrate. At a temperature difference of 14.3 °C, the device outputs a voltage of 51 mV, or 48 nW. Other researchers use polydimethylsiloxane (PDMS) as the filler-material surrounding the TEG legs [35], [36], [43]–

[45]. Francioso et al. [43], [44] measured a power of 4.18 nW at $\Delta T = 15$ K which, in their second optimization iteration, increased to 27 nW at $\Delta T = 10$ K. Jo et al. [36], [45] designed a TEG for implanting into the body. When attached to a human body, with a temperature difference of 7 K, the TEG generated 50 nW. While both of the previous authors used thin films to connect TEG legs, Suarez et al. [35] used liquid metal giving the TEG the ability to stretch. The maximum power from the device was 46.28 μW over a $\Delta T = 1.1$ K.

Both optimization approaches highlight the importance of improving TEG performance on a device level in a more comfortable manner, but do not consider the variety of environmental conditions the human body is exposed to on a daily basis. Of particular interest is the observation that thermal energy harvesting has been shown to have negative effects on human comfort due to a high heat flow from the skin resulting in a chilling effect [14], [31]. For the eventual success of on-body energy harvesting, the ability to understand what factors influence energy harvesting over the wide range of body placement and human factors is paramount to mitigating human discomfort without compromising the efficiency of the thermal energy harvester [46].

## 2.2 Smart Textiles

### *2.2.1 Energy Harvesting Textiles*

Electronic textiles, e-textiles, combine electrical, computer, and textile engineering into one platform to meet the demand for wearable computing systems [47]. The term e-textiles encompasses electrically conductive fibers and yarns as well as sensors, microchips, and other components embedded into textiles. Some basic electrical components, capacitors and

resistors, can be made with conductive yarn [48]–[50] using traditional knitting techniques such as intarsia and jacquard knitting. Sophisticated functionality and components, such as energy harvesters and sensors, require modification at the material level instead of at knit or grid patterning. Most bulk materials used in electronics are rigid with poor mechanical properties for flexible applications. Researchers use different approaches to address this issue, one of which is using organic materials and polymers to fabricate components in place of silicon [51]. In textile applications, this results in various polymeric coatings to functionalize textiles for various electronic applications. In this thesis, a focus is placed on applications involving thermal energy harvesting.

An approach to harvesting thermal energy from the body involves functionalizing the textile or fiber itself. The first thermal energy harvester suitable for textiles was developed by Yadav et al. in 2008 [37]. The authors made a thermoelectric fiber via Ag and Ni thermal evaporation. The fiber produced a maximum of 2 nW over seven thermocouples at a $\Delta T = 6.6$ K. In 2012, Hewitt et al. [52] developed an energy harvesting fabric. The fabric was a hybrid piezoelectric and thermoelectric energy harvester. To achieve this, the fabric comprised several layers of PVDF (polyvinylidene fluoride) sandwiched between alternating n- and p-type CNT (carbon nanotube)/PVDF layers. Thus, the fabric generated power when deformed and when exposed to a temperature gradient. While carbon nanotubes have poor thermoelectric properties, others have investigated CNT-based TEGs due to the flexibility and lightness of CNTs. Kim et al. [53] fabricated a TEG by functionalizing CNT mats to power a glucose sensor. The resulting generator was a thin film device with the potential for textile integration demonstrating a power output of 1.75 μW at a $\Delta T = 32$ K.

PEDOT:PSS (poly(3,4-ethylenedioxythiophene):poly(4-styrenefulfonate)) is another common material used in fabricating textile-based energy harvesters. Du et al. [54] demonstrated a TED device based on dipping polyester fabric into a mixture of PEDOT:PSS and graphite. They report a maximum power factor of 0.025 μW $m^{-1}$ $K^{-1}$ at 398 K for the coated fabric with 15 wt% graphite loading. This research expanded on their previous work on PEDOT:PSS coated fabric strips [55]. The authors report a 4.3 mV output produced from 5 thermoelectric strips at a $\Delta T = 75.2$ K. Finefrock et al. [56] dipped nylon fibers into a solution of $Ag_2Te$ nanocrystals to add thermoelectric properties to the fibers. The untreated nanocrystals are n-type, while p-type nanocrystals are found after annealing the coated nylon. Using both fiber types, the authors generated 0.8 nW at a 20 K temperature difference. The power increased to over 5 nW when the p-type material was replaced with a conducting polymer. Lee et al. [57] created thermoelectric textiles by weaving n- and p-type yarns by twisting electrospun polymer nanofibers that are coated with $Bi_2Te_3$ and $Sb_2Te_3$. Plain weave, garter stitch, and zigzag stitch structures produced 1 μW, 0.21 μW, and 0.24 μW at a $\Delta T = 50$ K, respectively. Ryan et al. [58], [59] used textile dyeing processes to deposit PEDOT:PSS onto silk and cotton yarns. The authors note that the outer layer of silk fibers showed a high degree of interaction with the PEDOT:PSS. Then, they demonstrate two uses of the silk in e-textiles: (1) replace wires that serve as interconnects for transferring data and (2) to act as p-type legs in a fabric-based TEG. A 26 element energy harvester with dyed silk as the p-type legs and a silver wire as the n-type legs produced 12.3 nW of power at $\Delta T = 66$ °C. Another interesting fabric based TEG was proposed by Wu and Hu [60], which demonstrated a multi-wall carbon nanotube (MWCNT) doped solution with nonionic waterborne polyurethane (NWPU) using both n- and p-type

MWCNTs. Polyester yarns were then dipped in the solution and dried a total of five times. The thermoelectric yarns were embroidered into a 3D fabric, or spacer fabric, and connected in series at the top and bottom of the fabric using conducting paint as seen in Figure 2.2. When placed on the distal forearm, the TEG generated 0.1242 mV at a $\Delta T = 10.7$ °C.

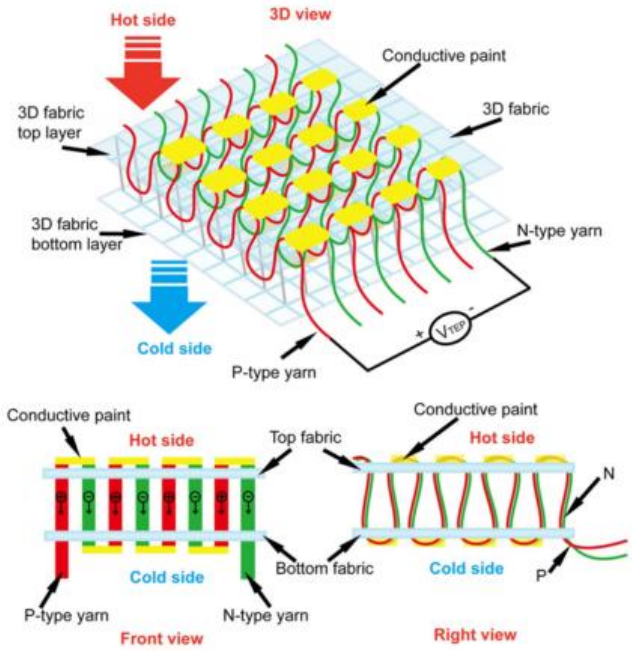


**Figure 2.2** Isometric, front, and right side views of spacer fabric with embroidered TE yarns [50].

Printing is another approach to incorporating electronic and energy harvesting functionality into textile platforms [51]. Electronic conductivity is added to textiles by printing conductive inks onto the fabric itself or onto a thermoplastic polyurethane (TPU) layer that is then laminated onto the fabric.

Thin films are common substrates for printing TE inks and materials. Screen-printing is one of the simplest approaches to deposit materials onto a substrate. It is particularly useful in depositing high viscosity materials. Cao et al. [61], [62] printed thermoelectric pastes onto

Kapton®. The Kapton® substrate enables large flexion and deformation of the thermocouples without significant defects forming. The first thermocouple they fabricated generated 48 nW at a $\Delta T = 20$ °C. The group expanded on this research and lowered TE material resistivity. The updated prototype with eight thermocouples produced 40.3 nW when exposed to the same temperature gradient. Ankireddy et al. [63] produced a similar device by dispenser printing silver and nickel pastes onto Kapton®. Strips of these TEGs, for a total of 31 thermocouples, were placed normal to a waste heat system and showed the highest power generation of 14.6 μW at $\Delta T = 113$ °C. Other printed thermocouples on thin film substrates produced 10.5 μW for 50 couples at $\Delta T = 20$ K [64], 20.5 μW from 60 legs at 20 K temperature difference [65], 4.18 nW from 100 thermocouples at thermal gradient of 15 °C [44], a 0.085 μW $K^{-2}$ $cm^{-1}$ power factor [66], and 1.2 mW $cm^{-2}$ with $\Delta T = 50$ K [67]. Itoigawa et al. [68] added an additional step to the thin film TEG fabrication. The group bent the TEG film into a sinusoid between heat sink and absorber sheets resulting in a flexible TEG. Instead of common $Bi_xTe_x$ or $Sb_xTe_x$ materials, Lee et al. [69] screen printed ZnSb onto a thin film. This device showed a power density of 0.22 mW $cm^{-2}$ at a 70 K temperature difference. Also of note is a TEG fabricated by sputtering TE materials onto paper [70]. The authors optimized the TEG design deposited the TE materials in a helical pattern, which enabled the TEG to stretch out of plane [71].

Some researchers have also printed TE materials directly onto a fabric substrate. Kim et al. [72], [73] used dispenser printing to print n- and p-type legs directly onto a polymer fabric thus embedding the material into the textile matrix. A polyimide film attaches underneath the fabric to shield the skin from the TEG. Conductive thread was used to connect the legs. At an ambient temperature of 5 °C, the TEG produced 224 nW of power when worn on the body. Another

group [74] screen-printed thermoelectric pastes onto glass fabric. They added PDMS to isolate the device and improve mechanical stability. The authors report a power density of 3.8 mW $cm^{-2}$ at a 50 K temperature gradient. Shin et al. [75] optimized TE inks to improve the viscosity for printability. Following printing on a glass fabric, the authors hot pressed the substrate resulting in the ink binders burning off. The defects left from the binders scattered phonons and improved the ZT of the material. Lu et al. [41] printed nanostructured thermoelectric materials onto silk fabric and connected the legs with silver foil. The TEG generated 15 nW of power at a $\Delta T = 35$ K. It should be noted that this device was not encapsulated like the aforementioned generators. Rabari et al. [76] also dispenser printed TE materials onto a fabric; however, the fabric used was very porous and the device was designed so that the TE materials filled designated pores. When worn on an arm, the TEG produced 1.3 mV.

### *2.2.2 Knit Textiles for Wearables*

All of the aforementioned smart textiles consist of applying a material to a finished textile. Modifying the structure and type of textile is another way to add smart functionality. Knitting a fabric offers several advantages over weaving including high extensibility and recovery and a reduced number of manufacturing processes. However, knitting with smart or functionalized yarns poses a unique challenge in that the yarn is inter-looped with itself. In contrast, a woven textile consists of multiple yarns laid parallel to each other in the warp and weft directions. A nonwoven textile, created from fibers and not yarn, also lacks material distortion as fibers are compressed together in a random orientation, without bending individual fibers. Thus, a smart

knit must be comprised of a yarn material that withstands large amounts of strain and repeated bending.

When referencing a knit textile, it is helpful to understand the scale of reference. Abel et al. [77], [78] defined a knit structure hierarchy seen in Figure 2.2. This scale can be modified further to include features of the yarn and fibers used, but for the purposes of this thesis, only the material properties as a member of the first level, the knitted loop, are considered. At second level, specific stitches define patterns, create texture, and shape the garment. This is where the interface between electronics and knits most prominently exists.

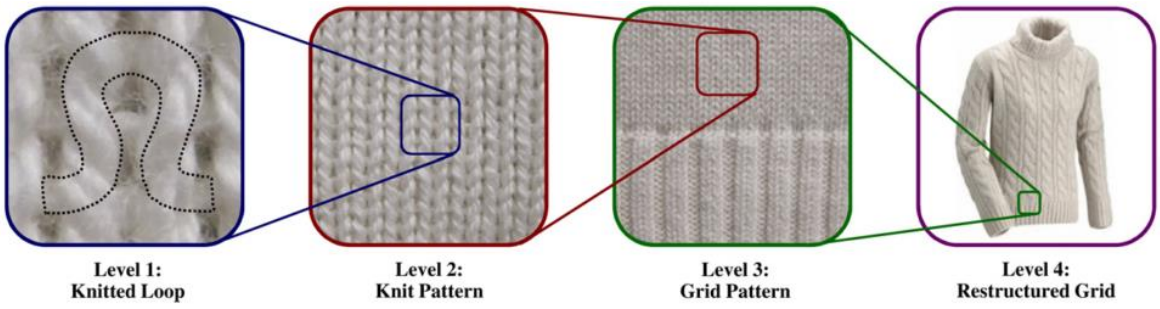


**Figure 2.3** Each level of a knit garment hierarchy as described in literature by Abel et al [77]

One benefit of using specific knit structures for e-textiles is the minor changes of properties due to mechanical stresses. Rather than designing an electrical interconnect in a serpentine or horseshoe line to accommodate stretching, no modifications are necessary since any deformation is absorbed by the geometry of the knit stitch. Jost et al. [48], [50] developed knit supercapacitors by defining interdigitated patterns at Level 3: Grid Pattern as seen in Figure 2.4. The intarsia technique allowed the authors to seamlessly integrate conductive yarns into specific patterns based on the intended application of the smart garment. Jost demonstrated

supercapacitors by knitting alternate courses of conductive yarn and inert yarn and then proposed a connected garment with several functions using conductive yarn as interconnects and sensors. Modifying materials used at the knit pattern level has not been reported yet, but the approach could enable other applications of conductive yarn.

Knitted sensors and actuators demonstrate new opportunities in wearable technology and body monitoring. Abel et al. [77], [78] knit a shape memory alloy (SMA) wire to explore different actuation motions. By modifying the stitch or the grid design, the authors curled and folded the wires into different 3D designs.

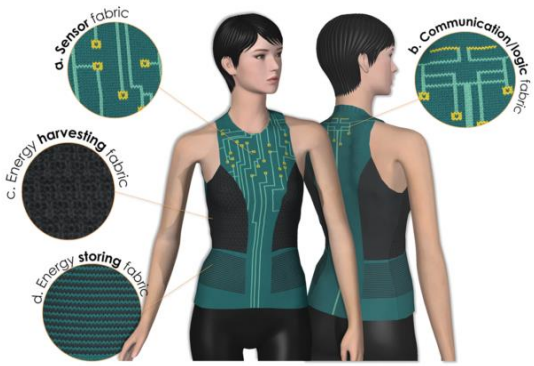


**Figure 2.4** Various patterns that demonstrate specific applications including, sensing, communication, energy harvesting, and energy storing, of knitted conductive yarn [45]

## 2.3 Modelling the Microclimate

### *2.3.1 Modelling Knit Morphology*

For a mathematical model of heat and mass transport in textiles to be accurate, one must accurately model the morphology of the textile. Much attention has been devoted to accurately representing knit structures in simulations due to their complexity. The first attempt to recreate a knitted pathway was performed by Chamberlain, [79] who created a 2D model in 1926, and

Peirce [80], who created a 3D model based on Chamberlain's 2D model in 1947. Others [81]–[83] built off these models and developed a model suitable for predicting fabric dimensions, but not for computer generated models.

Kurbak [84] began developing a method to generate an accurate computer-aided knit morphology in the late 1990s. Rather than modelling the pathway as a series of splines, Kurbak based his model on a series of ellipses connected by helical arms, as seen in Figure2.5a. In addition to modelling plain and jersey knit geometries, Kurbak modelled other stitches including tuck, rib, purl, miss, full and half cardigan, lacoste, and spacer knits [85]–[91]. To do so, Kurbak mapped a series of nodes in 3D from various geometrical derivations using Python. The plot is imported into 3DS-MAX software where yarn geometry and properties are added. In addition to modelling other stitches, Kurbak also considered several nuances of textiles that arise during and post manufacturing such as yarn relaxation, fabric curling, spirality, knit tightness, and post-wash relaxation.

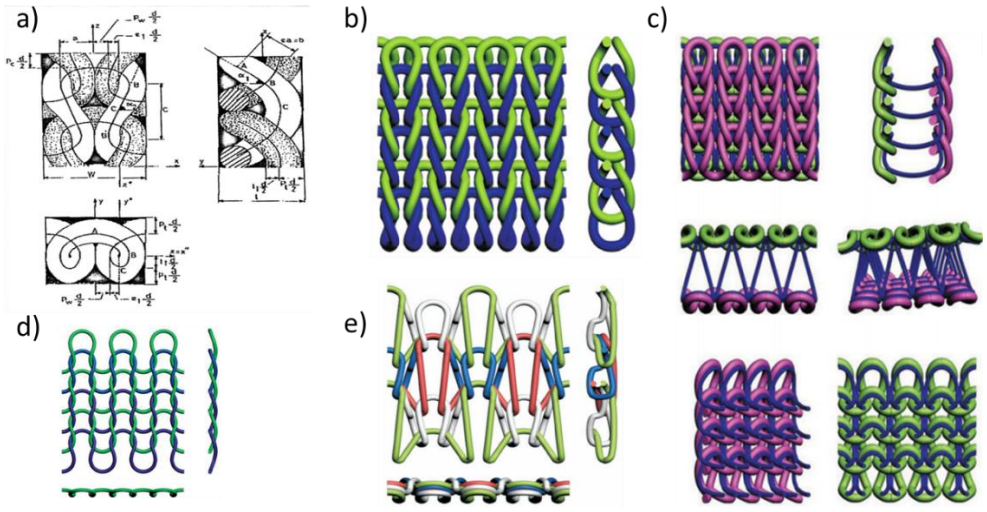


**Figure 2.5** Models of a) 2D jersey b) 1x1rib c) spacer d) 3D jersey and e) piqué stitch geometries as modelled by Kurbak [85].

Another approach to computer generated knit fabric modelling was demonstrated by Yuksel et al. [92]. Rather than mapping the yarn pathway, the morphology was generated using a pattern of meshes, seen in Figure 2.6a. Each element of the mesh comprised a 2.5D representation of yarn curves. The yarn curves followed cubic Catmull-Rom spline pathways. Different stitches could be generated by using mesh elements with different yarn pathways and a different number of sides, as seen in Figure 2.6a. This method enabled the authors to model complex knit patterns with correct knit shaping and fabric draping.

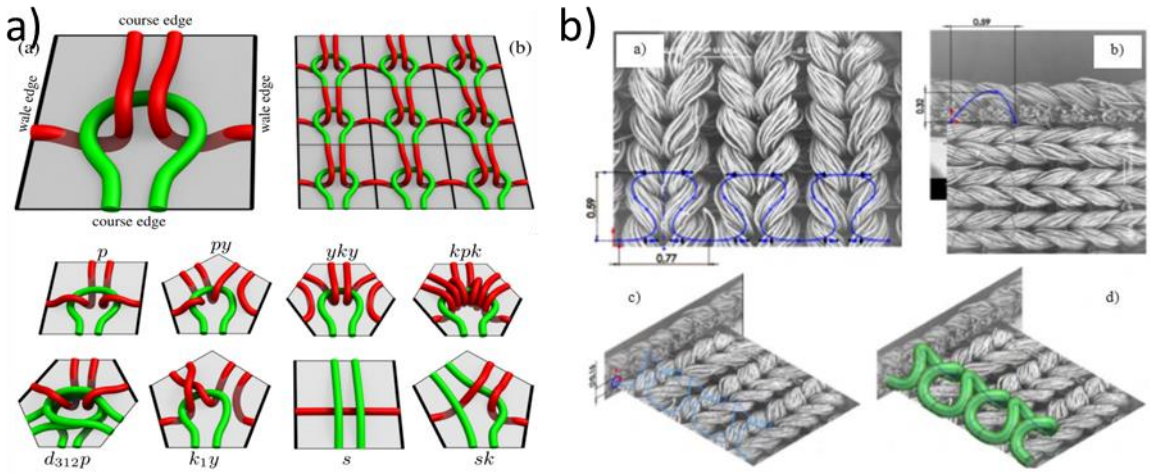


**Figure 2.6** (a) Model of stitches via mesh elements as reported by Yuskel et al. [92] (b) Puskarz et al. jersey stitch model from scanned knit fabric. [93]

Puskarz [93] created the geometric model used in finite volume simulations by mapping the knit structure shape based on electron micrographs of their knit swatches, demonstrated in Figure 2.6b. After importing the micrograph image into SolidWorks, Puskarz traced the yarn path using non-uniform rational B-spline (NURBS) curves. The author then generated a swept extrude to form the 3D yarn geometry.

### *2.3.2 Modelling Heat Transfer in Textiles*

Modeling textiles accurately is difficult due to the complexity of the system. One needs to consider the structure of the textile (woven, nonwoven, or knit), the three-dimensional nature of fabric, the material properties of the yarn used, and the interfaces between yarns. Additionally, a yarn is composed of individual fibers that are considered separate bodies in finite element analysis. Textiles are typically modeled following a finite element method [94] and much of literature focuses on woven textiles rather than knit.

Thermal management of electronic systems is widely studied to improve component performance and reduce the chance of overheating. Additionally, thermal management regarding textiles and clothing is widely studied to prevent hypothermia or hyperthermia and to improve thermal comfort [4], [95], [96]. However, few studies have investigated the thermal relationship between electronic components and textiles when considering wearable devices. This is a crucial constituent to the advance of this field as many electronics generate heat during operation. This heat must be accounted for and either stored or dissipated in the textile so as not to disturb the thermal comfort of the user.

Heat transfer through textiles and porous media is a complex phenomenon. Thus, when looking at heat and moisture transfer through textiles, many researchers assume the textile as a simple bulk substrate or as a porous/webbed substrate. Few account for detailed stitch geometries and weave patterns. Puskarz and Krucinska [93], [97], [98] performed flow simulations, via the finite volume method, in Solidworks that describe the heat transport phenomena in knitted fabric. To achieve this, they simplified the morphology of the knit and assumed the yarn to be a monofilament with isotropic properties. They supplement these models with thermography

studies of knit samples. The results showed that most thermal energy propagates through the most vertical stitch section. In further studies, the knit geometry was refined to account for multi-filament yarn with twist inserted into the yarn. The authors note that using a multi-filament model resulted in significant differences from that of the monofilament. This is due to the contribution of air gaps between fibers in the multi-filament model. After conducting experimental tests by imaging textiles on a hot plate, the authors concluded that the simulations complemented the experimental results. They state that the key variables in the model are the raw material properties while yarn structural properties are less significant.

### *2.3.3 Modeling the Human - Environment Microsystem*

Maintaining thermo-physiological comfort via temperature and humidity control is widely considered a priority by most workplaces. As such, the mechanisms of moisture and heat transport away from the human body have been widely studied and characterized. Wissler [99] proposed the first mathematical model of the human thermal system with respect to a simplified human geometry composed of 6 cylinders, each representing a section of the body. Many researchers have expanded upon this model into study of the climate immediately surrounding a human body, the microclimate, taking into consideration clothing, transient effects and more complex human geometries. [9], [11], [100]–[103] Figure 2.7 [101] shows the human body-clothing-environment system with (a) and without (b) clothing over different body segments. This model assumes that the heat transfer within the human body can be broken into 4 concentric regions: the core, muscle, fat and skin, which are all controlled by blood

circulation, represented as a separate node. Thermal regulation of the body is achieved via several control processes: vasodilation, vasoconstriction, perspiration, and shivering. [104]

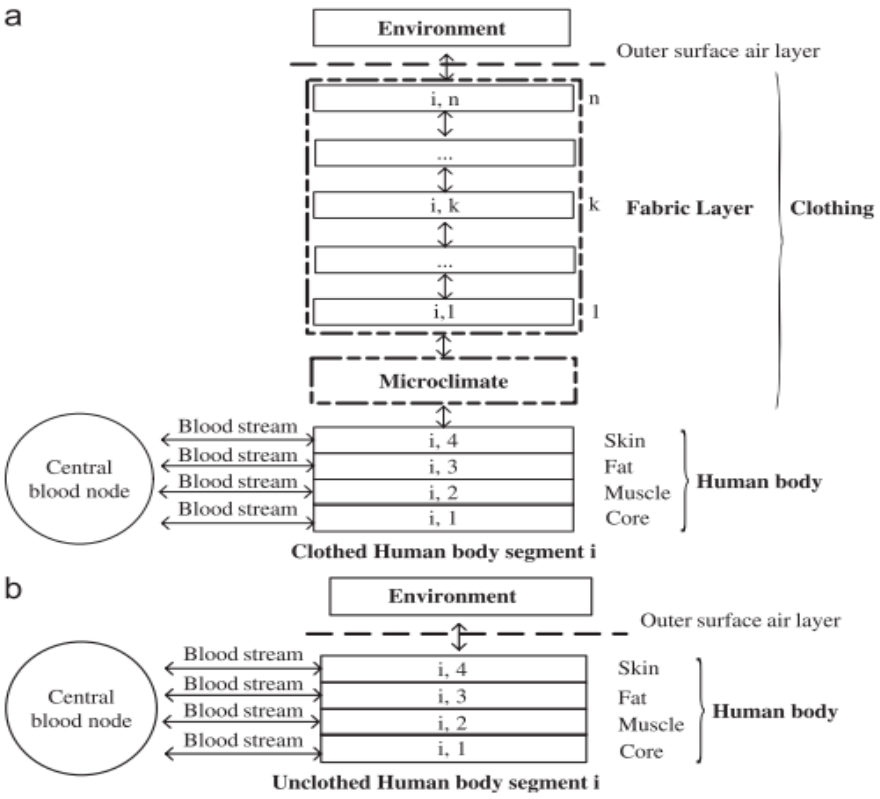


**Figure 2.7** (a) Expanded and (b) simplified node breakdown for heat generation and transfer from the body to the environment.

The simplest representation of the heat transfer away from the body at the skin surface is denoted in Eq. 1

$$S = M_{sk} \pm R \pm C \pm E_{sk} \quad (1)$$

where $S$ is the rate of storage of body heat, $M_{sk}$ is the net rate of metabolic heat exchange to the skin surface, $R$ is the radiant heat exchange, $C$ is the rate of conductive heat transfer, and $E_{sk}$ is the net rate of evaporative heat transfer at the skin surface. [11] A more complete

summary of the heat balance equations that correspond to Figure 2.7 are given by Wan and Fan [101] as follows:

$$C_{i,1}\, {dT_{i,1}}/{dt} = Q_{i,1} - B_{i,1} - D_{i,1} - RES_{i,1} \quad (2)$$

$$C_{i,2}\, {dT_{i,2}}/{dt} = Q_{i,2} - B_{i,2} + D_{i,1} - D_{i,2} \quad (3)$$

$$C_{i,3}\, {dT_{i,3}}/{dt} = Q_{i,3} - B_{i,3} + D_{i,2} - D_{i,3} \quad (4)$$

$$C_{i,4}\, {dT_{i,4}}/{dt} = Q_{i,4} - B_{i,4} + D_{i,3} - Q_{t,i} - E_i \quad (5)$$

$$C_{blood}\, {dT_{blood}}/{dt} = \sum_{i=1}^{16} \sum_{j=1}^{4} B_{i,j} \quad (6)$$

where *C* is the heat capacity of the body, *T* is the temperature, *Q* is the rate of internal heat production, *B* is the heat exchange between each body node and central blood node, *D* is the heat transmitted by conduction between layers, *RES* is the respiratory heat loss, and *E* is the latent heat loss from skin, with respect to node (i,j). In this notation, node 1 represents the core, node 2 is muscle, node 3 is fat, and node 4 is skin. A separate node for the central blood supply is assumed. Equations 2-5 summarize the heat balance of the core, muscle, fat, and skin respectively, while equation 6 represents the heat balance of the central blood system.

None of the aforementioned equations includes the effect of clothing on thermal and moisture transport away from the body. Wan and Fan [101] consider this critical component of the model as clothing ventilation can cause up to a 50% reduction in thermal insulation and up to 88% reduction in evaporative resistance, [105] based on level of activity. The addition of clothing creates a region between the skin and bottom layer of fabric with distinct temperature and

humidity levels referred to as the human microclimate. The heat balance equation of this region is

$$V_{mc,i} Cv_a \, {dT_{mc,i}}/{dt} = h_c\left(T_{i,4} - T_{mc,i}\right) - h_c\left(T_{mc,i} - T_{cl,i,1}\right) - Q_{vent} \quad (7)$$

where $V$ is the volume of the microclimate, $Cv$ is the volumetric heat capacity, $h_c$ is the convective heat transfer coefficient, $T$ is the temperature at a designated node, and $Q$ is the heat loss due to ventilation. Sweat is accounted for by the following moisture balance equation

$$V_{mc,i} \, {dC_{mc,i}}/{dt} = h_m\left(P_{sk,i} - P_{mc,i}\right) - h_m\left(P_{mc,i} - P_{cl,i,1}\right) - \dot{m}_{vent,i} \quad (8)$$

where $C$ is the water vapor concentration, $h_m$ is the convective moisture transfer coefficient, $P$ is the water vapor pressure at a designated node, and $m$ is the moisture loss from the microclimate due to ventilation.

## 2.4 SUMMARY

Each of the subjects previously discussed: thermal energy harvesting, electronic and smart textiles, and human microclimate and knit modelling, have considerable depth and are ongoing areas of research. The research produced in each of the fields remains relatively isolated from the others. As such, one challenge is finding parallels in the fields and using those similarities to create a multidisciplinary project, the summary of which is seen in Figure 2.8.

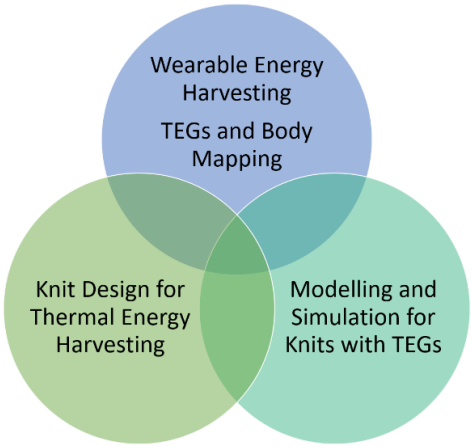


**Figure 2.8:** Venn diagram of the interrelated topics discussed in this thesis.

The goal of this thesis is to study the interaction of TEGs with the human body and knit textiles via body mapping, to determine the interaction of knit structures with thermal energy harvesting and thermal comfort, and to use simulations to correlate heat transfer from the body and environmental conditions to improving textile integration methods. Each aspect of the project influenced the others, visually demonstrated in the Figure 2.8. Due to this relationship, it is difficult to discuss one aspect of the project without mentioning the others. The next chapters are individual articles that display the iterative design process used in this thesis. The next chapter discusses the proof of concept data that highlighted the important parameters to focus on in the later chapters.

# CHAPTER 3: Human and Environmental Analysis of Wearable Energy Harvesting

Amanda Myers, Ryan Hodges, and Jesse Jur
**As published in Energy Conversion and Management*

## 3.1 OVERVIEW

In considering wearable energy harvesting, one must recognize the wide array of factors that lead to variations of energy harvesting. The objective of this work is to define analytical methods to study the effect of environmental and human factors on thermal energy generator (TEG) performance in a variety of use case scenarios. A test method for evaluating the performance of a TEG in a wearable form is developed and demonstrated using both in-lab and out-of-lab procedures. The fabrication procedure of an energy harvesting wearable device demonstrates a method of integrating rigid devices into a flexible substrate. The wearable device is used in a human trial, which covered a series of activities in different environmental conditions. The results of these trials demonstrate the significant effect of movement, or convection, on thermal energy harvesting. Humidity levels do not have a significant correlation to power; however, wet bulb temperature must be taken into consideration due to the additional cooling effect of evaporation on temperature. The data collected indicates that while dry-bulb temperature does not have the greatest effect on TEG power generation, wet-bulb temperature is indicative of TEG performance. Additionally, user generated movement is the main consideration when designing a wearable device with TEGs as it had the largest effects on power generation. The results of this work quantify how a wearable device will perform

throughout daily activities, allowing the definition of an operational scenario of a self-powered wearable device while choosing the most appropriate design for a particular application. This work also provides a foundation for exploring how textiles can enable the design of unique wearable devices. This will lead to further investigation into quantifying the effect that the construction of a textile has on TEG performance as well as on consumer comfort.

## 3.2 Introduction

Recent advances in low power electronics, including semiconductor on chip and radios are enabling opportunities in wearable devices that utilize sources of energy outside the use of a battery. In wearable devices, batteries add both bulk and weight to a device reducing its perceived comfort [1]–[4], and also require plug-in recharging that can seem burdening to the consumer. While low power electronics enable strategies in reducing the battery size or improving the operating lifetime between battery charges, the ability to use energy harvesting directly from the body has been suggested as an alternate source of power. Studies exploring mechanical and thermal energy harvesting have shown promise in guiding energy harvesting materials design, but have been limited to benchtop and short term use case studies [5]–[8]. The energy harvesting packaging design for on-body use has a number of complex design criteria that define the device comfort and performance. For example, the on-body location of the device identifies form factor, flexibility, materials used, etc. that need to be considered with regard to user comfort. The device performance is highly dependent on human factors that are even more influential to the performance of the energy harvester [9]–[11]. For a thermal energy generator (TEG), human factors include the temperature difference between the surface of the

skin and ambient air, air velocity over the TEG, and the humidity of the ambient air, resulting in a complex combinatorial effect on the energy harvesting ability of the TEG. The influence of these variables is dependent on the harvester's location on the body. This work aims to explore testing strategies for determining the effect of human factors related to thermal energy harvesting, including environmental influences and position, or location, of energy harvesting, which thereby enables future strategic design of the materials surrounding the energy harvesting for improving performance.

Prior research has shown that thermal energy harvesting offers a consistent supply of energy for wearable energy harvesting purposes[28]–[30], [36], [37]. Of particular note is the work conducted by Leonov et al. [24], [28], [30], [31] that have demonstrated TEG performance in a watch-based and shirt based platforms. Their research demonstrated that the key challenge of thermal energy harvesting from the body is the temperature differential between the body and microclimate surrounding the device that ultimately limits the energy that can be harvested. The common approach to improve thermal energy harvesting is to include a heat spreader and/or a heat sink to improve power output and maintain a temperature gradient across wearable TEGs. The rigid and bulkiness of the heat sink comes at the expense the perceived comfort of the device. Settaluri et al. [38] characterized and optimized a heat sink and heat spreader system for use with a wearable TEG wristband, acquiring a power density of 28.5 $\mu W/cm^2$. Another is the fabrication of flexible or fiber-based TEGs [8], [39]–[41] which improves the TEG-to-skin contact. Both of these methods highlight the importance of improving TEG performance on a device level in a more comfortable manner, but do not consider the variety of environmental conditions the human body is exposed to on a daily basis.

Of particular interest is the observation that thermal energy harvesting has been shown to have negative effects on human comfort due to a high heat flow from the skin resulting in a chilling effect [14], [31]. For the eventual success of on-body energy harvesting, the ability to understand what factors influence energy harvesting over the wide range of body placement and human factors is paramount to mitigating human discomfort without compromising the efficiency of the thermal energy harvester.

The purpose of this work is to quantify the effects of transient environmental conditions and human scenarios on the efficiency of a body-worn TEG via controlled laboratory experiments and human trial studies. The controlled tests presented in this work characterize the TEG with defined heat loads, air velocities, and heat sinks to define TEG integration strategies. Using these design strategies, a wearable platform is used to collect experimental data directly from a human in true indoor and outdoor conditions. As part of the device design, a novel printed circuit board (PCB) design was constructed to simultaneously monitor the environmental conditions, activity level of the human, and the instantaneous power generated by the TEG device. Data was collected using this platform in real time with human subjects performing different activities that changed motion and environmental conditions. The results of this work identify specific environmental variables that show the largest effect on the energy harvested and analysis is performed to define correlations between motion intensity and power generation. Finally, a power map based on activity and external environment is defined that can be used to estimate TEG efficiency in future studies.

## 3.3 TEG CHARACTERIZATION

Several tests were performed in a controlled laboratory setting to characterize the response of the TEGs (Laird Technologies: OT08, 18, F0, 0505, 11) used in this study. In a benchtop analysis, finned heat sinks with values of 10 °C/W, 4.6 °C/W, and 1.9 °C/W (CTS Electronics Components) were each applied to the TEG with matched load (4.4 Ω) and the power output recorded. The TEG was placed in contact with a thin layer of polydimethylsiloxane (PDMS) situated in contact with a hot plate. The PDMS served as a thermal simulant to skin (the thermal conductivity of PDMS is 0.15 W/mK [106] while the thermal conductivity of the epidermis layer of skin ranges from 0.2 – 0.5 W/mK [107]) and the PDMS was able to dampen the effects of the temperature fluctuations of the hot plate with minor spatial variability. A hot plate temperature of 37 °C resulted in a PDMS exposed surface temperature of 35 °C, which is an average temperature of human skin.[108] During all experiments, the ambient air temperature remained between 21-22 °C. After the TEG power output reached steady state in stagnant air (~30 min), an air flow of 1.2 m/s was provided using a small fan placed 15 cm away from the heat sink edge to simulate the airflow induced by a human walking pace [26]. This setup is similar to that demonstrated previously in testing for a material's Seebeck coefficient for a TEG placed on the body [109].

The effect of spacing between TEGs was evaluated by placing two TEGs in series at increasing spaces. The spacing between the TEGs ranged from 0 mm to 6 mm as measured between the neighboring edge of each device, and held in place with in a structural mold. The TEGs were placed on the heated PDMS with a matched resistive load (8.8 Ω) and the experiment outlined previously was repeated.

### 3.4 TEG Characterization Results

The results of laboratory-controlled TEG characterization tests, presented in Fig. 4.1, provide two observations that are key to energy harvesting at low temperature differentials across a TEG; first, convection over the TEG improves the steady state power generation and second, heat sink properties are not proportional to power generation. The first trend in Fig. 4.1a shows an increase in power generated when air convection is used to remove heat from the TEG (after 30 min of stagnant air). The second trend observed is that the power harvested is not proportional to heat sink thermal properties. As shown, a decrease in power generated when the improved, 1.9 °C/W heat sink is used as compared to the 4.6 °C/W, both of which are improved compared to the 10 °C/W heat sink. This is directly attributed excess cooling provided by the better heat sink, that, without a change in heat input begins to limit the TEG performance. On a human, this result would be observed as a cooling sensation at the location of the TEG.

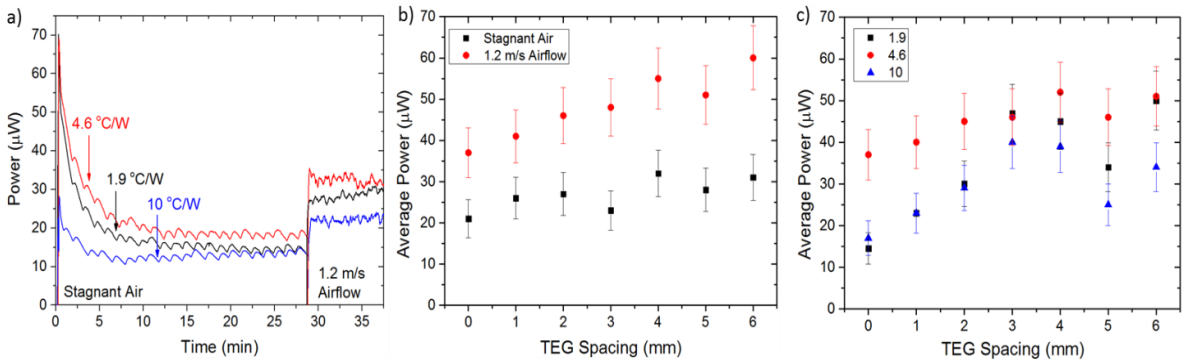


**Figure 3.1** Heat sink comparison with constant heat input for a single TEG. (a) Air flow and spacing comparison showing the average power output of two TEGs with varied spacing and constant heat input. (b) The 4.6 °C/W heatsink displays the largest average power values. This heat sink is evaluated in both stagnant and moving air. (c) A comparison of the average power output between each of the heat sinks (units in °C/W) in constant airflow.

When the heat transfer from the heat sink is larger than what can be provided from skin, it may be possible that the cooling effect is observed at distances beyond the area of the skin that is directly in contact with the skin. In essence, this would induce a design constraint with respect to the spacing of two TEGs that exists at the heat spreading, skin side of the TEG. That is, when two TEGs are separated by a large distance, the total power harvested will be larger as compared to two TEGs intimately in contact. It is important to note that this would suggest that the heat flow from the skin cannot be considered to be constant, as thermal effects would be observed from the neighboring TEG. To test this hypothesis, the effect of spacing between TEGs was evaluated by placing two TEGs in series at increasing spaces.

As shown in Fig. 4.1b, the total power harvested from the two TEGs increases with an increase in the spacing distance between TEGs. This trend is more pronounced with the addition of airflow across the device. A comparison of the spacing effects for each heat sink when subjected to air flow is provided in Fig. 3c. As observed in the analysis of a single TEG (Fig. 4.1a), the 4.6 °C/W heat sink harvests more power when compared to the 1.9 and 10 °C/W heat sinks. As the spacing is increased (~4 to 6 mm), the increase power harvested is less impacted by the spacing of the TEGs, indicating that the spacing of the TEGs is sufficient to not impede on the neighboring TEG's heat flow (or pull). The importance of this result cannot be underestimated when it comes to designing multiple TEGs within close proximity for on-body energy harvesting. It is noted that potential factors that influence this spacing impact include the internal TEG design (fill factor, junction spacing, leg height) as well as the heat spreader and heat sink. From a comfort level, the rigid TEG spacing will also impact that the flexibility of package and therefore influence the thermal contact resistance between the skin

and TEG. While additional work needs to be conducted to relate all of these factors, for the purpose of this work the construction of the multiple TEG package will assume that 6 mm spacing is sufficient to maximize the potential energy harvesting.

### 3.5 EHSS Platform Design

A unique energy harvesting platform was developed that allows for simultaneous energy harvesting and storage evaluation alongside incorporation of sensors. The battery-powered platform and corresponding source code is based on the TI SensorTag development kit. The evaluation system is specifically designed to measure the useable current and voltage from an energy harvester the power consumption from a suite of sensors. Moreover, the PCB dimensions and communication allow for simple on-body testing. The system's primary differentiation to commercial systems is its application as a testing platform for real time power management profiles necessary for development of on-body self-powered sensor systems.

The energy harvesting subsystem (EHSS) allows for the wireless transmission of multiple sensor and energy harvesting data via Bluetooth LE. It measures harvested voltage and current levels from thermoelectric, piezoelectric, and/or solar energy harvesting devices delivered to a variable load. In addition, the system measures 3-axis accelerometer data, 3-axis gyroscope data, ambient temperature, and humidity. A block diagram for the system is seen in Fig. 2. Output from the TEG is first sent to a transformer and boost converter (LTC3108) [110] before getting sent to measurement and load circuits. Other sensor data communicates directly with the microcontroller using an I2C interface. The firmware for the on-board microcontroller has been developed to wirelessly transmit all sensor data and is designed for future expansion

should additional sensing modalities be required. The accelerometer data is transmitted to an app on a Bluetooth-enabled device at a rate of 100 Hz while all other data rates are set to 1 Hz. Additionally, the app logged each data point to allow for real time plotting and for the data to be accessed at a later point.

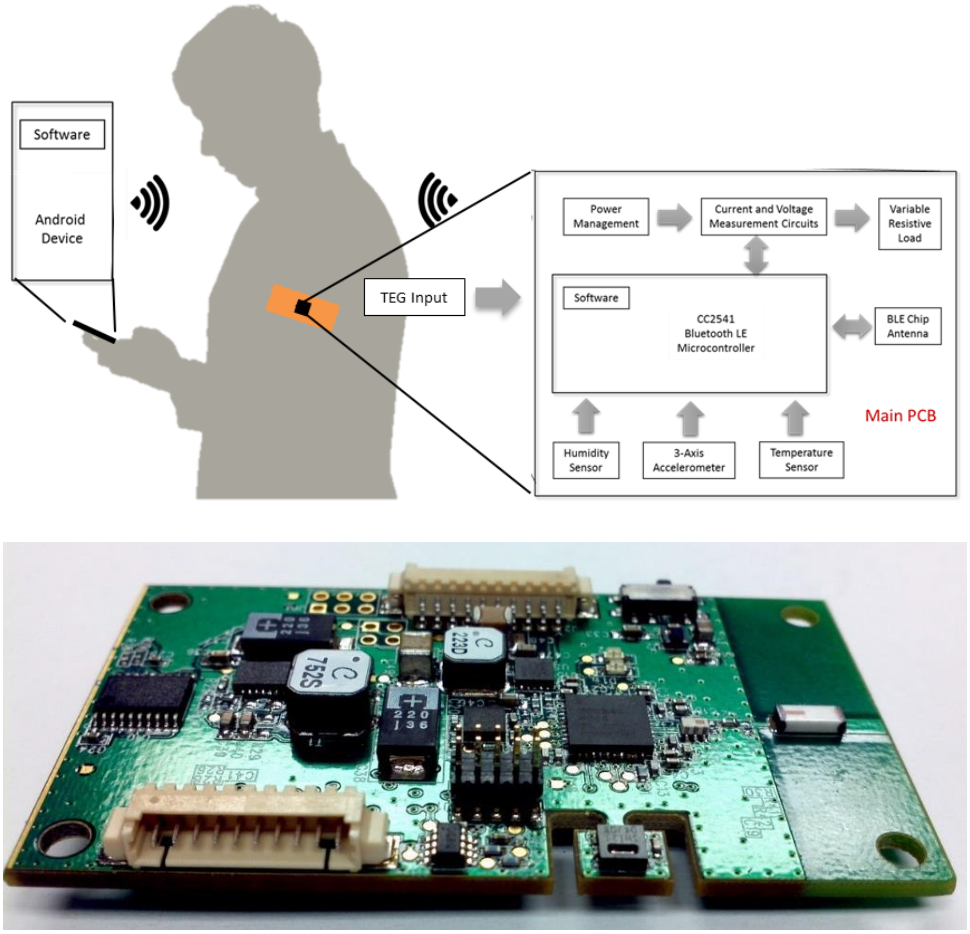


**Figure 3.2** A block diagram of the EHSS showing armband to BTE-device communication and the top view of the populated PCB.

## 3.6 Device Assembly

The construction of the wearable TEG devices is outlined below in terms of the formation of the flexible TEG integration into a textile assembly and the construction of a novel evaluation

platform for communicating the data wirelessly from the body to an Android tablet. Finally, the experimental design for the human trial study is described.

The design for integrating a series of TEGs into a flexible package is outlined in Fig. 1a. Pyralux® (Dupont), a flexible Kapton substrate that is coated in Cu on one side, serves as the flexible substrate which connects the TEGs. Pyralux® substrate is prepared using a die cutter to create five holes, 4.9 mm x 4.9 mm, spaced 6 mm apart horizontally as dictated by the controlled lab experiments presented. A mask applied to the Pyralux® defines the Cu connections between TEGs. The exposed Cu is etched by submersing the substrate in ferric chloride for >15 min. The mask is removed to expose the copper interconnects. The TEG is integrated into the cut out holes by first placing a Bi-Sn low temperature solder on the Cu coated sides to the gap that the TEG are placed, with the phalanges of each TEG maintaining direct contact with the solder. The substrate with the TEGs is cured in a reflow oven for 420 s at a maximum temperature of 150 °C.

The flexible substrate with the TEGs integrated is embedded in a textile multilayered structure comprising of Cu-coated taffeta, a polyethylene nonwoven textile, and jersey polyester knit. The Cu taffeta acts as a heat spreader between the skin and lower header of the TEGs. The polyethylene is included as structural support of the TEGs and as an insulating layer between the top and bottom of the TEGs. The polyester knit serves as the base fabric for the wearable device. The top edges of the band are sewn together and a 30 mm x 125 mm area is cut from the knit and Cu taffeta is sewn in its place. Small holes are cut in the outer polyester layer and in the inner polyethylene layer for TEG insertion. A fastener is attached to the band to accommodate size variations between human subjects. The TEG series attaches to the band

using alumina thermal paste on the TEG/Cu taffeta interface. Aluminum heat sinks, exposed to the environment, adhere to each TEG header with carbon tape. The final profile of the assembly is demonstrated in Fig. 1c. The data collection board, EHSS, is mounted to each of the devices via a mesh pocket. The pocket provides mechanical protection for the electronics without inhibiting any sensing modalities. The resulting devices as worn by a mannequin are displayed in Fig. 1b.

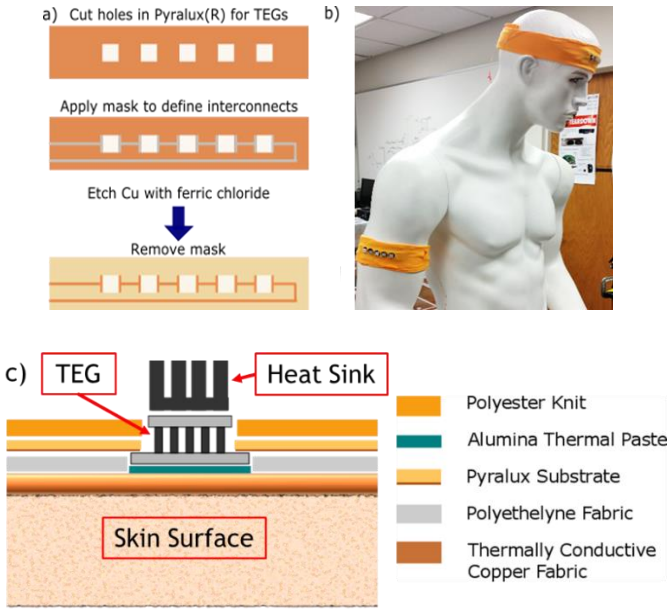


**Figure 3.3** a) Overview of flexible circuit fabrication process b) Fabricated headband and armband c) Profile view of device assembly

## 3.7 Design of Experiments

Three male participants (25 – 50 yrs, 168 – 185 cm, 59 – 82 kg) volunteered for a human trial study designed to observe how energy harvesting trends change as the user transitions between different environments and movement profiles and acquire to preliminary data for the design of an integrated thermal energy harvesting garment. An outline of the human trial study is

provided. First, a thermal imaging camera (FLIR E50) is used to map the distribution of the participants' skin temperature. This information is used to compare energy harvesting areas on the body as well as define an approximate skin temperature for each area. The participant then put on the headband or armband and adjusted the compression of the band as they found comfortable. The subject then participated in several pre-determined activities summarized in Table 1: walking, running, and resting. Each activity is performed for at least 15 min while the data on the temperature, acceleration, humidity, and TEG voltage was collected wirelessly on an Android tablet. The participant completed each activity in both an indoor and outdoor setting.

**Table 3.1** Indoor and outdoor temperatures for each activity during the study.

| *Participant Activity (15 min each)* | *Indoor Ambient Temperature (°C)* | *Outdoor Ambient Temperature (°C)* |
|---|---|---|
| *Rest* | 26 ± 2 | 30 ± 2 |
| *Walk* | 26 ± 2 | 28 ± 3 |
| *Run* | 26 ± 2 | 28 ± 5 |

### 3.8 HUMAN TRIAL RESULTS

Thermal imaging was first conducted to determine the average initial skin temperature of the forehead (38 °C) and the upper arm (36 °C) while in standard room conditions of ~21 °C. The pressure exerted by the device on the body was measured with a force sensitive resistor but was below the range of sensitivity so it is noted as < 0.1 psi. The following figures and results demonstrate the analysis procedure used in this study; however, not all data from individual participants is provided.

As shown in Fig. 4, the movement of subject 1 strongly influences the amount of power harvested from the TEGs. The instantaneous power, temperature, and movement intensity are shown in the top of Fig. 4 with respect to three movement scenarios: running, walking, and sitting. The temperature and power relationship is most obvious in Fig. 4a, outdoor running. However, the impact of ambient temperature on instantaneous power increases as the subject's movement decreases, indicating that the instantaneous power is more influenced by air flow rather than dry-bulb temperature. When the subject is seated, instantaneous power levels decrease to a negligible amount. The rate of energy harvesting with each movement scenario is shown in Fig. 4d. The rate of energy harvesting while running is approximately 0.021 mJ/s which decreases to 0.013 mJ/s while walking. The rate decreases to 0.001 mJ/s while the subject is seated. This vast difference in energy harvesting rates is another example of the significant effect air flow has on TEG performance.

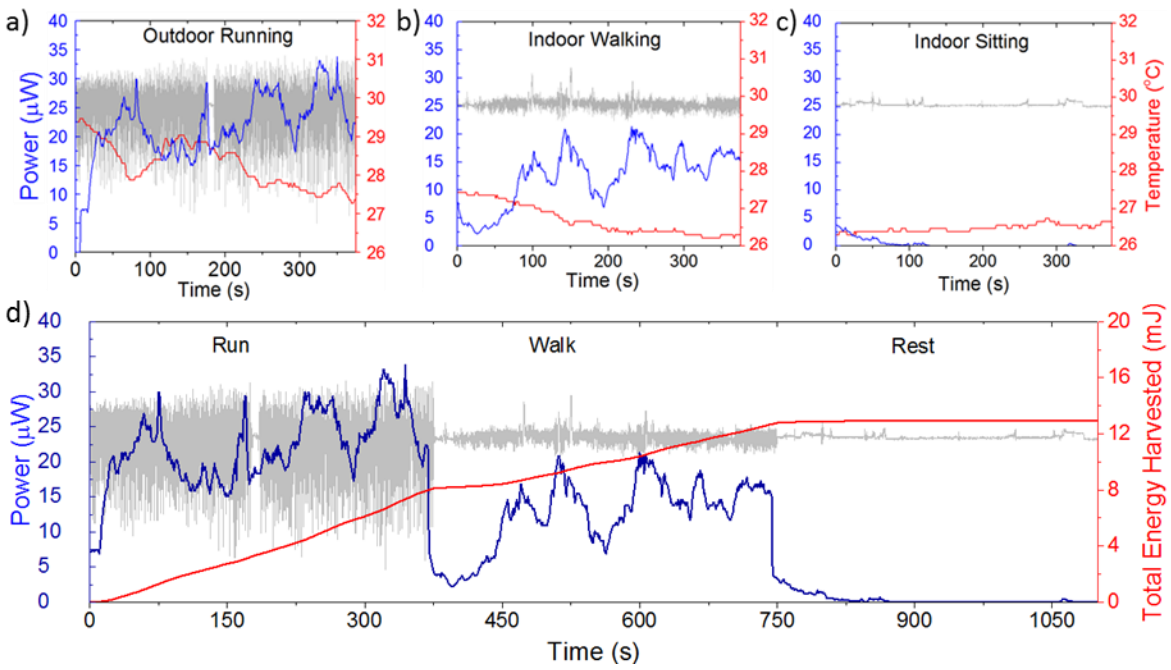


**Figure 3.4** The instantaneous power (blue) from a five TEG armband as compared to ambient temperature (red) and accelerometer magnitude (gray) for the subject running (a) walking (b) and sitting (c). All scenarios compared only to movement displayed in (d) with accelerometer magnitude (gray) and instantaneous power (blue) and the rate of energy harvesting or additive amount of energy harvested per unit time (red).

In summary, the energy harvesting data shows an increase in the energy harvesting rate with an increase in movement and also confirms the inverse relationship of temperature and instantaneous power. Based on the energy harvesting rates during various test scenarios, movement, or wind flow, is considered a significant factor and changes in ambient temperature has less of an effect while the subjects are running or walking. While seated, temperature became the dominant variable for determining the rate of energy harvesting.

## 3.9 Temperature Analysis

A thorough analysis was performed on a single subject to identify any trends that may exist within the raw data. Instantaneous power, external temperature, and external humidity plots for the running activity from the headband and armband are shown in Fig. 5, respectively. An inverse correlation is observed between the ambient temperature and the instantaneous power levels of the armband. The relative humidity does not appear to have a significant effect on the instantaneous power generation during the running activity (Fig. 5a), however a slight inverse correlation between humidity and energy harvesting is seen in the walking activity (Fig. 5b). As air velocity across the heat sink increases (i.e. as the subject moves faster), it can be assumed that the environmental microclimate surrounding the TEG can change in a short time period. Therefore, when determining the temperature gradient across a wearable TEG, it must take into account both the relative humidity and the temperature of the environment. This can be done with the use of a psychometric chart or through the conversion of the measured dry-bulb temperature to wet-bulb temperature via the method outlined in Stull. [111]

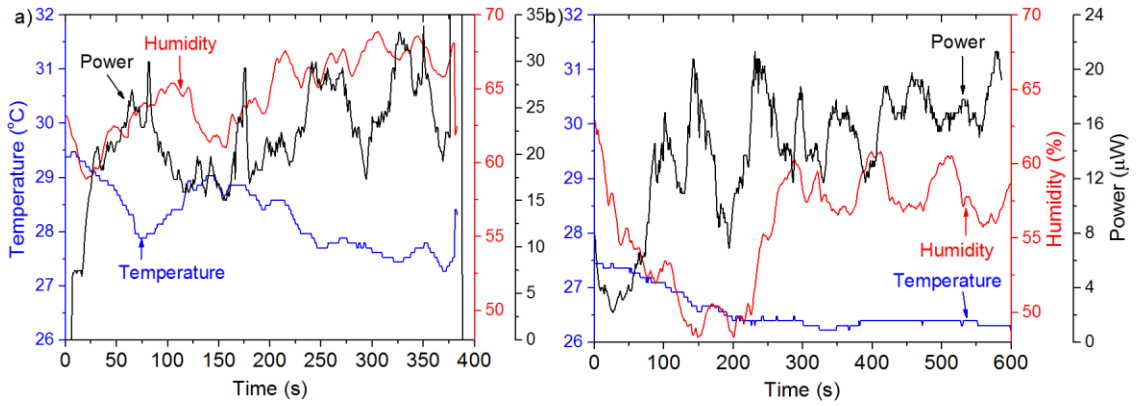


**Figure 3.5** Comparison of power (black) harvested to that of temperature (blue) and of humidity (red) for the subject running (a) and walking (b).

The power and temperature correlation is examined in Fig. 6, showing two distinct clusters identified which correspond to each movement, walking and running. The clusters show a linear trend as seen in the armband output (Fig. 6a). A linear fit of the clusters results in an R-squared value greater than 0.5 for each cluster. While this confirms that the linear response is accurate, the large deviation from the linear trend from subject 2 indicates that the armband did not have secure contact with the skin and may have motion artifacts.

The relative humidity did not show a significant influence on the TEG power when compared directly in Fig. 5; however, when used to calculate the ambient wet-bulb temperature, a change in the shape of the clusters is noted. The linear trends seen in the dry-bulb temperature comparison from subject 2 is not visually apparent in Fig. 6b. This implies an even greater influence of movement on power output when one accounts for relative humidity.

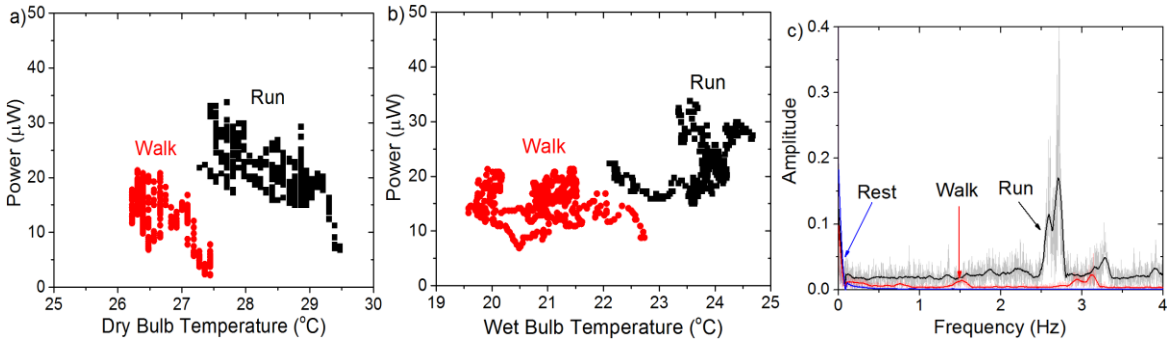


**Figure 3.6** The instantaneous power clusters generated as compared to dry-bulb temperatures where clusters are linear (a) and wet-bulb temperature where the clusters show more scattering (b) smoothed FFT evaluation of accelerometer data from human trials comparing peak amplitude, intensity of foot impact to frequency pace of foot impact, for the armband (c)

To investigate the geometrical change in clusters with relative humidity considered, cluster area was measured with respect to each activity and subject. Namely, the horizontal and

vertical ranges of each cluster were identified and the percent change in area between the dry-bulb temperature clusters and the wet-bulb temperature clusters was calculated as seen in the table below.

**Table 3.2** Geometric dimensions of clusters in Fig 6. Note that the vertical range does not change since the amount of power produced does not change.

| | Height (μW) | Dry-Bulb Width (°C) | Wet-Bulb Width (°C) | Change in Area (%) |
|---|---|---|---|---|
| *Run* | 18.78 | 2.20 | 2.57 | 16.80 |
| *Walk* | 14.55 | 1.22 | 3.15 | 61.27 |

For the subject, the addition of humidity in the power and temperature comparison expanded the range of temperatures recorded, resulting in an overall increase of the cluster area. The linearity of all data decreased when wet-bulb temperature is considered.

This indicates that when estimating the power output of a body-worn thermal energy harvesting device, one can increase the accuracy of the power estimate by using wet-bulb temperature regardless of whether the subject is indoors or outdoors. To improve the accuracy of the estimate further, the intensity of activity of the subject should be considered as well.

## 3.10 Accelerometer Analysis

The speed of someone as they move forward is correlated to the frequency at which their foot strikes the ground when walking or running. Walking and running repetitive movements with clear peak frequencies (Fig. 6c) while resting shows no clear movement trends from the accelerometer data. The frequency of foot strike and intensity of foot strike (the amplitude) were found by performing a Fast Fourier Transform (FFT) on the accelerometer data, seen in

the background of Fig. 6c. The data was smoothed using the Savitzky-Golay method with a 7 point window (Fig. 6c foreground). The average frequency of foot strike when walking is between 1.5 and 2 Hz with a mean amplitude of 0.055 ± 0.01. When running, the strike rate increases to ~ 2.5 Hz with an average impact amplitude of 0.311 ± 0.05. The frequency and intensity of the foot strikes increase with the subjects' pace.

Similar to the rate of energy harvesting, the strike intensity nearly doubles as the participant speeds up from a walk to a run, confirming the close correlation of thermal energy harvesting efficiency to movement. When performing the analysis, only the values from the x-axis of the accelerometer were evaluated. The data from each axis was compared and found to have little to no trend variation from that of the x-axis data.

### 3.11 Subject to Subject Variability

The accelerometer data was converted to velocity for further analysis. To do so, the raw data was converted from units of g (force) to $m/s^2$ and then integrated. The following figures investigate the reliance of thermal power harvested to subject velocity and to wet-bulb temperature. Fig. 7a and 7b compare power trends while each subject was running wearing the armband. The data confirms larger amounts of power at higher velocities, but the contour plots between subjects are vastly different. One reason for this is the level of contact the armband makes with the skin for each subject. It is difficult to quantify exact contact pressure due to differing comfort levels and amounts of hair between subjects. As the contact pressure changes, the area of the contour is likely to change as well. In the same manner, the use of different TEGs, heat spreaders, or heat sinks will affect the size and layout of the plot.

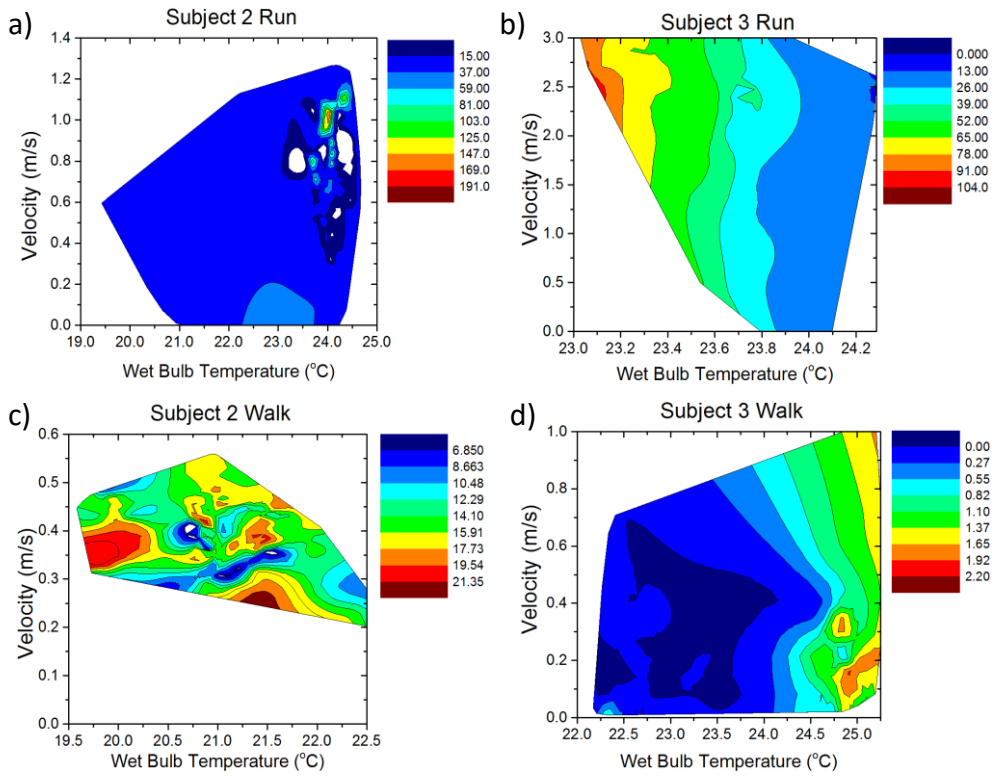


**Figure 3.7** Contour mapping of power generated in μW for a color scale from blue to red (red is the largest power value) with respect to wet-bulb temperature and subject velocity. The activity from one subject is shown on the left and another is shown on the right.

A similar trend between the power response to body location of the wearable device can be noted when the subject is walking, as seen in Fig. 7c and 7d. Again, the areas with largest power generation are associated with lower temperatures and higher velocities. Discrepancies between the power generation trends are due to subject variability. To see if these observations apply when all movements and subjects are directly compared to each other, each activity from each subject was mapped on the contour plot seen in Fig. 8. This confirms the trends previously noted: the most thermal power will be generated when the temperature gradient is largest and when the subject is generating the most air flow over the cold side of the TEGs. It should be

noted that Fig. 7 and Fig. 8 allow for the prediction of the energy harvested amongst individuals and groups of individuals. This prediction allows for the boundaries that support power management profiles for future self-powered devices. In addition, the methods serve as a benchmark for materials and device improvement.

When comparing the on body location of the TEGs, one must look at the use case scenario. While the armband has lower instantaneous power levels, the rate of energy harvesting while the subject is moving is significantly higher than the headband; indicating that it would harvest more energy over a longer period of time while in motion. This suggests that the armband platform is better suited for a consumer who is consistently active throughout the day. In future scenarios, power generation trends will also depend on the location of TEGs on the body. Each potential location on the body has benefits and drawbacks in terms of ideal location for thermal energy harvesting. Therefore, it is necessary to consider a consumer who may have different movement scenarios throughout the day. The results of the thermal energy harvesting body map guide the design and placement of other wearable energy harvesting devices to meet this requirement.

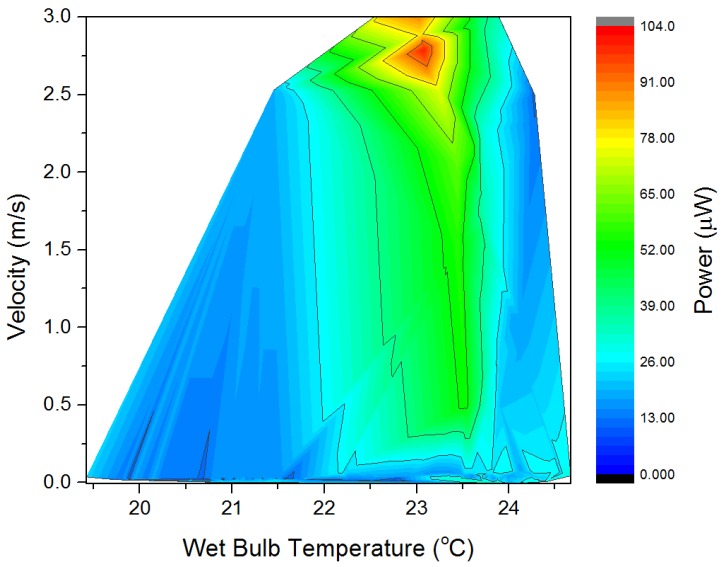


**Figure 3.8** Contour map of thermal energy harvested from the armband as a function of subject speed and wet-bulb temperature for all subjects. On the scale from blue to red, blue represents the lowest instantaneous power value in µW.

## 3.12 CONCLUSION

In summary, the work completed in this study determine the effect environmental and human factors have on thermal energy generator (TEG) performance in a variety of scenarios. A test method for assessing the performance of a TEG in a wearable form is detailed and demonstrated. The fabrication procedure of an energy harvesting device demonstrates a method of integrating rigid devices into a flexible substrate. The wearable device is used in a human trial which covered a series of activities in different environmental conditions. The results of these trials demonstrate the significant effect of movement, or convection, on thermal energy harvesting. Humidity levels do not have a significant correlation to power; however wet-bulb temperature must be taken into consideration due to the additional cooling effect of evaporation on temperature. While the amount of power generated varied between individuals,

the combined data sets match expected trends. The combined data quantifies how a wearable device will perform throughout daily activities for a group of individuals. This allows someone to define the operating scenario for a self-powered wearable device while choosing the most appropriate design for a particular application. It also sets a benchmark for exploring how textiles can enable the design of unique wearable devices which will lead to further investigation into quantifying the effect that the construction of a textile has on TEG performance as well as on consumer comfort.

# CHAPTER 4: Effects of Knit Parameters on Thermal Energy Harvesting

## 4.1 Overview

As efforts to improve wearable energy harvesting continue to focus on device and material performance, another area of optimization, the device's immediate environment, must be considered as well. Thermal energy harvesting from the human body relies heavily on temperature gradients and movement, but is also affected by how the device is worn. Textiles either aid or hinder energy harvesting efforts, so they must be characterized with regard to the complex human- textile- energy harvesting- environment microsystem. The aim of this work is to create a knit textile model with an integrated thermal energy harvester and to simulate how changes in the knit parameters influence energy harvesting. Finite-element simulations developed in this work are used to explore how convection changes the heat flux through both the textile and thermoelectric generator (TEG). We also identify which knit structure properties are able to improve thermal energy harvesting by modifying the environment immediately surrounding the TEG in the simulations. These simulations provide critical guidance for the integration of wearable technology with knit textiles. To validate the simulations, textile swatches were knit and characterized accordingly. The results of this work show how the stitch density has a significant effect on air permeability of the textile and corresponds to heat flow induced by convection. Heat flux through the system is highest when the textile has either an open-cell structure, a low stitch density, that promotes convection or a closed-cell structure, high stitch density, which promotes heat flux via conduction. This work is the base of

investigating other devices and textiles and their effects on the human body. The information from these simulations will guide both garment and electronic system design for wearable technology.

## 4.2 Introduction

Thermal properties of textile structures and electronic thermal management are active fields of research in both academia and industry. However, few studies have investigated the thermal relationship between electronic components and textiles. As the wearable technology market continues to grow [12], this relationship is becoming a crucial constituent to the market's advancement as many electronics generate heat during operation. This heat must be accounted for and either stored or dissipated in the textile so as not to disturb the thermal comfort of the user. Thermal comfort is a subjective parameter but can be considered the point at which heat produced in the body is equivalent to heat rejected by the body. [17] Another potential roadblock for wearable technology progress is the method used to power wearable devices. Because batteries are bulky, heavy, and unable to be washed, energy harvesting, also known as energy scavenging, is an ongoing area of interest. While the human body produces several sources of energy, e.g. heat and movement, [15] thermal energy harvesting shows the most promise for wearable technology due to the body's ability to consistently produce heat. Harvesting body heat via the thermoelectric (TE) effect or the pyroelectric effect is well documented [31], [34], [39] as is integrating TE devices into textiles [30], [112] and creating TE textile materials [55], [113].

The amount of heat generation from the body is related to metabolic activity, measured in METs, with the goal of maintaining a core temperature of ~ 37 °C. Metabolic heat generated from activity may be measured by oxygen uptake rate. The created energy is then released in several ways: i) metabolic heat transferred through the skin surface ii) heat of vaporization and convection from respiration and iii) external work. [9], [11] Metabolic rates range from 0.7 – 12 MET for an average adult with a skin surface area of 1.8 $m^2$ [11], [17] which equates to 40 – 700 $W/m^2$ based on activity level. Not all of this energy contributes to energy harvesting as approximately 7% is lost through respiration and even more is lost via external work efficiency [9].

When one dons a garment, heat flows from the body to the textile in the form of either conduction, evaporation or radiation. It is important to note that conduction is a simplified mechanism for convection within the microclimate, or the air gap between skin and textile. We assume the air gap between textile and skin act as a conductor rather than a convective area due to stagnate microclimate conditions [104], [114]. This assumption also holds true for the microclimate between the skin and TEG interface. When sweating, a garment absorbs the fluid and wicks it to the cloth-environment interface via capillary action. During exercise, this increase in evaporation becomes a significant form of heat loss from the body. Skin emissivity and radiative heat transfer are minor thermal losses when compared to the other methods of heat transfer [115]–[119].

This study corroborates thermal management research because the environment immediately surrounding the TEG surface is within the thermal and velocity convective boundary layers of the skin [120], [121]. The ambient conditions within these layers can be vastly different from

the universal environment. In order to improve energy harvesting efficiency, one must know the characteristics of the TEG's immediate surroundings. In the case of wearable harvesting, these surroundings include the garment, human body, and environment. Textile surfaces are particularly difficult to study due to the high factor of surface roughness at the top and bottom interfaces. The surface roughness strongly contributes to the type of flow occurring, as it induces turbulent flow [122]. Additionally, the device can disrupt the surface of the fabric. In the example of a TEG, the device can act as either a heat sink or source, which not only influences the shape and duration of the thermal boundary layer, but also disrupts the heat flow through the textile.

When heat flow through the TEG reaches 15 – 25 $mW/cm^2$, the person wearing the TEG may begin to feel a cooling sensation that can lead to discomfort. This approaches the maximum heat flow from the distal forearm, 30 $mW/cm^2$. [14] These values vary from person-to-person depending on the position of the TEG on the body, personal sensitivities to the environment, and the local thermal resistance of the body. The ideal energy harvesting conditions occur when heat flow into the textile (from the body via radiation and conduction) is equivalent (or slightly less than) to the heat flow leaving the TEG via convection. [24] In other words, the ideal scenario occurs when much of the heat flow from the body is directed to a TEG.

Herein, this work will demonstrate a model for evaluation of the heat transfer properties of a knit textile with regard to how the textile's structural and thermal properties affect thermal energy harvesting. We identify which knit properties improve thermal energy harvesting by modifying the environment immediately surrounding the TEG. Thus, we correlate convection coefficients to the desired heat flow range, i.e. in a cold climate; a textile structure with a lower

convection coefficient and higher thermal absorptivity moves the system to equilibrium. Likewise, in a warm climate, a knit structure with a high surface roughness (high convection coefficient and low thermal absorptivity) is necessary to promote heat flow away from the body. This modelling technique lays a foundation for studies with more complex circuitries in integrated wearable technology.

## 4.3 Experimental Procedures

### *4.3.1 Modeling and Simulation Parameters*

The entirety of the modeling and fluid simulations were completed in Solidworks2016. A schematic of the resistive network for the complex human-textile-TEG microclimate is shown in Figure 4.1b. The air gap at the skin and textile interface is considered a conductive area with no convection, as seen in previous literature [123], [124]. The skin and textile interfaces also show evaporative resistance that arises when sweat is present. For the modeling performed in this work, evaporative resistance and heat loss are not considered.

A single jersey knit stitch was drawn based on Non-Uniform Rational B-Spline (NURBS) curves as described in Puszkartz et al. [93], [97] and Kurbak et al. [84], [88], [90]. The stitch served as a pattern template for the jersey textile model. A cut extrusion through the center of the textile provided the space for modeling a TEG. The TEG is modeled as a bulk extrusion through the hole created in the previous step. Symmetry effects were accounted for by enabling periodicity in the X and Y computational domain directions.

The porous nature of textiles requires the need for determining effective thermal conductivity values based on the bulk thermal conductivity and the percent composition of each material. The effective thermal conductivity for the textiles was calculated using the following equation

$$k_{eff} = (1 - \varphi)k_a + \varphi k_p \quad (1)$$

where $\varphi$ is the percent composition of polymer, $k_p$ is the thermal conductivity of polymer, and $k_a$ is the thermal conductivity of air. The polymer chosen in this work was polyester. Individual thermal conductivities of the polyester and air, 0.04 and 0.025 W $m^{-1}$ $K^{-1}$ respectively, were acquired from literature. [93], [125] Thermal properties of the TEG block are defined in a similar way. Since the considered TEGs comprise of bismuth telluride legs, alumina headers, and air in the empty spaces, the thermal conductivity and specific heat follow the same ratio calculation as demonstrated in Eq. 1. According to Suarez et al [8] the ideal fill factor for an energy harvesting thermoelectric module is approximately 20%. Assuming a 20% fill factor, $k_{TEG}$ = 0.06056 W $m^{-1}$ $K^{-1}$ and specific heat, $c_p$ = 109.604 kJ $kg^{-1}$ $K^{-1}$ were determined.

The tightness of the knit is a key factor in its thermal and moisture management properties. The tightness factor of a knit follows [126]

$$TF = \sqrt{tex}/L \quad (2)$$

where L is the length of a single loop in cm and tex is the yarn count. Several knit models were created, each with a different tightness factor while assuming the same yarn. Knit models and their corresponding swatches of the loosest and tightest stitches, tightness factors of 1.79 (a compression garment) and 7.16 (a scarf or light sweater) respectively, are shown in Figure 4.1.

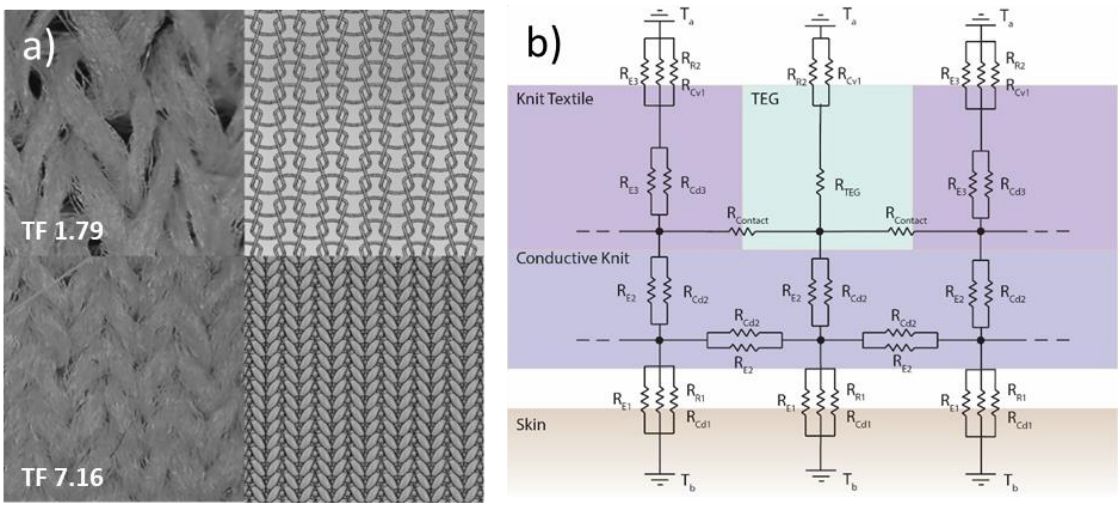


**Figure 4.1** a) Knit swatch (left) and CAD simulation (right) of samples with tightness factors of 1.79 and 7.16. b) Resistance network of human microclimate with integrated TEG and conductive heat spreading textile.

The Solidworks Flow Simulator was used to complete a heat transfer simulation at room temperature, 298 K, seen in Figure 4.2. Four simulations ran for each knit density, each with a different airflow velocity in the x-direction. Simulations were run for 0, 1, 2, and 3 m $s^{-1}$ airflows, which ranges from a stationary person to one running at a 7 min per mile pace. Both laminar and turbulent effects are accounted for and k-ε parameters are defined for the turbulent flow. The simulations' aim is to look at the effect of different environmental conditions on a textile system already in contact with the skin. Thus, the starting temperature of the solid geometries is set to 300 K. In addition, gravitational effects are taken into consideration and the gap between skin and textile is attributed with conduction, not convection.

It is important to note that the skin does not generate heat, but rather dissipates it. Accordingly, it would be erroneous to assign a heat generation or heat transfer rate to the skin geometry. Instead, the bottom surface of the skin geometry is assigned a heat flux equivalent to 1 MET,

58.2 W $m^{-2}$. This is representative of the body's thermoregulation system maintaining a core temperature of 37 °C while the person is at rest. To account for various thermal losses as heat travels from the core to epidermal skin, the skin geometry is assigned temperature-dependent thermal conductivity values from 180 – 600 $cm^2$ K $W^{-1}$ based on results reported by Leonov et al. [14]. It should be noted that the thermal resistance of soft tissue and skin varies significantly across individuals, body location, and skin moisture content so the results shown could vary with changes in skin thermal properties.

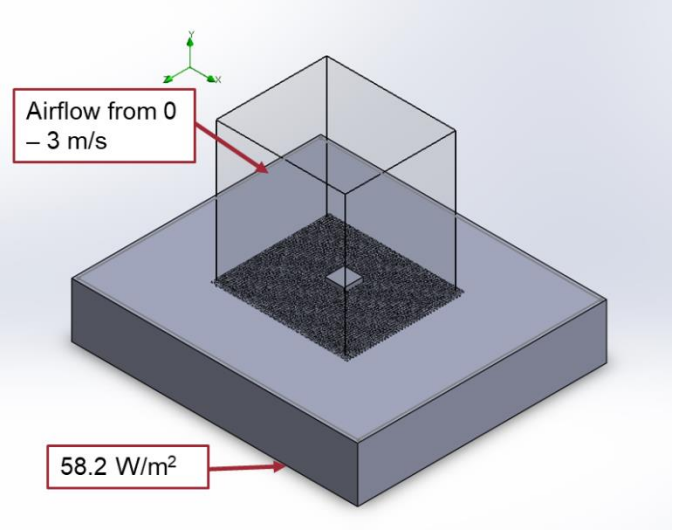


**Figure 4.2:** The boundary conditions and computational domain established in the Solidworks Flow Simulator

In addition to running simulations on TEGs integrated into knits with increasing stitch densities, a simulation of a single TEG on the body is performed without any surrounding textile. This accounts for a knit tightness factor of zero and gives the other results context for how the addition of a knit textile changes the heat flux away from the body. To reduce processing time, the mesh for each simulation was limited to < 5000 cells for each simulation.

### *4.3.2 Knit Sample Fabrication and Characterization*

A series of knit samples was created to verify the results of the simulations. Samples were knit on a 15 gauge Shima Seiki Mach 2XS Whole Garment knitting machine. Single jersey swatches were knit with stitch lengths ranging from 4 mm to 7 mm. The yarn, 35 denier Sapona, dictates this range because of the elastic content of the yarn. The yarn stretches significantly so care must be taken to ensure the yarn does not become tangled in the knitting needles. Two of the resulting swatches, seen in Figure 4.1a, show the top view of the loosest and tightest stitch densities. Samples cut from the swatches are used to characterize the textile thermal properties summarized in Table 4.1. The samples were tested for $Q_{max}$, thermal conductivity, and air permeability based on ASTM standards F1868-17, and D737-04.

Each knit sample underwent air permeability tests following ASTM D737-04 guidelines. Tests were performed in a laboratory setting with atmospheric temperature and relative humidity set to 21 ± 1 °C and 65 ± 2 %, respectively. Samples were clamped with a 1" diameter of the fabric exposed to airflow and an 8 mm orifice was used for the 6 and 7 mm stitch length samples while a 6 mm orifice was used for the 4 and 5 mm samples. Ten trials ran for each knit sample. The pressure differential was read from the manometer and converted to permeability units. The relationship of air permeability and knit tightness factor is demonstrated in Figure 4.3.

After air permeability tests, the samples were tested for thermal resistance on a sweating hot plate following ASTM F1868-17 guidelines. Samples were tested using the Kawabata Evaluation System Thermolabo instrument (KES-F7). The instrument consists of the following: a box with a thin copper heat capacitor inside, a water-cooled wet-box for a consistent base temperature, and an insulated hot plate in a box with temperature controls.

Each sample was weighed according to ASTM D3776 before determining thermal properties. The dry heat transport rate was found by placing each specimen on the guarded hot place at 35 °C and measuring the heat transfer through the material. The resulting thermal resistance values of each sample are seen in Table 4.1.

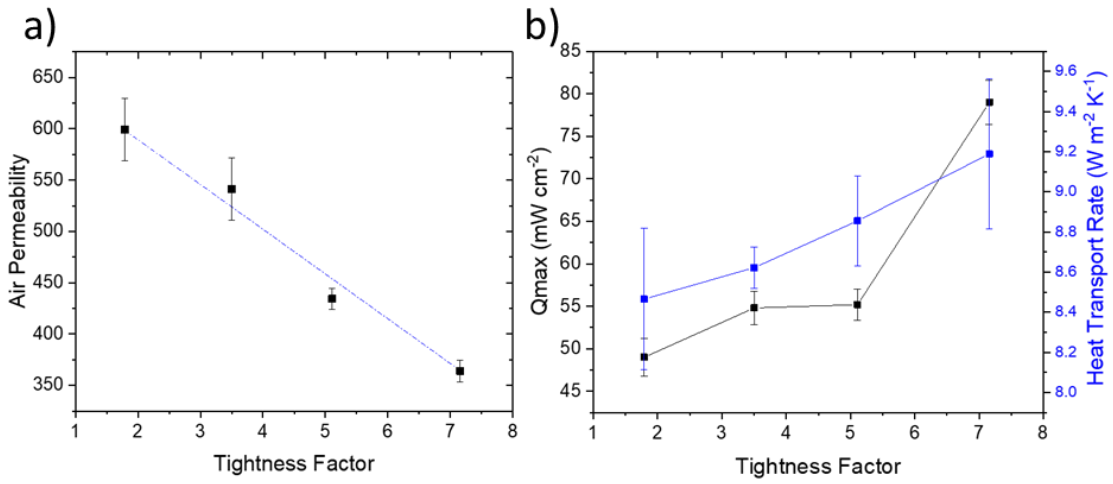


**Figure 4.3:** Results of textile characterization for various stitch densities. a) Air permeability has a negative correlation to tightness factor. b) The heat transport rate and $Q_{max}$ values have a positive correlation to tightness factor.

The $Q_{max}$ test was also performed on the Kawabata Evaluation System (KES-F7). This test characterizes the thermal feel of the fabric when initially touched. A larger $Q_{max}$ value indicates rapid heat transfer from the body to fabric, resulting in the fabric feeling cool. Swatches were conditioned in laboratory settings of 21 °C and 65% relative humidity for several days. The thermal transport value of the knit swatch peaked at 0.2 s after initial contact with the measurement system. The power consumption from the test plate heater indicates the amount of heat passing through the knit in W $m^{-2}$. Both the technical face and the technical back of the knit samples are tested five times and the average of the sample is reported in Table 4.1.

**Table 4.1** Textile characterization for jersey knits of varying tightness factor according to ASTM standards

| Tightness Factor | Air Permeability [$ft^3/(min/ft^2)$] | Thermal Resistance [$m^2$ K/W] | Qmax [$mW/cm^2$] |
|---|---|---|---|
| ***1.79*** | 599.2 ± 30.4 | 0.118 ± 0.005 | 49.0 ± 2.2 |
| ***3.5*** | 541.4 ± 30.2 | 0.116 ± 0.001 | 54.8 ± 1.9 |
| ***5.11*** | 434.4 ± 10.3 | 0.113 ± 0.003 | 55.2 ± 1.8 |
| ***7.16*** | 363.9 ± 10.5 | 0.109 ± 0.004 | 79.0 ± 2.6 |

## 4.4 Model Results

The results of the jersey knit simulation confirm expected fluid behavior. Heat transfer next to the knit surface is increased due to a higher convection coefficient. This convection coefficient increases with increasing wind speed and with knit tightness. This is due to an increase in surface roughness per unit area, for as knit density increases the amount of rough yarn in a given area also increases. However, as the velocity of airflow increases, the turbulent intensity decreases and the thermal boundary layer thickness decreases.

We see the TEG is responsible for the majority of heat flux normal to the heat source. However, no clear trend is seen in the surface heat flux values seen in Figure 4.4d. Rather, the overall heat flux from the textile and TEG surfaces confirms the hypothesized trend. A loose stitch density promotes high heat transfer through the fabric due to high porosity in the knit structure. The tightest stitch density also promotes increased heat transfer through the fabric due to the increased fill factor of the yarn. The lowest heat flux values are attributed to the textile with a tightness factor of 3.5. While the heat flux from the TEG surface is similar to that of other tightness factors, the convection induced by fabric porosity decreased with the decrease in porosity. Additionally, the yarn fill factor is not high enough to encourage heat flow via conduction to compensate for the loss in convection.

The contact resistance between the sides of the TEG and the fabric were expected to reduce the heat flux through the TEG due to lateral heat transfer from the TEG to the knit. This phenomenon is observed as the tightness factor increases. However, as tightness factor increases past 3.5, the lateral heat loss remains steady. We attribute this to the changing geometry of the textile. When the stitch density increases, the thickness of the textile decreases so the overall contact surface area between textile and TEG remains constant.

## 4.5 Discussion

While the heat flux away from the TEG surface did not follow the expected trend, investigations into other thermal properties showed interesting results. The results of the knit sample characterization tests, shown in Figure 4.2, follow expected trends with the density of the knit. As the tightness factor increases, the space between stitches increases as well. Therefore, air permeability is observed to be the highest at low tightness factor values where the textile has large air gaps. The size of these air gaps decreases linearly with increasing stitch density (tightness factor), resulting in near linear decrease in air permeability. Similarly, the thermal resistance of the samples decreases with increasing stitch density. This is expected as the as the ratio of air to polymer yarn decreases with an increasing tightness factor. As such, the $Q_{max}$ value has a positive correlation to tightness factor. Likewise, the increase in yarn volume lowers the thermal resistance of the sample, which can lead to increased heat flow from the body to the textile upon initial contact. Based on these results, we expect to see a parabolic relationship of energy harvested to knit density in later studies.

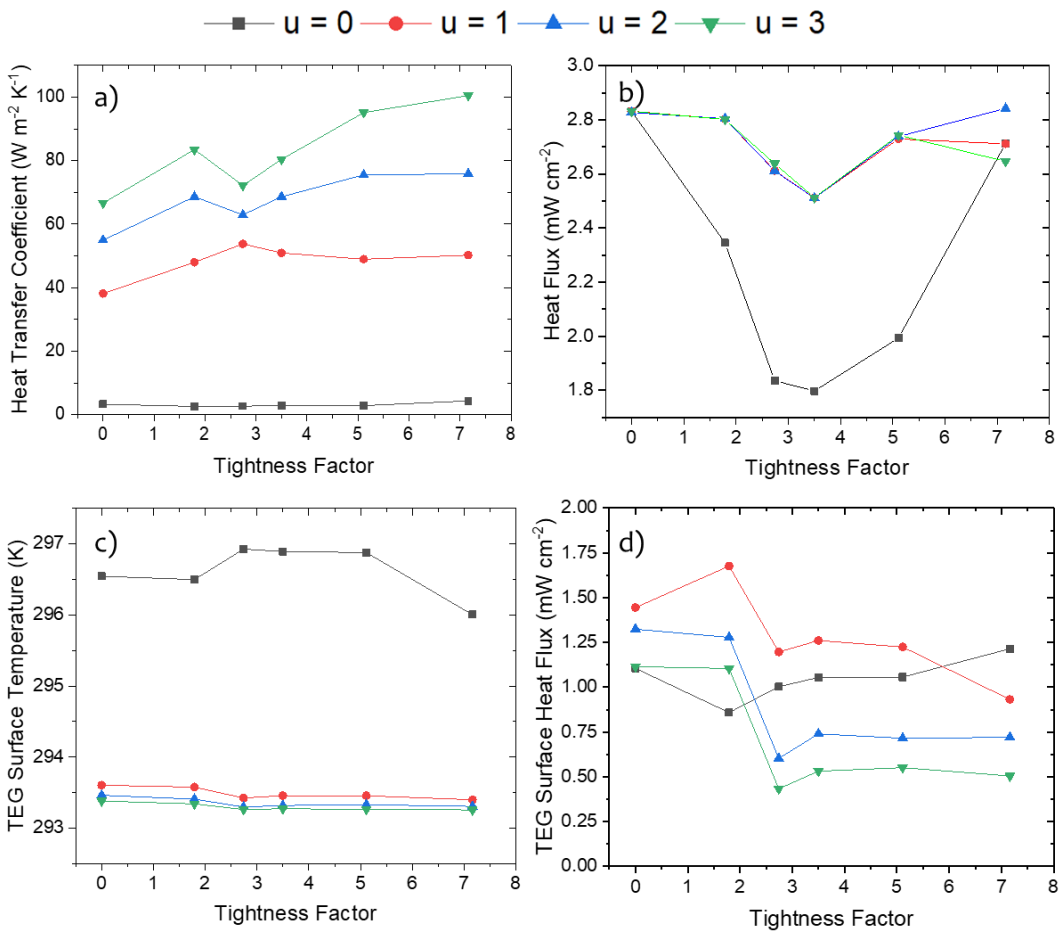


**Figure 4.4:** Simulation results for a range of knit tightness with increasing airflow velocities (u) from 0 to 3 m/s. a) Heat transfer coefficient as measured from the surface of the TEG. b) Heat flux away from the body as measured from the surfaces of the knit and TEG. c) Surface temperature of the TEG. d) Heat flux rejected from the surface of the TEG.

The heat transport rate, found in the thermal resistance test, increases with the tightness factor. While polyester yarn is a poor thermal conductor, its thermal conductivity is still higher than that of air. This results in better conductive heat transport through the fabric, when the stitch density is higher, i.e. there is more yarn to promote conduction. This trend confirms the heat flux results from the simulations for the upper tightness factors. The simulations also show increased heat flux at the lower stitch densities. The thermal resistance test does not include

convection as it only characterizes the textile itself. The overall heat flux increases because the looser stitches result in better convective heat transport through the fabric as confirmed in the air permeability characterization.

The addition of convection drastically lowers the TEG surface temperature, which was expected based on the results discussed in Myers et al. [46] where the introduction of movement had a significant effect on power generation and ambient temperature showed minor effects. Increases in airflow speed continued to lower the surface temperature, but the decrease was insignificant. Figure 4.3d demonstrates the overall effect of the knit structure on the heat flux through the TEG. The presence of a textile with low stitch density increases the surface heat flux from the TEG. We attribute this to improved convective heat transport at low tightness factors, which also introduce turbulence into the flow. As the tightness of the knit increases, conduction becomes the dominant method of heat transport through the fabric so the knit's effect on the TEG heat flux lessens. The heat flux also decreases because the contact resistance between textile and TEG decreases causing some heat flow to be directed laterally.

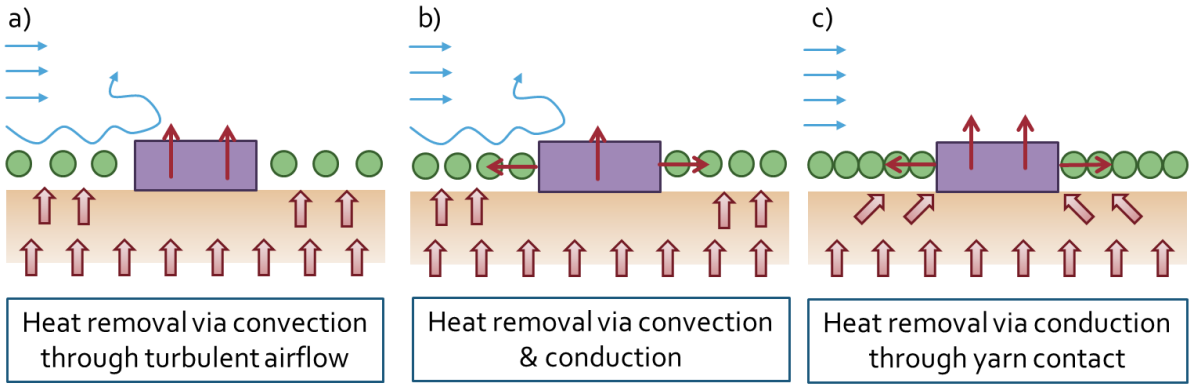


**Figure 4.5:** Schematics of the three heat flux scenarios that result from changes in tightness factor from loosest (a) to tightest (c)

The best way to compare the heat flux scenarios is through visual aid, Figure 4.5. Gaps in the textile layer permit heat to flow away from the body without disturbance. The gaps also induce turbulent airflow immediately next to the textile surface, which aids in heat removal. As the stitch density increases, the gaps in the textile layer decrease in size, blocking the heat flow through the knit. As a result, the heat is directed towards the TEG increasing the heat flux through the TEG, theoretically leading to increased power generation. However, the high stitch density introduces a contact resistance between the TEG and surrounding textile and between loops of yarn. Some heat flow through the TEG is lost to the textile due to this contact, but not enough to significantly influence the power generation. A combination of convection and conduction heat flows, Figure 4.5b, result when the textile is tight enough to contact the TEG but loose enough to have air gaps between the stitches. As seen in Figure 4.4b, the most of the heat is removed without passing through the TEG. Thus, when considering electronic devices integrated into knit textiles, the textile structure should be considered as it changes heat flow through the microclimate and affects thermal comfort.

## 4.6 Conclusion

In summary, we created a simulation for an integrated TEG in a knit textile and confirmed its results using thermal characterization methods on textile swatches with varying stitch density. This work demonstrates the effect of some knit parameters, namely stitch length, on the heat flux through a wearable TEG. The tightness factor, controlled by stitch length, changes both convective and conductive heat flow through the textile and, as such, changes the heat flow through the TEG. While some TEG heat flux is redirected laterally when stitch density

increases, the $Q_{max}$ and heat transport coefficient of the textile improve cooling at the skin level. These results lay a foundation not only for detailed textile modelling, but also for multi-faceted modelling that includes electronics, materials, fluids, and the human thermoregulatory responses. Additional textile details such as yarn filament, yarn twist, and knit stitch type will add a new level of understanding in how garments are designed and how electronics and other devices can be integrated into textiles. Other details, such as heat generating devices, resistors, sensors, and other electronics will increase our ability to design advanced wearable technologies that are discreet and comfortable to wear. As such, this model of a textile-integrated TEG provides a starting point from which modelling wearable technology on the human body can advance.

# CHAPTER 5: Thermal Energy Harvesting Body Map and On-Body Characterization

## 5.1 Overview

To improve thermal energy harvesting from the body, a complex set of microclimates, components, and functions must be considered in relation to each other. While much literature on energy harvesting improvements highlights the importance of device and material optimization, little focus has been geared towards improving the system as a whole. The objective of this work is to integrate thermal energy harvesters into a knit textile and to generate a map of locations and scenarios for thermal energy harvesting on the body. Previous results, discussed in Chapters 3 and 4, led the design of a knitted shirt with structured stitches that promote energy harvesting. The fabrication procedure of a thermal energy-harvesting shirt demonstrates a method of integrating rigid components into a conformal substrate. The shirt is used in a human trial, which covered a series of activities in different environmental conditions. The preliminary results of these trials show areas for detailed analysis and for future studies. Challenges encountered during the study identify what improvements must be made to acquire conclusive data and the study will be performed a second time to address these issues. As wearable technology advances, this work can be referenced as a foundation for investigating textile design based on human factors and device functionality.

## 5.2 INTRODUCTION

The onset of wearable technology innovation and, recently, large public acceptance of smart wearable devices is providing new opportunities for improving quality of life. Rapid improvements in sensing capabilities signal processing techniques and wireless communication options mean that product developers have an ever-expanding marketplace. Wearable technology is also projected toward health monitoring due to the necessity of continuous monitoring of chronic illnesses. Limiting this advancement is that current devices are still large, bulky and intrusive to the user's everyday life in part due to the large battery or periodic need for battery recharging necessary for continuous monitoring at high sensor duty cycles. The power management of wearables devices are overall viewed as a strategic drawback toward marketability and longevity of use by the user. [127]

Energy harvesting from the human body facilitates innovation in wearable devices and smart textiles. As demand for smarter devices and textiles increases, so does the demand for effective power supply and management for these systems. Conventional sources of power, such as batteries and capacitors, are inconvenient to the user in that they are heavy, require frequent charging, and have a large footprint relative to other electronics. Thus, investigations into energy harvesting from the human body via numerous methods are necessary. Thermoelectric (TE) materials and devices have the potential to resolve the demand for lightweight and convenient sources of power.

Thermoelectricity is a phenomena well documented in literature. Improving the efficiency of a TE device is the focus of much of the current research. Researchers aim to do this by improving the ZT of the material, decreasing interstitial resistance losses, or adding heat-

spreading materials to one or both sides of the TE device. Additionally, most TE improvements are demonstrated on a wearable platform, typically a watch or wristband, to highlight their suitability in wearable applications. However, most of these devices are rigid and non-conformal to the human body, which not only decreases TE efficiency but also can cause some discomfort depending on the application. Other efforts to create flexible TEGs rely on non-porous substrates such as Kapton® or polydimethylsiloxane (PDMS) to provide flexibility, but these substrates are not breathable and could cause discomfort when worn.

Only recently has more attention been shifted towards developing textile-based or textile-integrated wearable TE devices. Leonov et al. demonstrated an assembly of TE generators (TEGs) integrated into a shirt. Myers et al. showed a series of TEGs in a headband and armband. Kim et al. printed TE materials onto polyester-based fabric. Outside of printing TE materials onto a film or textile, others coat the textile fibers, yarns, or fabric with TE materials or polymers. While this technology is still in its infancy, it shows promise for wearable applications as the TE coated textiles retain breathability and flexibility.

As critical as device optimization is for realizing TE powered wearable devices, one must also consider the device surroundings when improving TEG efficiency. This is partially addressed by adding a heat spreader and heat sink to the bottom and top surfaces of the TEG, but other factors such as integration method, textile surroundings, and body location must be considered. The effects of these factors vary with activity and environment, so one must consider the range of dynamic activities and environments the wearable device will encounter.

## 5.3 METHODOLOGY

### *5.3.1 Shirt Design and Fabrication*

The human trial study followed the procedure outlined in Myers et al. [46] and 10 subjects were recruited to participate. Each participant wore a knit shirt with five TEGs integrated at the following locations: the front of the bust line, the wrist, under the arm, on top of the shoulder, and the center of the back. Locations were chosen based on average thermal resistance or temperature of the skin [8], [31] and the range of environmental variables the TEG would be exposed to i.e. more motion on the wrist due to arm movement and increased skin temperature under the arm.

The information from previous experiments, covered in Chapter 3, guides the knit design of the shirt. To reduce knitting production errors, only jersey and rib, structures are used in the design. Thermal properties of the knit structures were investigated and the results are described in Chapter 4. Accordingly, the sleeves of the shirt are constructed with a 1x1-rib knit that provides more insulation surrounding the TEG and supplies increased mechanical support via compression. The knit structure of the shirt is designed in Apex3 software, seen in Figure 5.1a, and knit on a 15G Shima Seiki Mach 2XS Whole Garment machine. The shirt is knit with 3 ends of 70 den. Sapona yarn. Sapona yarn is a multifilament polyester yarn with a spandex core. Following knitting, the shirt is steamed and heat pressed.

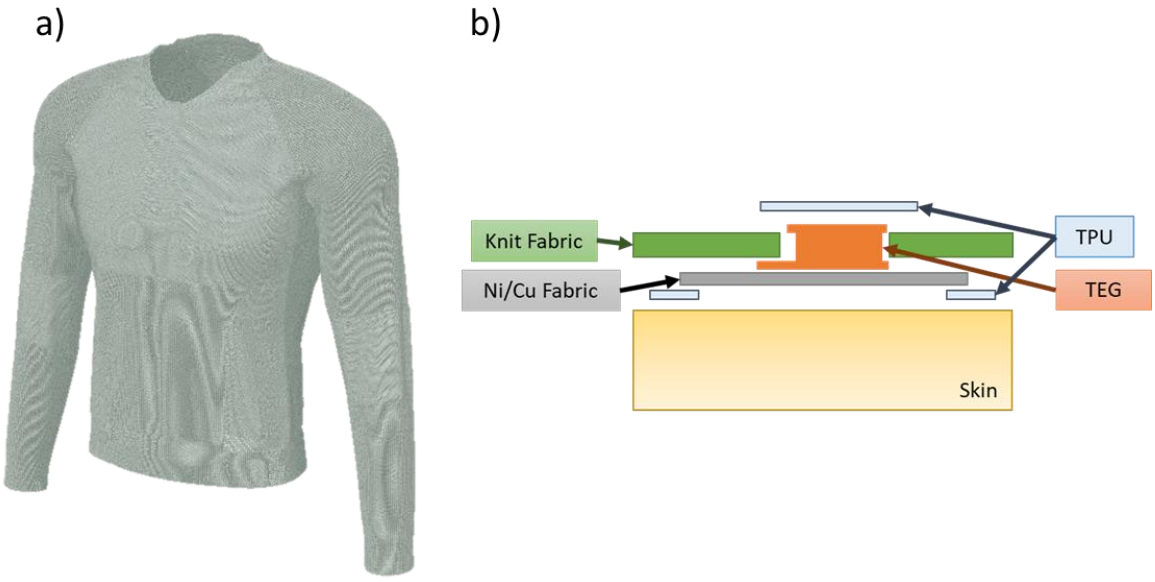


**Figure 5.1** a) A rendering of the knit shirt design with two knit structures, 1x1 rib and jersey. b) Profile view of TEG integration into the shirt with materials used.

Then, a TEG (Laird OT20, 30, F2A, 0610, 11, EP, W2.25) is integrated into the knit so that the body serves as the heat source and heat flux is normal to the skin. Five 5 x 9 mm holes are cut in the shirt using a laser cutter to accommodate each TEG at the specified sites. Nickel/Copper coated fabric serves as a heat spreader for each TEG. The fabric is cut into 10 x 19 mm rectangles and adhered to the inside of each TEG hole by hot pressing thermoplastic polyurethane (TPU) mesh (Bemis BFF 3914) over the edge of the heat spreader. A final layer of the TPU mesh is laminated over the top of the integrated TEG to secure the device to the shirt. Figure 5.1b shows a cross section of this integration technique.

### *5.3.2 Energy Harvesting Measurement System Design*

An energy harvesting measurement system (EHMS) resides next to each TEG, the block diagram of which is seen in Figure 5.2. Each circuit board records the open circuit voltage of

the TEG and has a temperature sensor and accelerometer that record temperature, ambient pressure, humidity, and acceleration in the X, Y, and Z directions. This gives an accurate description of the environmental conditions exposed to each TEG.

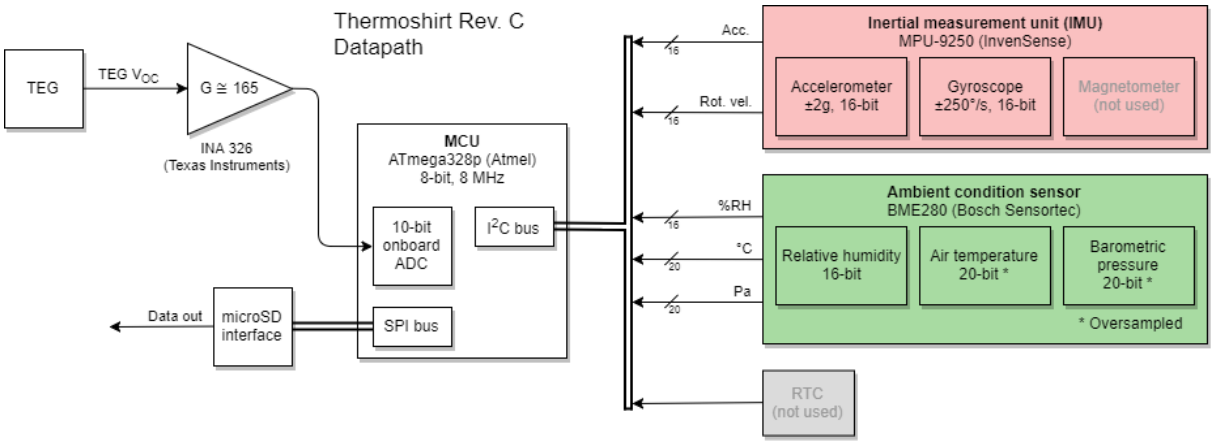


**Figure 5.2** Block diagram for the EHMS.

In this experiment, the predicted maximum power output of the thermoelectric device being measured under a given set of operating conditions is derived from the open-circuit voltage across the two device leads. Due to the size of the TEGs themselves, and the relatively low thermal gradient across them, the voltage being measured is quite small, approximately 10 to 20 mV during saturation. As such, the TEG leads are connected to the inputs of an instrumentation amplifier (INA326, Texas Instruments) to sample and amplify the generated voltage between the two leads, while presenting the TEG with a very high input impedance. This instrumentation amplifier has adjustable gain, which is set by varying the resistance between two of the amplifier's pins in conjunction with a fixed resistor and capacitor between a third pin and system ground. This was done using a mechanical linear potentiometer

wired in a rheostat (variable resistance) configuration, connected to a test point on either side to facilitate resistance measurement. The final amplified output signal, prior to measurement by the microcontroller's onboard ADC, was routed through a passive RC low-pass filter with a cutoff frequency of approximately 1.33 KHz to reduce any transient noise.

An 8-bit, AVR-family microcontroller (ATmega328p, Atmel) forms the heart of the EHMS. This microcontroller handles both system data buses - $I^2C$, which connects all the peripheral sensors, and SPI, where data logs to the SD card are made. Further, the microcontroller's onboard 10-bit ADC and internal 3.3 V reference voltage is used to read the filtered amplifier output, rather than a discrete ADC elsewhere on the board.

The system clock signal is generated by an 8 MHz ceramic resonator. The ATmega328p is rated for use up to a supply voltage of 5 V, but at 3.3 V the maximum specified clock frequency is between 8 and 10 MHz. As a result, this choice of microcontroller and operating voltage places an inherent limit on the maximum operating speed of the system, which proved to be a limiting factor for the overall data acquisition rate. Ultimately, the polling rate for the full suite of sensors (including writing the collected data to the SD card) ended up being slightly faster than 30 Hz.

The main system voltage is set at 3.3 V, allowing for reduced power consumption and direct compatibility with the peripheral sensors chosen for inclusion in the final system. While this could have been accomplished in a 5 V system using several level-shifters, this ultimately proved to be far too bulky for the size constraints of the system, regardless of whether dedicated shifting ICs or discrete transistors were used for this purpose. Perhaps most importantly, 3.3

V operation allowed for the direct use of a LiPO battery for primary system power, using only a linear LDO regulator in lieu of a more complex switching supply

For this system, two identical 3.3 V linear regulators (MIC5219, Microchip) are used to condition the voltage supplied by the battery, prior to this voltage being passed to the nearly solid power plane running throughout most of one of the interior layers of the EHMS. Based on the expected achievable output current of the regulator selected for use, a second regulator was added to supply the SD card interface, while the primary regulator supplies the rest of the board. Once assembled, the tested device current was approximately 12 mA idle/quiescent with no firmware loaded, and approximately 25 mA while actively recording based on the firmware version used during all of the human trials. Note that while these were not used in any of the existing firmware variants, the microcontroller used has several low-power features available for use. It is likely that with additional firmware modifications, this current consumption could likely be reduced to some extent. These power-saving strategies entail the possibility of a reduced maximum sampling rate, so these were not incorporated into the original firmware design due to the already relatively low current consumption of the device.

The power management system for the board includes decoupling capacitors throughout. Almost all decoupling capacitors were placed on the opposite side of the PCB from their associated components, both to allow for ease of reflow soldering and because this configuration is reportedly a more efficient decoupling strategy when power planes are also used. As part of the onboard power management system, an included Micro-USB port and LiPO battery charge controller IC (MCP73831, Microchip) allows for in-system charging of the LiPO batteries used to power the system during data collection.

In addition to measurement of the voltage generated by the TEG, additional peripheral sensors were used to track other environmental and activity-related variables. In a single measurement cycle, the microcontroller runs an ADC measurement, and then polls each of these peripheral sensors for the desired output data, which is digitally encoded by each sensor's internal hardware, allowing for all of these subsystems to share an $I^2C$ bus for data transfer.

Ambient environmental conditions, percent relative humidity, barometric pressure, and ambient temperature, were all recorded with a single integrated IC (BME280, Bosch Sensortec). Care was taken to ensure that the portion of the EHMS on which this sensor was mounted was not separated from the surrounding air by either the device enclosure or other obstacles. This component was deliberately facing away from the wearer's body, to maximize airflow and to minimize parasitic heat transfer from the body ensuring the most accurate results possible. Humidity, pressure, and temperature were measured and reported to the microcontroller with 16-, 20-, and 20-bit precision, respectively. Units for these values are percent relative humidity, pascals, and degrees Centigrade, respectively.

Activity of the wearer was estimated using linear and rotational acceleration measurements performed by an inertial measurement unit ("IMU") IC (MPU-9250, Invensense). Both of these values were measured by the onboard accelerometers and gyroscopes for the X, Y, and Z-axes, both with 16-bit precision and with units of mg (1/1000 of one g) and degrees per second, and ranges of ±2g and ±250°/s, respectively.

A standard micro-SD card interface, connected to the microcontroller over an SPI bus, served as the main data storage location for the system. This had the advantage of providing a straightforward interface for data logging from the microcontroller, as well as an easy method

for exporting this collected data from the board at the end of a trial. The disadvantage to this method was the comparatively large footprint of the SD card receptacle, which represented the largest single component on an already space-constrained layout.

A large (10 MΩ) shunt resistor was placed between the non-inverting input of the amplifier and system ground, in order to provide an input bias current return path. Both inputs of the instrumentation amplifier generate a small, but nonzero, input bias current. Because the TEG is only connected to the rest of the circuit through these inputs and not to system ground, unless a path to ground is provided, these currents will result in floating or saturation of the amplifier output level, preventing accurate reproduction of the scaled input signal. This extra resistor was added to provide the required bias current return path, and a large value was chosen to minimize the parasitic effect this has on the amplifier's measured input voltage difference, while still allowing for appropriate discharge response in the event of saturation. While this appears to have largely achieved the intended result, based on the recorded data, there were still a few instances of brief saturation of the amplifier output signal that were observed during a few of the trials.

The EHMS and battery were housed by a three-piece protective enclosure, Figure 5.3b, designed to fit the profile of the board itself to minimize interference with the wearer. The EHMS and battery both fit into a base component, and a second lid piece fits over the EHMS to secure the electronics in place. The battery is placed into its housing, which is tilted to reduce the overall on-body contact area, and secured with a second lid, at which point the battery leads are passed around the device and secured to the board's power connector. Inclusion of cutouts in the enclosure where appropriate allows for insertion and

removal of the SD card, TEG leads, and battery, as well as limited testing of on-device parameters (gain resistance, etc.) without removing the device from its enclosure. A series of attachment loops, located around the perimeter of the enclosure, allowed for attachment to the underlying garment using ordinary fabric stitching. All of the custom enclosure parts were fabricated using a resin SLA printer (Formlabs Form 2) using engineering-grade "tough" resin.

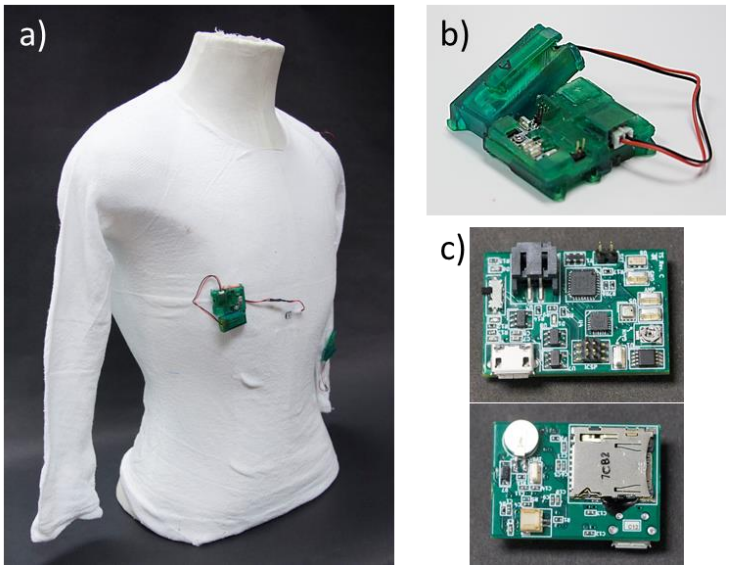


**Figure 5.3** a) The knit shirt on a mannequin showing the location of the TEG and corresponding circuit board and case for the torso location. b) The EHMS case. c) Top and bottom views of the EHMS.

### *5.3.3 Trial Procedures and Participants*

Three adult male participants weighing between 68 – 90 kg and four adult female participants weighing between 45 - 68 kg volunteered for the study. The volunteers completed an initial survey to assess their perceived level of fitness ranging from 'poor' to 'great'. Physiological data was also reported to better assess potential variables in the energy harvesting data.

Participants were asked to wear the energy-harvesting shirt while performing a series of activities: (i) running/jogging outdoors (ii) walking outdoors (iii) working or sitting indoors. Each activity was done for 10 – 15 min and each TEG on the shirt was sending data to their respective EHMS simultaneously. Each shirt, with EHMS removed, was hand washed after use in the trial.

Prior to each trial, the gain-setting resistance for each board was measured (and adjusted as necessary) to allow for derivation of the gain and subsequent conversion of the recorded results into the actual measured output voltage. During the trials, the nominal gain was set at approximately 165x, with board-to-board variation between 163x and 169x considered acceptable. Comparison of measurements between trials suggests that this mechanical component was not overly susceptible to change due to motion or vibration (which could possibly generate inaccuracies in the derived TEG voltage), and the PCB enclosure was designed to help minimize the risk of accidental contact with the potentiometer. That said, one development goal for future versions of the device would be the use of a digital potentiometer IC (such as the AD5272 from Analog Devices), controlled by the microcontroller over one of the existing digital buses on the board, in lieu of a mechanical potentiometer. This would realize three improvements to the current design: firstly, the device gain would be made even more immune to external interference; secondly, gain readback could be accomplished automatically and stored in the trial log, reducing system preparation time for future trials; and finally, the gain could be actively scaled during the trial, to allow for improved measurement resolution over a wider scale of voltage levels..

**Table 5.1:** Volunteer responses to physiological survey. Level of fitness is self-professed ranging from poor, average, good, and great**.**

| | ***Gender*** | ***Height [cm]*** | ***Weight Range [kg]*** | ***Level of Fitness*** |
|---|---|---|---|---|
| 1 | M | 175.26 | 68 – 80 | Good |
| 2 | F | 167.64 | 56 – 68 | Average |
| 3 | F | 160.02 | 56 – 68 | Average |
| 4 | M | 193.04 | 80 – 90 | Good |
| 5 | F | 162.56 | 56 – 68 | Great |
| 6 | M | 170.18 | 68 – 80 | Good |
| 7 | F | 149.86 | 45 - 56 | Average |

## 5.4 RESULTS

The results of the trial enabled a study of some physiological effects on thermal energy harvesting. Each participant donned the shirt as a base layer, seen in Figure 5.4d; women wore a sports bra underneath. The spandex content in the yarn resulted in a ‘one-size-fits-all’ shirt so each shirt was the same size, but fit each participant differently. In other words, the contact between skin and TEG varies due to how the shirt stretches over different body types. Trials began with participants jumping and then assuming a ‘T’ position to calibrate the accelerometers. Following this, each volunteer walked outside for 15 min, ran outside for 15 min, and then rested inside for 15 min. This activity order results in a high skin temperature during the resting period, which increases the power generated, as seen in Figure 5.4a.

The results from the walking and running portions of the trial are summarized in Figure 5.4b and Figure 5.4c respectively. This can likely be attributed to similar sweat or skin temperature responses to ambient temperature and humidity and will be investigated in detail in following experiments.

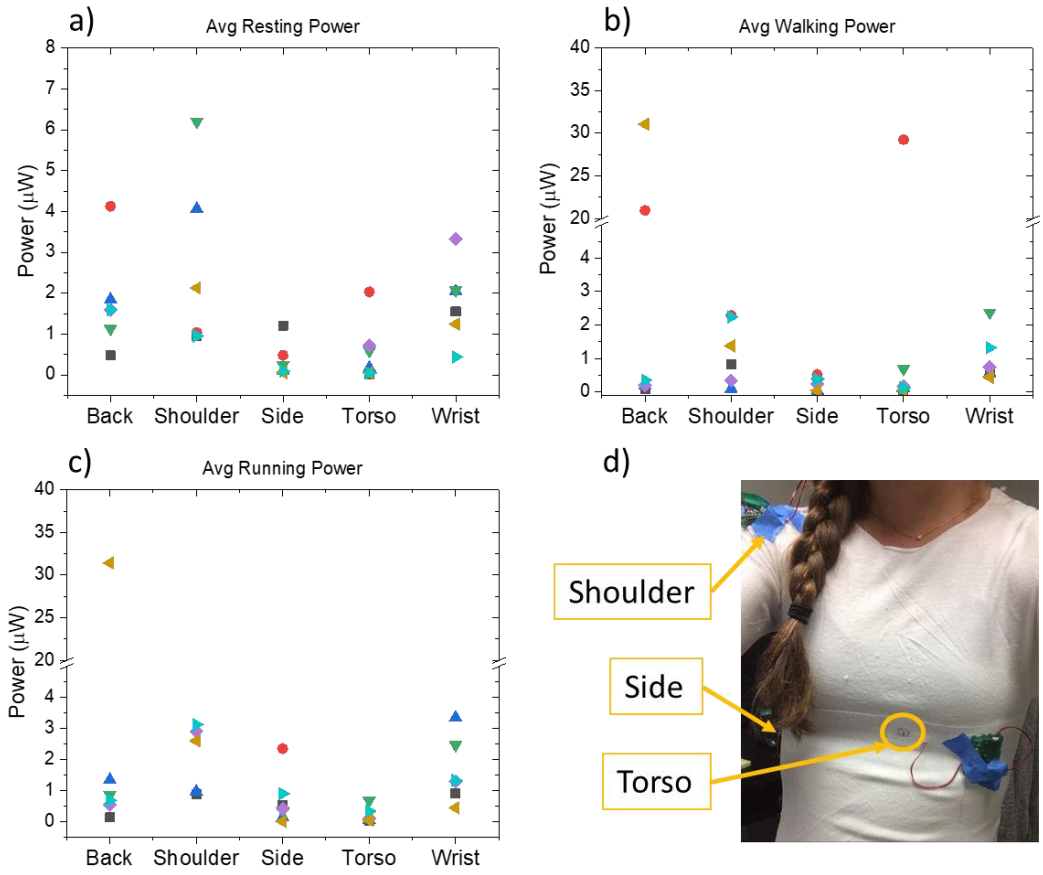


**Figure 5.4** a) Average power generated from each location on every participant while the participant was resting. b) Average power generated from each location while participants walked. c) Average power generated from each TEG location while participants ran. d) Participant wearing the fully assembled shirt (Wrist and Back locations not shown).

## 5.5 Discussion

### *5.5.1 Movement Analysis*

The accelerometer data is recorded for the X, Y, and Z directions at each TEG location. Due to uncertainty errors in deriving velocity from accelerometer data, the data was normalized and described as a movement intensity ratio. To do this, the values in each direction were averaged and the average from the whole dataset was subtracted to account for the effect of gravity in

each location and direction. The absolute value of these data points was then converted from mg's to g's. The magnitude of the accelerometer vector was calculated from the three directions. Finally, we took the absolute value of the change in accelerometer values for each of the data points. The resulting number demonstrates an average-adjusted acceleration vector that describes movement in terms of an intensity ratio where zero is stagnant and one is critical acceleration.

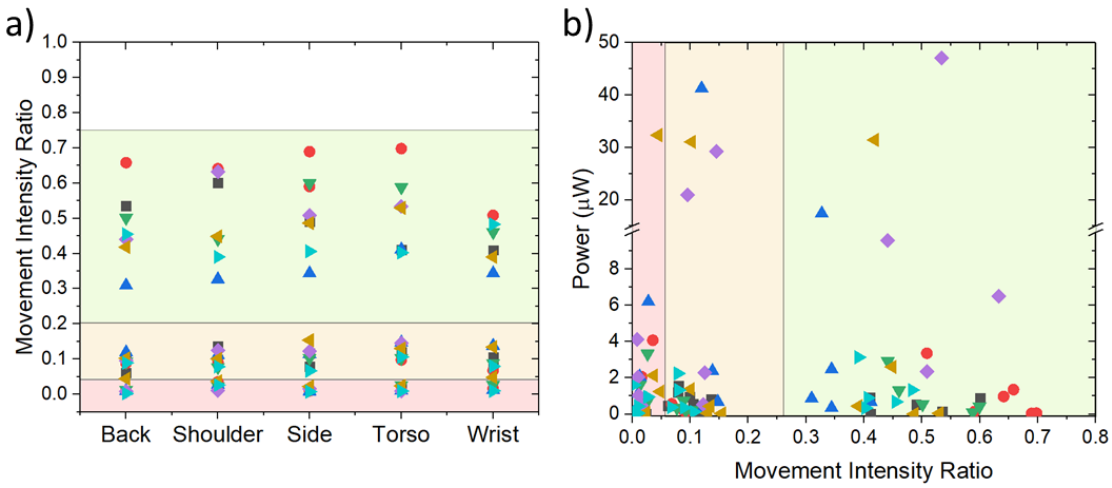


**Figure 5.5** a) Movement intensity ratio as calculated for each location on the body. Three distinct clusters representing resting, walking, and running are seen and represented by red, yellow, and green shading respectively. b) Average power generation as a function of the movement intensity ratio. Shading is transferred from values in (a).

The resulting intensity ratio values are seen in Figure 5.5a. The background shading is representative of the prescribed activity where red, yellow, and green correspond to resting, walking, and running respectively. Little to no movement is seen during resting for each body location. While walking, there is some, but not a significant amount of, variation in movement intensity based on both body location and participant. The differences in movement intensity

while running correspond to the speed at which the participant ran. While the wrist movement was expected to be higher than other locations due to arm swinging, it was not subjected to the same impact vibrations that the locations on the trunk of the body was. The remaining locations are relatively consistent in intensity.

The average power generated from each location as compared to movement is shown in Figure 5.5b. The high power values during resting, the last activity performed, are from increased skin temperature from running. Should the resting activity start the trial procedure, the average power values would likely decrease. Power values above 20 μW are outliers caused by data interruptions or signal saturation during the trial and the author does not consider these values accurate.

### *5.5.2 Temperature Analysis*

The amount of power a TEG produces depends on the temperature difference across the hot and cold sides of the device. The EHMS was designed with a sensor to monitor ambient temperature, humidity, and pressure. Because of the small distance between sensing unit and the human body and the order of completed activities, the recorded data was likely affected by increased body temperature from the activities. This is highlighted in Figure 5.6d and Figure 5.6e where many of the reported power values reside on the higher end of the temperature spectrum while resting, the final activity, and the values are on the lower end of the temperature spectrum while walking, the first activity. While we expect to see a negative correlation between power generation and ambient temperature, seen in Figure 5.6f, the average power values from the trial only show a slight decrease, if any, with increased temperature.

### *5.5.3 Physiological Analysis*

The average power values from each volunteer are compared to their respective body mass index (BMI) values, seen in Figure 5.6a, Figure 5.6b, and Figure 5.6c. The BMI values are found from the participants' height and approximate weight and every participant falls into the normal category as defined by the National Institute of Health [128]. While walking, the effect of BMI on the power generated is not significant, but there is a notable difference in power generation related to BMI while the volunteers were resting or running. This indicates that a person's level of fitness has some effect on thermal energy harvesting, the extent of which will be explored in a later study.

### *5.5.4 Body Mapping*

The main goal of the trial was to compare thermal energy harvesting over body area. The center of the chest, center of the back, top of the shoulder, on the side of the chest under the arm, and the wrist are the locations studied in this trial. The most straightforward comparison of each location occurs while the participants rest, since no external factors, i.e. wind or humidity, are at play. Figure 5.6a shows the average power generated from each participant at each location during the resting activity. Interestingly, the shoulder location consistently showed the largest average power across all participants. A possible explanation for this is the combination of good exposure to the ambient environment, good skin contact, and proximity to the neck, which houses major blood vessels. The power generated at the back and wrist locations is comparable while resting, and the torso and side-body locations are the worst locations for thermal energy harvesting.

Walking and running activities, Figure 5.6b and Figure 5.6c, show a similar location trend to the resting activity. The shoulder and wrist have the highest average power generated. Areas on the trunk of the body, the back, torso, and side, appear to be poor locations for thermal energy harvesting.

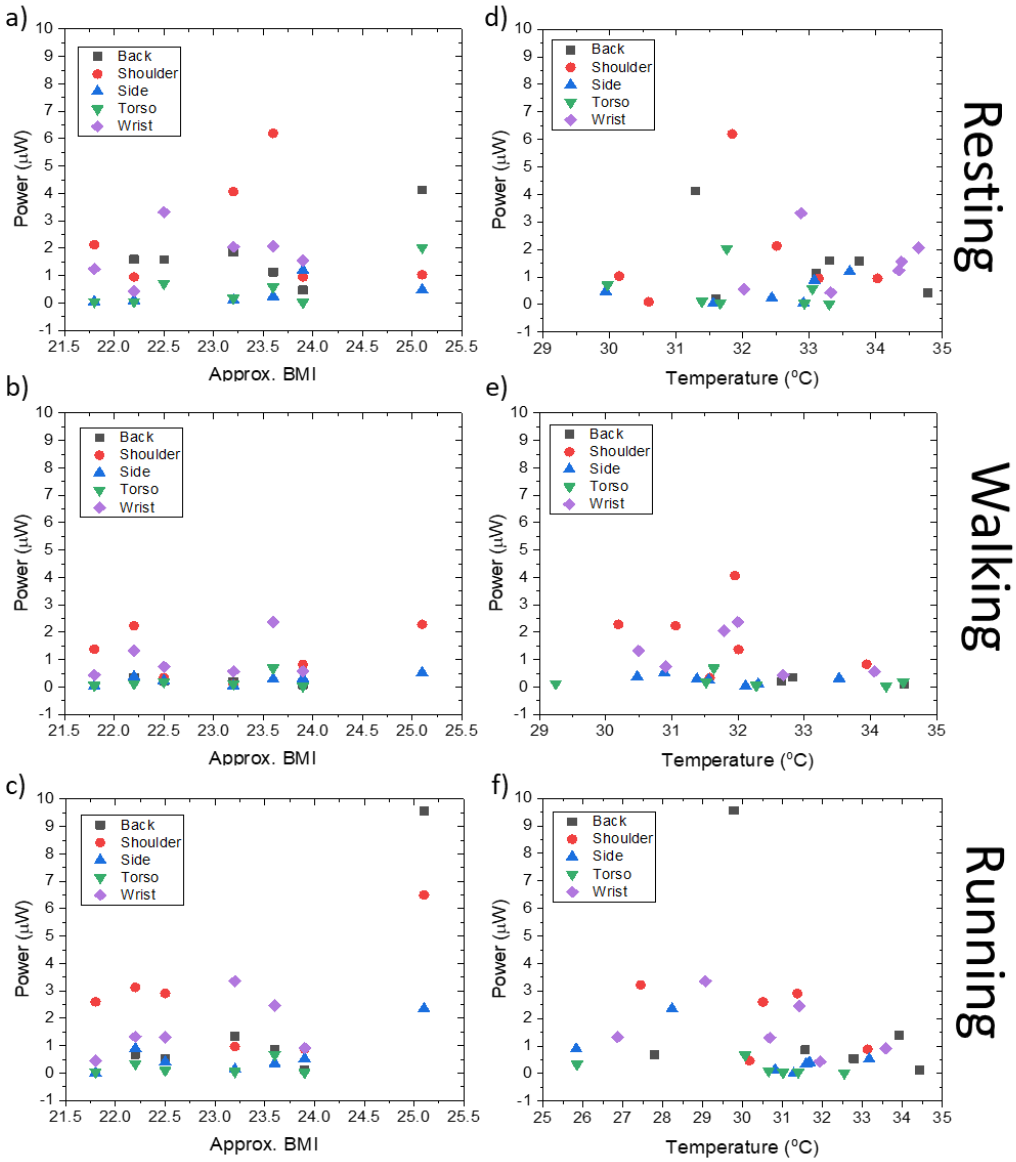


**Figure 5.6** a) - c) Average power output while resting, walking, and running, respectively, from each TEG as a function of the participants' estimated BMI. d) - f) Average power values as a function of recorded ambient temperature for resting, walking, and running, respectively.

## 5.6 CONCLUSION

The human trial procedures outlined in this study provided a foundation for following studies to build on. However, several challenges encountered must be addressed in order to obtain meaningful data. First, the yarn used for the shirt was not suitable for this application. The elasticity of the yarn caused fit issues, with regard to TEG contact resistance, and dulled the effect of different knit structures. It is recommended that a heavier yarn be used to highlight these structural differences and to study their effect on thermal energy harvesting. Second, the EHMS is bulky and should be easier to apply and remove from the shirt. This could be achieved by using a flexible polymer for the electronics case and by streamlining the profile of the circuit board. Finally, accelerometer data does not give an accurate description of a person's velocity so a sensor that can monitor speed should be added. Another option is to utilize a motion capture system to verify movement and velocity.

In summary, thermoelectric harvesting from the human body was studied to determine TEG response to changing activity levels and to create a thermal energy harvesting body map. A seamless shirt was designed with specific knit structure placement and five TEGs were integrated at the following locations: chest, side torso, back, shoulder, and wrist. An energy harvesting measurement system (EHMS) was designed to monitor the output of each TEG while collecting information on the surrounding environment. Each TEG had a corresponding EHMS so the size of the board was constrained to a small footprint. The shirt was worn by participants who volunteered to complete several activities: resting, walking, and running. The preliminary trial results show the effect of convection on thermal energy harvesting and compared energy harvesting levels over the upper body. TEGs placed on the back, torso, and

side of the body showed the lowest power values for all activities performed in the trial. While conclusions cannot be drawn from the data acquired in this study, the results of this work identify specific areas for future studies and optimization. Moving forward, the challenges in this trial will be addressed and a thorough analysis of data will be performed.

# CHAPTER 6: Conclusion and Future Work

## 6.1 Summary and Conclusion

To improve thermal energy harvesting from the body, a complex set of microclimates, components, and functions must be considered in relation to each other. While much literature on energy harvesting improvements highlights the importance of device and material optimization, little focus has been geared towards improving the system as a whole. The objective of this work is to integrate thermal energy harvesters into a knit textile and to generate a power generation map for locations and scenarios from thermal energy harvesting on the body. A test method for evaluating the performance of a TEG in a wearable form is developed and demonstrated using both in-lab and out-of-lab procedures. The fabrication procedure of an energy harvesting wearable device demonstrates a method of integrating rigid devices into a flexible substrate. The wearable device is used in a human trial, which covered a series of activities in different environmental conditions. The outcomes of these trials demonstrate the significant effect of movement, or convection, on thermal energy harvesting. Finite-element simulations explored how convection changes the heat flux through both the textile and thermoelectric generator (TEG). We also identify which knit properties improve thermal energy harvesting by modifying the environment immediately surrounding the TEG in the simulations. These simulations provide critical design considerations for integrating wearable technology with knit textiles. Textile swatches were knit and characterized accordingly for validation of the model results. The stitch density has a significant effect on air permeability of the textile and corresponds to heat flow induced by convection. Previous results led the

design of a knitted shirt with structured stitches that promote energy harvesting. The shirt is used in a human trial, which covered a series of activities in different environmental conditions. The results of these trials confirm the significant effect of convection on thermal energy harvesting in addition to mapping energy harvesting levels over the torso. While body temperature near the core is higher than the extremities, the identified ideal locations for thermal energy harvesting, the wrist and shoulder, have more exposure to the environment. TEGs placed on the back, torso, and side of the body showed the lowest power values for all activities performed in the trial. The results of this work quantify how smart garment design should include consideration of the use case scenario and where thermal energy harvesters are located. As wearable technology advances, this work can be referenced as a foundation for investigating textile design based on human factors and device functionality. Because there are several aspects of this project that can be continued in detail, future work will be covered in three sections: i) modelling, ii) textile design, and iii) body mapping.

## 6.2 Future Work in Modelling

The modelling work detailed in Chapter 4 lays a foundation for building sophisticated models of both textiles and the human microclimate. Only one knit structure was investigated in this project so one immediate continuation of the modelling work is to include multiple knit structures and designs in the current model. The knit geometry can also include fibers and yarn twist, as both of these properties change the amount of air considered in the problem. Another, equally important, textile property consideration is human sweat and the associated evaporative heat loss. Knit geometry plays a large role in wicking sweat from the body and

can be used for directing the flow of sweat through the textile. The addition of evaporative heat loss requires the computation software to have multiphase functionality that was not present in the Solidworks flow simulation. Knit textiles have unique mechanical properties that could yield insight into additional functionality from knit structures. Running complex mechanical, electrical, and fluid simulations simultaneously will highlight the unique properties of knit textiles and enable designers and engineers to create advanced smart garments.

Various electronic components integrated with a textile model has not been considered. This work only investigated the effects of thermal energy harvesters on the surrounding textile and vice versa. Many other components that are used in wearable devices such as sensors, electrodes, actuators, and batteries can generate heat that must be accounted for when designing the textile housing for these devices. Additionally, the added weight from electronic components should be modelled so a textile structure can be modified to support the device. Therefore, there is much work to be done on investigating the interaction of textiles and electronic devices.

## 6.3 Future Work in Textiles for Electronics

The textiles industry is large and well-established. Only simple knit textiles were studied in this project. This leaves woven, non-woven, and more complex knit textiles that are not well documented regarding interactions with electronic or smart garments. Garment construction can consist of several types of textiles which can also be used in designing wearable devices. Investigating textile fabrication and construction to accommodate electronic components will create opportunities for highly engineered garments that are still attractive to the average

consumer. Much of these design considerations rely on constraints imposed by the use scenario, nevertheless, textile construction plays a significant role in creating smart garments. More specific to the continuation of this project, future work entails using novel knitting processes to prepare garments for electronic integration. Some of this requires studying yarn properties and modifying the properties of smart yarn materials to be compatible with current manufacturing practices. The other approach is to modify current equipment to accommodate technical yarns.

Should the resistance of conductive yarns decrease, their use in wearable electronics will increase. Applications would expand from electrodes to include interconnect traces or interactive areas of the garment (i.e. using an area as a switch that activates when touched). Conductive yarns are already being investigated for uses such as capacitors. Material innovations at the fiber level introduces the realm of entirely textile-based electronic components. This area is ripe with research and project possibilities that can build on the modelling and energy harvesting work described in this dissertation.

## 6.4 Future Work in Energy Harvesting Body Mapping

The energy harvesting body map currently consists of five locations that all exist on the upper body. In addition, the only energy harvesting method investigated thus far is thermoelectric. Numerous other energy-harvesting options exist for wearable applications. Pyroelectric, piezoelectric, photovoltaic, triboelectric, magnetic induction, and ambient RF harvesting are options for wearable energy harvesting that were not covered in this work. The logical next steps for the body mapping study would include piezoelectric energy harvesting (due to its

prevalence in wearable technology in watches) or photovoltaic energy harvesting. These harvesting methods can be studied individually or combined with the thermoelectric study to characterize the wearable harvesting capabilities.

The skin temperature was not measured in the human trials because all current methods of measurement are known to be inaccurate in ideal settings, more so in transient conditions. The device used to measure skin temperature must remain in one place for the duration of the trial to avoid excessive noise. This is not feasible with current technology so skin temperature data was not collected. The data would solidify the temperature difference across the TEG and identify how the heat flux away from the body changes with regard to activity. Other environmental factors, such as radiation exposure, would need to be monitored in the case of other energy harvesting methods being studied.

Finally, only the upper body was mapped in the study. Further exploration and mapping should include the lower body, extremities such as the feet and hands, and the head. Pants, gloves, shoes, and hats can act as substrates for integrating one or several energy harvesting devices. In addition, other locations on the upper body should be considered with regard to body shape. Many combinations of garments and harvesting methods can be explored and characterized, resulting in a full energy-harvesting guide for designing smart garments.

In conclusion, this dissertation discussed several design aspects pertaining to wearable technology, energy harvesting, and electronics integration. Many interesting projects investigate textile modifications for smart or electronic purposes, while still others look at optimizing thermal energy harvesting from the body. This work considered a multidisciplinary problem with several approaches to the solution. The overall goal was not to optimize energy

harvesting or create novel smart textiles but to investigate how the textile, energy harvester, and human body interact and affect one another. This information will be very useful in designing self-powered wearable electronics on garments or other textile platforms.

# BIBLIOGRAPHY


[1] K. Parsons, “Introduction to thermal comfort standards,” in *Conference: Moving Thermal Comfort Standards*, 2001, pp. 19–30.

[2] Y. Li, “The Science of Clothing Comfort,” *Text. Prog.*, vol. 31, no. 1–2, pp. 1–135, 2010.

[3] P. O. Fanger, “Assessment of thermal comfort practice,” *Occup. Environ. Med.*, vol. 30, pp. 313–324, 1973.

[4] R. De Dear, G. Brager, and U. C. Berkeley, “Developing an adaptive model of thermal comfort and preference,” *ASHRAE Trans.*, vol. 104, no. Part 1, pp. 1–18, 1998.

[5] C. Edifici, C. Codrea, M. Pollak, and P. Spies, “Human Body Energy Harvesting Thermogenerator for Sensing Applications,” in *International Conference on Sensor Technologies and Applications*, 2007, pp. 366–372.

[6] C. R. Saha, T. O’Donnell, N. Wang, and P. McCloskey, “Electromagnetic generator for harvesting energy from human motion,” *Sensors Actuators, A Phys.*, vol. 147, no. 1, pp. 248–253, 2008.

[7] A. Potnuru and Y. Tadesse, “Characterization of Pyroelectric Materials for Energy Harvesting from Human Body,” *Integr. Ferroelectr.*, vol. 150, no. 1, pp. 23–50, 2014.

[8] F. Suarez, A. Nozariasbmarz, D. Vashaee, and M. C. Ozturk, “Designing Thermoelectric Generators for Self-Powered Wearable Electronics,” *Energy Environ. Sci.*, vol. 9, no. 2099, 2016.

[9] A. Gagge and R. Gonzalez, “Mechanisms of Heat Exchange: Biophysics and Physiology,” *Handb. Physiol. Environ. Physiol.*, no. 1, pp. 45–84, 1996.

[10] K. Parsons, “Human Thermal physiology and thermoregulation,” in *Human Thermal Environments*, 2014, pp. 31–48.

[11] A. Gagge and Y. Nishi, “Heat exchange between human skin surface and thermal environment,” in *Handbook of physiology - reactions to environmental agents*, 1977, pp. 69–92.

[12] “Smart and Interactive Textiles Market for Industrial , Military and Defense , Medical and Healthcare Retail and Consumer , Transportation and Other Applications - Global Industry Analysis , Size , Share , Growth , Trends and Forecast ,” 2015.

[13] CCS Insight, “Wearable Technology,” 2016.

[14] V. Leonov and R. J. M. Vullers, “Wearable Thermoelectric Generators for Body-Powered Devices,” *J. Electron. Mater.*, vol. 38, no. 7, pp. 1491–1498, Jan. 2009.

[15] T. Starner and J. Paradiso, “Human generated power for mobile electronics,” *Low-power Electron. Des.*, vol. 1990, 2004.

[16] J. A. Paradiso and T. Starner, “Energy scavenging for mobile and wireless electronics,” *IEEE Pervasive Comput.*, vol. 4, no. 1, pp. 18–27, 2005.

[17] “No Title,” *ASHRAE Standard 55*. pp. 16–17, 2004.

[18] R. J. M. Vullers, R. van Schaijk, I. Doms, C. Van Hoof, and R. Mertens, “Micropower energy harvesting,” *Solid. State. Electron.*, vol. 53, no. 7, pp. 684–693, Jul. 2009.

[19] L. Mateu and F. Moll, “Review of energy harvesting techniques and applications for microelectronics (Keynote Address),” *Microtechnologies New Millenn. 2005*, pp. 359–373, 2005.

[20] Y. K. Tan and S. K. Panda, “Energy harvesting from hybrid indoor ambient light and thermal energy sources for enhanced performance of wireless sensor nodes,” *IEEE Trans. Ind. Electron.*, vol. 58, no. 9, pp. 4424–4435, 2011.

[21] S. Chalasani and J. M. Conrad, “A survey of energy harvesting sources for embedded systems,” *Conf. Proc. - IEEE SOUTHEASTCON*, pp. 442–447, 2008.

[22] Z. G. G. Wan, Y. K. K. Tan, and C. Yuen, “Review on energy harvesting and energy management for sustainable wireless sensor networks,” *2011 IEEE 13th Int. Conf. Commun. Technol.*, pp. 362–367, 2011.

[23] V. Misra *et al.*, “Flexible technologies for self-powered wearable health and environmental sensing,” *Proc. IEEE*, vol. 103, no. 4, pp. 665–681, 2015.

[24] V. Leonov and R. J. M. Vullers, “Wearable electronics self-powered by using human body heat: The state of the art and the perspective,” *J. Renew. Sustain. Energy*, vol. 1, no. 6, p. 62701, 2009.

[25] A. Harb, “Energy harvesting: State-of-the-art,” *Renew. Energy*, vol. 36, no. 10, pp. 2641–2654, Oct. 2011.

[26] P. D. Mitcheson, E. M. Yeatman, G. K. Rao, A. S. Holmes, and T. C. Green, “Energy Harvesting From Human and Machine Motion forWireless Electronic Devices,” *Proc. IEEE*, vol. 96, no. 9, pp. 1457–1486, 2008.

[27] M. Wahbah, M. Alhawari, B. Mohammad, H. Saleh, and M. Ismail, “Characterization of Human Body-Based Thermal and Vibration Energy Harvesting for Wearable

Devices," *IEEE J. Emerg. Sel. Top. Circuits Syst.*, vol. 4, no. 3, pp. 354–363, Sep. 2014.

[28] Z. Wang, V. Leonov, P. Fiorini, and C. Van Hoof, "Realization of a wearable miniaturized thermoelectric generator for human body applications," *Sensors Actuators A Phys.*, vol. 156, no. 1, pp. 95–102, Nov. 2009.

[29] J. W. Stevens, "Optimal design of small ΔT thermoelectric generation systems," *Energy Convers. Manag.*, vol. 42, no. 6, pp. 709–720, Apr. 2001.

[30] V. Leonov, C. Van Hoof, and R. J. M. Vullers, "Thermoelectric and Hybrid Generators in Wearable Devices and Clothes," in *2009 Sixth International Workshop on Wearable and Implantable Body Sensor Networks*, 2009, pp. 195–200.

[31] V. Leonov, "Energy Harvesting for Self-Powered Wearable Devices," in *Wearable Monitoring Systems*, A. Bonfiglio and D. De Rossi, Eds. Boston, MA: Springer US, 2011, pp. 27–49.

[32] M. Lossec, B. Multon, and H. Ben Ahmed, "Sizing optimization of a thermoelectric generator set with heatsink for harvesting human body heat," *Energy Convers. Manag.*, vol. 68, pp. 260–265, Apr. 2013.

[33] C.-C. Wang, C.-I. Hung, and W.-H. Chen, "Design of heat sink for improving the performance of thermoelectric generator using two-stage optimization," *Energy*, vol. 39, no. 1, pp. 236–245, Mar. 2012.

[34] P. Dziurdzia *et al.*, "Estimation and harvesting of human heat power for wearable electronic devices," *IOP Conf. Ser. Mater. Sci. Eng.*, vol. 104, no. 1, p. 12005, Jan. 2015.

[35] F. Suarez, D. P. Parekh, C. Ladd, D. Vashaee, M. D. Dickey, and M. C. Öztürk, "Flexible thermoelectric generator using bulk legs and liquid metal interconnects for wearable electronics," *Appl. Energy*, vol. 202, pp. 736–745, 2017.

[36] S. Jo, M. Kim, M. Kim, H. Kim, and Y. Kim, "Human Body Heat Energy Harvesting Using Flexible Thermoelectric Generator for Autonomous Microsystems," *Rsc.Org*, no. V, pp. 839–841, 2012.

[37] A. Yadav, K. P. Pipe, and M. Shtein, "Fiber-based flexible thermoelectric power generator," *J. Power Sources*, vol. 175, no. 2, pp. 909–913, Jan. 2008.

[38] K. T. Settaluri, H. Lo, and R. J. Ram, "Thin Thermoelectric Generator System for Body Energy Harvesting," *J. Electron. Mater.*, vol. 41, no. 6, pp. 984–988, Dec. 2011.

[39] J.-H. Bahk, H. Fang, K. Yazawa, and A. Shakouri, "Flexible thermoelectric materials

and device optimization for wearable energy harvesting," *J. Mater. Chem. C*, vol. 3, no. 3, pp. 10362–10374, 2015.

[40] A. Majumdar, S. Mukhopadhyay, and R. Yadav, "Thermal properties of knitted fabrics made from cotton and regenerated bamboo cellulosic fibres," *Int. J. Therm. Sci.*, vol. 49, no. 10, pp. 2042–2048, 2010.

[41] Z. Lu, H. Zhang, C. Mao, and C. M. Li, "Silk fabric-based wearable thermoelectric generator for energy harvesting from the human body," *Appl. Energy*, vol. 164, pp. 57–63, 2016.

[42] G. Delaizir *et al.*, "A new generation of high performance large-scale and flexible thermo-generators based on (Bi,Sb)2 (Te,Se)3 nano-powders using the Spark Plasma Sintering technique," *Sensors Actuators A Phys.*, vol. 174, pp. 115–122, 2012.

[43] L. Francioso, C. De Pascali, V. Sglavo, A. Grazioli, M. Masieri, and P. Siciliano, "Modelling, fabrication and experimental testing of an heat sink free wearable thermoelectric generator," *Energy Convers. Manag.*, vol. 145, pp. 204–213, 2017.

[44] L. Francioso *et al.*, "Flexible thermoelectric generator for wearable biometric sensors," *J. Power Sources*, vol. 196, no. 6, pp. 747–750, 2010.

[45] M. K. Kim, M. S. Kim, S. E. Jo, and Y. J. Kim, "Flexible thermoelectric generator for human body heat energy harvesting," *Electron. Lett.*, vol. 48, no. 16, pp. 1015–1017, 2012.

[46] A. Myers, R. Hodges, and J. S. Jur, "Human and environmental analysis of wearable thermal energy harvesting," *Energy Convers. Manag.*, vol. 143, pp. 218–226, Jul. 2017.

[47] M. Ghahremani Honarvar and M. Latifi, "Overview of wearable electronics and smart textiles," *J. Text. Inst.*, vol. 108, no. 4, pp. 631–652, 2017.

[48] K. Jost *et al.*, "Natural fiber welded electrode yarns for knittable textile supercapacitors," *Adv. Energy Mater.*, vol. 5, no. 4, pp. 1–8, 2015.

[49] K. Jost, G. Dion, and Y. Gogotsi, "Textile energy storage in perspective," *J. Mater. Chem. A*, vol. 2, no. 28, pp. 10776–10787, 2014.

[50] K. Jost *et al.*, "Knitted and screen printed carbon-fiber supercapacitors for applications in wearable electronics," *Energy Environ. Sci.*, vol. 6, p. 2698, 2013.

[51] M. Kimura, *Handbook of Smart Textiles*. 2014.

[52] C. A. Hewitt, A. B. Kaiser, S. Roth, M. Craps, R. Czerw, and D. L. Carroll,

"Multilayered carbon nanotube/polymer composite based thermoelectric fabrics," *Nano Lett.*, vol. 12, no. 3, pp. 1307–1310, 2012.

[53] S. L. Kim, K. Choi, A. Tazebay, and C. Yu, "Flexible power fabrics made of carbon nanotubes for harvesting thermoelectricity," *ACS Nano*, vol. 8, no. 3, pp. 2377–2386, 2014.

[54] Y. Du, J. Xu, Y. Wang, and T. Lin, "Thermoelectric properties of graphite-PEDOT:PSS coated flexible polyester fabrics," *J. Mater. Sci. Mater. Electron.*, vol. 28, no. 8, pp. 5796–5801, 2017.

[55] Y. Du *et al.*, "Thermoelectric fabrics: toward power generating clothing.," *Sci. Rep.*, vol. 5, p. 6411, 2015.

[56] S. Finefrock, X. Zhu, Y. Sun, and Y. Wu, "Flexible Prototype Thermoelectric Devices Based on Ag2Te and PEDOT:PSS Coated Nylon Fibre," *Nanoscale*, pp. 5598–5602, 2015.

[57] J. A. Lee *et al.*, "Woven-Yarn Thermoelectric Textiles," *Adv. Mater.*, pp. 5038–5044, 2016.

[58] J. D. Ryan, D. A. Mengistie, R. Gabrielsson, A. Lund, and C. M??ller, "Machine-Washable PEDOT:PSS Dyed Silk Yarns for Electronic Textiles," *ACS Appl. Mater. Interfaces*, vol. 9, no. 10, pp. 9045–9050, 2017.

[59] R. Kroon *et al.*, "Thermoelectric plastics: from design to synthesis, processing and structure-property relationships.," *Chem. Soc. Rev.*, vol. 45, no. 22, pp. 6147–6164, 2016.

[60] Q. Wu and J. Hu, "A novel design of wearable thermoelectric generator based on 3D fabric structure," p. 16, 2017.

[61] Z. Cao, E. Koukharenko, M. J. Tudor, R. N. Torah, and S. P. Beeby, "Screen printed flexible $Bi_2Te_3$-$Sb_2Te_3$ based thermoelectric generator," *J. Phys. Conf. Ser.*, vol. 476, p. 12031, 2013.

[62] Z. Cao, E. Koukharenko, R. N. Torah, J. Tudor, and S. P. Beeby, "Flexible screen printed thick film thermoelectric generator with reduced material resistivity," *J. Phys. Conf. Ser.*, vol. 557, no. 1, p. 12016, 2014.

[63] K. Ankireddy, A. K. Menon, B. Iezzi, S. K. Yee, M. D. Losego, and J. S. Jur, "Electrical Conductivity, Thermal Behavior, and Seebeck Coefficient of Conductive Films for Printed Thermoelectric Energy Harvesting Systems," *J. Electron. Mater.*, vol. 45, no. 11, pp. 5561–5569, 2016.

[64] A. Chen, “Thermal Energy Harvesting with Thermoelectrics for Self-powered Sensors : With Applications to Implantable Medical Devices , Body Sensor Networks and Aging in Place By Alic Chen A dissertation submitted in partial satisfaction of the requirements for the,” 2011.

[65] D. Madan, Z. Wang, A. Chen, P. K. Wright, and J. W. Evans, “High-performance dispenser printed MA p-type Bi0.5Sb 1.5Te3 flexible thermoelectric generators for powering wireless sensor networks,” *ACS Appl. Mater. Interfaces*, vol. 5, no. 22, pp. 11872–11876, 2013.

[66] C. Navone, M. Soulier, M. Plissonnier, and A. L. Seiler, “Development of (Bi,Sb) 2(Te,Se) 3-based thermoelectric modules by a screen-printing process,” *J. Electron. Mater.*, vol. 39, no. 9, pp. 1755–1759, 2010.

[67] J. H. We, S. J. Kim, and B. J. Cho, “Hybrid composite of screen-printed inorganic thermoelectric film and organic conducting polymer for flexible thermoelectric power generator,” *Energy*, vol. 73, pp. 506–512, 2014.

[68] K. Itoigawa, H. Ueno, M. Shiozaki, T. Toriyama, and S. Sugiyama, “Fabrication of flexible thermopile generator,” *J. Micromechanics Microengineering*, vol. 15, no. 9, pp. S233–S238, 2005.

[69] H. B. Lee, J. H. We, H. J. Yang, K. Kim, K. C. Choi, and B. J. Cho, “Thermoelectric properties of screen-printed ZnSb film,” *Thin Solid Films*, vol. 519, no. 16, pp. 5441–5443, 2011.

[70] J. P. Rojas, D. Conchouso, A. Arevalo, D. Singh, I. G. Foulds, and M. M. Hussain, “Paper-based origami flexible and foldable thermoelectric nanogenerator,” *Nano Energy*, vol. 31, no. August 2016, pp. 296–301, 2017.

[71] J. P. Rojas, D. Singh, D. Conchouso, A. Arevalo, I. G. Foulds, and M. M. Hussain, “Stretchable helical architecture inorganic-organic hetero thermoelectric generator,” *Nano Energy*, vol. 30, no. August, pp. 691–699, 2016.

[72] M.-K. Kim, M.-S. Kim, S. Lee, C. Kim, and Y.-J. Kim, “Wearable thermoelectric generator for harvesting human body heat energy,” *Smart Mater. Struct.*, vol. 23, no. 10, p. 105002, Oct. 2014.

[73] M. K. Kim and M. S. Kim, “Wearable thermoelectric generator for human clothing applications,” 2013, no. June, pp. 1376–1379.

[74] S. J. Kim, J. H. We, and B. J. Cho, “A wearable thermoelectric generator fabricated on a glass fabric,” *Energy Environ. Sci.*, vol. 7, no. 6, pp. 1–9, 2014.

[75] S. Shin *et al.*, “High-Performance Screen-Printed Thermoelectric Films on Fabrics,”

*Sci. Rep.*, vol. 7, no. 1, p. 7317, 2017.

[76] A. R. M. Siddique, R. Rabari, S. Mahmud, and B. Van Heyst, "Thermal energy harvesting from the human body using flexible thermoelectric generator (FTEG) fabricated by a dispenser printing technique," *Energy*, vol. 115, pp. 1081–1091, 2016.

[77] J. Abel, J. Luntz, and D. Brei, "Hierarchical architecture of active knits," *Smart Mater. Struct.*, vol. 22, no. 12, p. 125001, Dec. 2013.

[78] J. Abel, J. Luntz, and D. Brei, "A two-dimensional analytical model and experimental validation of garter stitch knitted shape memory alloy actuator architecture," *Smart Mater. Struct.*, vol. 21, no. 8, p. 18, Aug. 2012.

[79] J. Chamberlain, *Hosiery Yarns and Fabrics Vol. II*. Leicester College of Technology and Commerce, 1926.

[80] F. T. Peirce, "Geometrical Principles Applicable to the Design of Functional Fabrics," *Text. Res. J.*, vol. 17, pp. 123–147, 1947.

[81] G. A. V Leaf and A. Glaskin, "The Geometry of a Plain Knitted Loop," *J. Text. Inst. Trans.*, vol. 46, no. 9, pp. T587–T605, 1955.

[82] G. A. V. Leaf, "Models of the Plain-Knitted Loop," *J. Text. Inst. Proc.*, vol. 51, no. 2, pp. P61–P61, 1960.

[83] A. Demiroz and T. Dias, "A Study of the Graphical Representation of Plain-knitted Structures Part I: Stitch Model for the Graphical Representation of Plain-knitted Structures," *J. Text. Inst.*, vol. 91, no. 4, pp. 463–480, 2000.

[84] A. Kurbak, "Plain knitted fabric dimensions," *Text. Asia*, pp. 36–46, 1998.

[85] A. Kurbak, "Geometrical Models for Balanced Rib Knitted Fabrics Part I: Conventionally Knitted 1 x 1 Rib Fabrics," *Text. Res. J.*, vol. 79, no. 5, pp. 418–435, 2009.

[86] A. Kurbak and A. S. Soydan, "Basic Studies for Modeling Complex Weft Knitted Fabric Structures Part III: A Geometrical Model for 1 x 1 Purl Fabrics," *Text. Res. J.*, vol. 78, no. 5, pp. 377–381, 2008.

[87] A. Kurbak and O. Kayacan, "Basic Studies for Modeling Complex Weft Knitted Fabric Structures Part II: A Geometrical Model for Plain Knitted Fabric Spirality," *Text. Res. J.*, vol. 78, no. 4, pp. 279–288, 2008.

[88] A. Kurbak and T. Alpyildiz, "Geometrical Models for Balanced Rib Knitted Fabrics Part II: Applications of 1 x 1 Rib Model to Presser-Foot Knitted 1 x 1 Rib, Interlock

and Half Milano Rib," *Text. Res. J.*, vol. 79, no. 6, pp. 495–505, 2009.

[89] T. Alpyidiz and a. Kurbak, "A Geometrical Model for the Single Pique (Lacoste) Knits," *Text. Res. J.*, vol. 76, no. 11, pp. 861–867, 2006.

[90] O. Kayacan, A. Kurbak, and O. Kayacan, "Basic Studies for Modeling Complex Weft Knitted Fabric Structures Part V: Geometrical Modeling of Tuck Stitches," *Text. Res. J.*, vol. 78, no. 7, pp. 577–582, 2008.

[91] A. Kurbak and O. Ekmen, "Basic Studies for Modeling Complex Weft Knitted Fabric Structures Part I: A Geometrical Model for Widthwise Curlings of Plain Knitted Fabrics," *Text. Res. J.*, vol. 78, no. 3, pp. 198–208, 2008.

[92] C. Yuksel, J. M. Kaldor, D. L. James, and S. Marschner, "Stitch meshes for modeling knitted clothing with yarn-level detail," *ACM Trans. Graph.*, vol. 31, no. 4, pp. 1–12, 2012.

[93] A. K. Puszkarz, R. Korycki, and I. Krucinska, "SIMULATIONS OF HEAT TRANSPORT PHENOMENA IN A THREE-DIMENSIONAL MODEL OF KNITTED FABRIC," *AUTEX Res. J.*, vol. 16, no. 3, pp. 128–137, 2016.

[94] M. Sherburn, "Geometric and Mechanical Modelling of Textiles," 2007.

[95] ASHRAE Fundamentals, "Thermal Comfort," in *Handbook—Fundamentals*, 2009.

[96] E. Onofrei, A. M. Rocha, and A. Catarino, "The influence of knitted fabrics' structure on the thermal and moisture management properties," *J. Eng. Fibres Fabr.*, vol. 6, no. 4, pp. 10–22, 2011.

[97] A. K. Puszkarz and I. Krucinska, "The study of knitted fabric thermal insulation using thermography and finite volume method," *Text. Res. J.*, vol. 87, no. 6, pp. 643–656, 2017.

[98] A. K. Puszkarz and I. Krucinska, "Study of multilayer clothing thermal insulation using thermography and the finite volume method," *Fibres Text. East. Eur.*, vol. 24, no. 6, pp. 129–137, 2016.

[99] E. H. Wissler, "A mathematical model of the human thermal system," *Bull. Math. Biophys.*, vol. 26, no. 1, pp. 147–166, 1964.

[100] J. A. J. Stolwijk, "Control of body temperature," *Handb. Physiol. - React. to Environ. Agents*, pp. 45–67, 1977.

[101] X. Wan and J. Fan, "A transient thermal model of the human body-clothing-environment system," *J. Therm. Biol.*, vol. 33, no. 2, pp. 87–97, 2008.

[102] L. Yi, L. Fengzhi, L. Yingxi, and L. Zhongxuan, “An integrated model for simulating interactive thermal processes in human-clothing system,” *J. Therm. Biol.*, vol. 29, no. 7–8 SPEC. ISS., pp. 567–575, 2004.

[103] S. Murakami, S. Kato, and J. Zeng, “Combined simulation of airflow, radiation and moisture transport for heat release from a human body,” *Build. Environ.*, vol. 35, no. 6, pp. 489–500, 2000.

[104] S. I. Tanabe, K. Kobayashi, J. Nakano, Y. Ozeki, and M. Konishi, “Evaluation of thermal comfort using combined multi-node thermoregulation (65MN) and radiation models and computational fluid dynamics (CFD),” *Energy Build.*, vol. 34, no. 6, pp. 637–646, 2002.

[105] G. Havenith, R. Heus, and W. a. Lotens, “Resultant clothing insulation: a function of body movement, posture, wind, clothing fit and ensemble thickness,” *Ergonomics*, vol. 33, no. 1, pp. 67–84, 1990.

[106] J. E. Mark, *Polymer Data Handbook*, 2nd ed. Oxford University Press, 2009.

[107] R. C. Webb *et al.*, “Ultrathin conformal devices for precise and continuous thermal characterization of human skin.,” *Nat. Mater.*, vol. 12, no. 10, pp. 938–44, Oct. 2013.

[108] A. Martinez-Nicolas, E. Ortiz-Tudela, M. A. Rol, and J. A. Madrid, “Uncovering different masking factors on wrist skin temperature rhythm in free-living subjects.,” *PLoS One*, vol. 8, no. 4, p. e61142, Jan. 2013.

[109] M. Lossec, B. Multon, H. Ben Ahmed, and C. Goupil, “Thermoelectric generator placed on the human body: system modeling and energy conversion improvements,” *Eur. Phys. J. Appl. Phys.*, vol. 52, no. 1, p. 11103, Sep. 2010.

[110] M. Guan, K. Wang, D. Xu, and W.-H. Liao, “Design and experimental investigation of a low-voltage thermoelectric energy harvesting system for wireless sensor nodes,” *Energy Convers. Manag.*, vol. 138, pp. 30–37, 2017.

[111] R. Stull, “Wet-Bulb Temperature from Relative Humidity and Air Temperature,” *J. Appl. Meteorol. Climatol.*, vol. 50, pp. 2267–2269, 2011.

[112] M. Hyland, H. Hunter, J. Liu, E. Veety, and D. Vashaee, “Wearable thermoelectric generators for human body heat harvesting,” *Appl. Energy*, vol. 182, pp. 518–524, 2016.

[113] Y. Li, Y. Du, Y. Dou, K. Cai, and J. Xu, “PEDOT-based thermoelectric nanocomposites – A mini-review,” *Synth. Met.*, vol. 226, pp. 119–128, 2017.

[114] X. Xu and J. Werner, “A dynamic model of the human/clothing/environment-

system.," *Applied human science : journal of physiological anthropology*, vol. 16, no. 2. pp. 61–75, 1997.

[115] B. J. D. Hardy, "the Radiation of Heat From the Human Body," *Russell J. Bertrand Russell Arch.*, 1934.

[116] J. D. Hardy, "THE RADIATION OF HEAT FROM THE HUMAN BODY: III. The Human Skin as a Black-Body Radiator.," *J. Clin. Invest.*, vol. 13, no. 4, pp. 615–620, 1934.

[117] J. D. Hardy and C. Muschenheim, "the Radiation of Heat From the Human Body. Iv. the Emission, Reflection, and Transmission of Infra-Red Radiation By the Human Skin.," *J. Clin. Invest.*, vol. 13, no. 5, pp. 817–31, 1934.

[118] J. D. Hardy and C. Muschenheim, "Radiation of Heat From the Human Body. V. the Transmission of Infra-Red Radiation Through Skin," *J. Clin. Invest.*, vol. 15, no. 1, pp. 1–9, 1936.

[119] K. Parsons, "The Human Heat Balance Equation and the Thermal Audit," in *Human Thermal Environments*, 2003, pp. 33–57.

[120] A. Bejan, *Convection Heat Transfer*, 4th ed. John Wiley & Sons, 2013.

[121] F. Incropera, D. Dewitt, T. Bergman, and A. Lavine, *Fundamentals of Heat and Mass Transfer*. 2007.

[122] S. Toppaladoddi, S. Succi, and J. S. Wettlaufer, "Roughness as a Route to the Ultimate Regime of Thermal Convection," *Phys. Rev. Lett.*, vol. 118, no. 7, pp. 1–5, 2017.

[123] K. Min, Y. Son, C. Kim, Y. Lee, and K. Hong, "Heat and moisture transfer from skin to environment through fabrics: A mathematical model," *Int. J. Heat Mass Transf.*, vol. 50, no. 25–26, pp. 5292–5304, 2007.

[124] X. Xu and J. Werner, "A Dynamic Model of the Humall/Clothing/EnvirorlInent - System.," *Appl. Hum. Sci. J. Physiol. Anthropol.*, vol. 16, no. 2, pp. 61–75, Sep. 1997.

[125] N. Uçar and T. Yılmaz, "Thermal Properties of 1x1 2x2 3x3 Rib Knit Fabrics," *Fibres Text. East. Eur.*, vol. 12, no. 3, pp. 34–38, 2004.

[126] K. F. Choi and T. Y. Lo, "An Energy Model of Plain Knitted Fabric," *Text. Res. J.*, vol. 73, no. 8, pp. 739–748, 2003.

[127] S. Pal, "Futuristic Outlook of Wearable Technology in Key Applications," *Tech. Insights Reports*, 2015.

[128] National Institute of Health, “Body Mass Index Table.” [Online]. Available: https://www.nhlbi.nih.gov/health/educational/lose_wt/BMI/bmi_tbl.pdf. [Accessed: 16-Oct-2017].

[129] Xiao-Fei Teng, Yuan-Ting Zhang, C. C. Y. Poon, and P. Bonato, “Wearable Medical Systems for p-Health,” *IEEE Rev. Biomed. Eng.*, vol. 1, pp. 62–74, 2008.

[130] C. Pang, C. Lee, and K.-Y. Suh, “Recent advances in flexible sensors for wearable and implantable devices,” *J. Appl. Polym. Sci.*, vol. 130, no. 3, pp. 1429–1441, Nov. 2013.

[131] D.-H. Kim *et al.*, “Epidermal Electronics,” *Science (80-. ).*, vol. 333, no. 6044, 2011.

[132] T. Yamada *et al.*, “A stretchable carbon nanotube strain sensor for human-motion detection,” 2011.

[133] T. Sekitani, U. Zschieschang, H. Klauk, and T. Someya, “Flexible organic transistors and circuits with extreme bending stability,” 2010.

[134] D.-H. Kim *et al.*, “Materials for multifunctional balloon catheters with capabilities in cardiac electrophysiological mapping and ablation therapy,” 2011.

[135] E. J. D. Bronzino, “Neuman, M. R. ‘Biopotential Electrodes.,’” in *Medical Instrumentation: Application and Design*, 4th ed., Hoboken: John Wiley & Sons, 2010, p. 713.

[136] A. Searle and L. Kirkup, “A direct comparison of wet, dry and insulating bioelectric recording electrodes.,” *Physiol. Meas.*, vol. 21, no. 2, pp. 271–83, May 2000.

[137] P. J. Xu, H. Zhang, and X. M. Tao, “Textile-structured electrodes for electrocardiogram,” *Text. Prog.*, vol. 40, no. 4, pp. 183–213, Dec. 2008.

[138] Y. M. Chi, S. Member, T. Jung, S. Member, and G. Cauwenberghs, “Dry-Contact and Noncontact Biopotential Electrodes :,” vol. 3, pp. 106–119, 2010.

[139] P. J. Xu, H. Zhang, and X. M. Tao, “Textile-structured electrodes for electrocardiogram,” *Text. Prog.*, vol. 40, no. 4, pp. 183–213, Dec. 2008.

[140] A. Gruetzmann, S. Hansen, and J. Müller, “Novel dry electrodes for ECG monitoring.,” *Physiol. Meas.*, vol. 28, no. 11, pp. 1375–90, Nov. 2007.

[141] H.-C. Ha-Chul Jung *et al.*, “CNT/PDMS Composite Flexible Dry Electrodesfor Long-Term ECG Monitoring,” *IEEE Trans. Biomed. Eng.*, vol. 59, no. 5, pp. 1472–1479, May 2012.

[142] J.-Y. Baek, J.-H. An, J.-M. Choi, K.-S. Park, and S.-H. Lee, “Flexible polymeric dry

electrodes for the long-term monitoring of ECG," *Sensors Actuators A Phys.*, vol. 143, no. 2, pp. 423–429, May 2008.

[143] P. Salvo, R. Raedt, E. Carrette, D. Schaubroeck, J. Vanfleteren, and L. Cardon, "A 3D printed dry electrode for ECG/EEG recording," *Sensors Actuators A Phys.*, vol. 174, no. null, pp. 96–102, Feb. 2012.

[144] K.-P. Hoffmann and R. Ruff, "Flexible dry surface-electrodes for ECG long-term monitoring.," *Conf. Proc. IEEE Eng. Med. Biol. Soc.*, vol. 2007, pp. 5740–3, Jan. 2007.

[145] R. Ma, D.-H. Kim, M. McCormick, T. Coleman, and J. Rogers, "A stretchable electrode array for non-invasive, skin-mounted measurement of electrocardiography (ECG), electromyography (EMG) and electroencephalography (EEG).," *Conf. Proc. IEEE Eng. Med. Biol. Soc.*, vol. 2010, pp. 6405–8, Jan. 2010.

[146] J.-W. Jeong *et al.*, "Capacitive Epidermal Electronics for Electrically Safe, Long-Term Electrophysiological Measurements," *Adv. Healthc. Mater.*, vol. 3, no. 5, pp. 642–648, May 2014.

[147] C.-Y. Chen, C.-L. Chang, T.-F. Chien, and C.-H. Luo, "Flexible PDMS electrode for one-point wearable wireless bio-potential acquisition," *Sensors Actuators A*, vol. 203, pp. 20–28, 2013.

[148] C.-Y. Chen *et al.*, "A Low-Power Bio-Potential Acquisition System with Flexible PDMS Dry Electrodes for Portable Ubiquitous Healthcare Applications," *Sensors*, vol. 13, no. 3, pp. 3077–3091, Mar. 2013.

[149] C.-T. Lin, L.-D. Liao, Y.-H. Liu, I.-J. Wang, B.-S. Lin, and J.-Y. Chang, "Novel dry polymer foam electrodes for long-term EEG measurement.," *IEEE Trans. Biomed. Eng.*, vol. 58, no. 5, pp. 1200–7, May 2011.

[150] Tong InOh *et al.*, "Nanofiber Web Textile Dry Electrodes for Long-Term Biopotential Recording," *IEEE Trans. Biomed. Circuits Syst.*, vol. 7, no. 2, pp. 204–211, Apr. 2013.

[151] J.-W. Jeong *et al.*, "Capacitive epidermal electronics for electrically safe, long-term electrophysiological measurements.," *Adv. Healthc. Mater.*, vol. 3, no. 5, pp. 642–8, May 2014.

[152] H.-C. Jung *et al.*, "CNT/PDMS composite flexible dry electrodes for long-term ECG monitoring.," *IEEE Trans. Biomed. Eng.*, vol. 59, no. 5, pp. 1472–9, May 2012.

[153] F. Xu and Y. Zhu, "Highly conductive and stretchable silver nanowire conductors.," *Adv. Mater.*, vol. 24, no. 37, pp. 5117–22, Sep. 2012.

[154] H. J. Johnston, G. Hutchison, F. M. Christensen, S. Peters, S. Hankin, and V. Stone, "A review of the in vivo and in vitro toxicity of silver and gold particulates: Particle attributes and biological mechanisms responsible for the observed toxicity," *Crit. Rev. Toxicol.*, vol. 40, no. 4, pp. 328–346, Apr. 2010.

[155] F. M. Christensen *et al.*, "Nano-silver – feasibility and challenges for human health risk assessment based on open literature," *Nanotoxicology*, vol. 4, no. 3, pp. 284–295, Sep. 2010.

[156] Y. Xiong *et al.*, "The role of surface chemistry on the toxicity of ag nanoparticles.," *Small*, vol. 9, no. 15, pp. 2628–38, Aug. 2013.

[157] S. Yao and Y. Zhu, "Wearable multifunctional sensors using printed stretchable conductors made of silver nanowires," *Nanoscale*, vol. 6, no. 4, p. 2345, 2014.

[158] L. Song, A. C. Myers, J. J. Adams, and Y. Zhu, "Stretchable and reversibly deformable radio frequency antennas based on silver nanowires.," *ACS Appl. Mater. Interfaces*, vol. 6, no. 6, pp. 4248–53, Mar. 2014.

[159] Z. Cui, F. R. Poblete, G. Cheng, S. Yao, X. Jiang, and Y. Zhu, "Design and operation of silver nanowire based flexible and stretchable touch sensors," *J. Mater. Res.*, vol. 30, no. 1, pp. 79–85, Jan. 2015.

[160] Yugang Sun, Brian Mayers, and Thurston Herricks, and Y. Xia*, "Polyol Synthesis of Uniform Silver Nanowires: A Plausible Growth Mechanism and the Supporting Evidence," 2003.

[161] B. Wiley, Y. Sun, and Y. Xia, "Synthesis of Silver Nanostructures with Controlled Shapes and Properties," *Acc. Chem. Res.*, vol. 40, no. 10, pp. 1067–1076, Oct. 2007.

[162] S. Grimnes and Ø. G. Martinsen, *Bioimpedance and Bioelectricity Basics*, 2nd ed. Amsterdam, 2008.

[163] W. Franks, I. Schenker, P. Schmutz, and A. Hierlemann, "Impedance Characterization and Modeling of Electrodes for Biomedical Applications," *IEEE Trans. Biomed. Eng.*, vol. 52, no. 7, pp. 1295–1302, Jul. 2005.

[164] C.-H. Liu and X. Yu, "Silver nanowire-based transparent, flexible, and conductive thin film," *Nanoscale Res. Lett.*, vol. 6, no. 1, p. 75, 2011.

[165] W. J. Lee, M. Y. Lee, A. K. Roy, K. S. Lee, S. Y. Park, and I. In, "Poly(dimethylsiloxane)-protected Silver Nanowire Network for Transparent Conductor with Enhanced Oxidation Resistance and Adhesion Properties," *Chem. Lett.*, vol. 42, no. 2, pp. 191–193, Feb. 2013.

[166] E. Berardesca, “EEMCO guidance for the assessment of stratum corneum hydration: electrical methods,” *Ski. Res. Technol.*, vol. 3, no. 2, pp. 126–132, May 1997.

[167] Y. Yamamoto and T. Yamamoto, “Characteristics of skin admittance for dry electrodes and the measurement of skin moisturisation,” *Med. Biol. Eng. Comput.*, vol. 24, no. 1, pp. 71–77, Jan. 1986.

[168] O. G. Martinsen and S. Grimnes, “Facts and myths about electrical measurement of stratum corneum hydration state.,” *Dermatology*, vol. 202, no. 2, pp. 87–9, Jan. 2001.

[169] S. Björklund *et al.*, “Skin membrane electrical impedance properties under the influence of a varying water gradient.,” *Biophys. J.*, vol. 104, no. 12, pp. 2639–50, Jun. 2013.

[170] X. Huang *et al.*, “Epidermal impedance sensing sheets for precision hydration assessment and spatial mapping.,” *IEEE Trans. Biomed. Eng.*, vol. 60, no. 10, pp. 2848–57, Oct. 2013.

[171] D.-H. Kim *et al.*, “Epidermal Electronics,” *Science (80-. ).*, vol. 333, no. 6044, pp. 838–843, Aug. 2011.

[172] S. Yao and Y. Zhu, “Nanomaterial-enabled stretchable conductors: Strategies, materials and devices,” *Adv. Mater.*, vol. 27, no. 9, pp. 1480–1511, 2015.

[173] F. Xu and Y. Zhu, “Highly Conductive and Stretchable Silver Nanowire Conductors,” *Adv. Mater.*, vol. 24, no. 37, pp. 5117–5122, Sep. 2012.

[174] R. Ivanic, I. Novotny, V. Rehacek, V. Tvarozek, and M. Weis, “Thin film non-symmetric microelectrode array for impedance monitoring of human skin,” *Thin Solid Films*, vol. 433, no. 1–2, pp. 332–336, Jun. 2003.

[175] S. Yao and Y. Zhu, “Nanomaterial-Enabled Dry Electrodes for Electrophysiological Sensing: A Review,” vol. 68.

[176] A. Cömert, M. Honkala, and J. Hyttinen, “Effect of pressure and padding on motion artifact of textile electrodes.,” *Biomed. Eng. Online*, vol. 12, p. 26, Jan. 2013.

[177] J. G. Webster and J. W. (John W. Clark, *Medical instrumentation : application and design*. John Wiley & Sons, 2010.

[178] X. Huang, W.-H. Yeo, Y. Liu, and J. A. Rogers, “Epidermal differential impedance sensor for conformal skin hydration monitoring.,” *Biointerphases*, vol. 7, no. 1–4, p. 52, Dec. 2012.

[179] Øs. G. Martinsen, S. Grimnes, and E. Haug, “Measuring depth depends on frequency

in electrical skin impedance measurements," *Ski. Res. Technol.*, vol. 5, no. 3, pp. 179–181, Aug. 1999.

[180] K. Ito, K. Furuya, Y. Okano, and L. Hamada, "Development and characteristics of a biological tissue-equivalent phantom for microwaves," *Electron. Commun. Japan (Part I Commun.*, vol. 84, no. 4, pp. 67–77, Apr. 2001.

[181] T. Yamamoto *et al.*, "Development of electromagnetic phantom at low-frequency band.," *Conf. Proc. ... Annu. Int. Conf. IEEE Eng. Med. Biol. Soc. IEEE Eng. Med. Biol. Soc. Annu. Conf.*, vol. 2013, pp. 1887–90, Jan. 2013.

[182] H. N. Mayrovitz, "Assessing Free and Bound Water in Skin at 300 MHz Using Tissue Dielectric Constant Measurements with the MoistureMeterD," in *Lymphedema*, Cham: Springer International Publishing, 2015, pp. 133–148.

[183] C. M. Sheehy, P. A. Perry, and S. L. Cromwell, "Dehydration: Biological Considerations, Age-Related Changes, and Risk Factors in Older Adults," *Biol. Res. Nurs.*, vol. 1, no. 1, pp. 30–37, Jul. 1999.

[184] S. M. KLEINER, "Water," *J. Am. Diet. Assoc.*, vol. 99, no. 2, pp. 200–206, Feb. 1999.

[185] J. Chan, S. F. Knutsen, G. G. Blix, J. W. Lee, and G. E. Fraser, "Water, other fluids, and fatal coronary heart disease: the Adventist Health Study.," *Am. J. Epidemiol.*, vol. 155, no. 9, pp. 827–33, May 2002.

[186] C. Van Mieghem, M. Sabbe, and D. Knockaert, "The clinical value of the ECG in noncardiac conditions.," *Chest*, vol. 125, no. 4, pp. 1561–76, Apr. 2004.

[187] A. C. Myers, H. Huang, and Y. Zhu, "Wearable silver nanowire dry electrodes for electrophysiological sensing," *RSC Adv.*, vol. 5, no. 15, pp. 11627–11632, Jan. 2015.

[188] A. Caduff, F. Dewarrat, M. Talary, G. Stalder, L. Heinemann, and Y. Feldman, "Non-invasive glucose monitoring in patients with diabetes: a novel system based on impedance spectroscopy.," *Biosens. Bioelectron.*, vol. 22, no. 5, pp. 598–604, Dec. 2006.

[189] A. Caduff, E. Hirt, Y. Feldman, Z. Ali, and L. Heinemann, "First human experiments with a novel non-invasive, non-optical continuous glucose monitoring system.," *Biosens. Bioelectron.*, vol. 19, no. 3, pp. 209–17, Nov. 2003.

[190] M. van Dooren, J. J. G. (Gert-J. de Vries, and J. H. Janssen, "Emotional sweating across the body: Comparing 16 different skin conductance measurement locations," *Physiol. Behav.*, vol. 106, no. 2, pp. 298–304, May 2012.

[191] A. Nakasone, H. Prendinger, and M. Ishizuka, "Emotion Recognition from

Electromyography and Skin Conductance," *Proc. 5th Int. Work. Biosignal Interpret.*, 2005.

[192] J. Di *et al.*, "Stretch-Triggered Drug Delivery from Wearable Elastomer Films Containing Therapeutic Depots," *ACS Nano*, vol. 9, no. 9, pp. 9407–9415, Sep. 2015.

[193] J. Nuutinen, R. Ikäheimo, and T. Lahtinen, "Validation of a new dielectric device to assess changes of tissue water in skin and subcutaneous fat.," *Physiol. Meas.*, vol. 25, no. 2, pp. 447–54, Apr. 2004.

# APPENDIX

# APPENDIX A: OTHER PUBLISHED WORKS

## Wearable Silver Nanowire Dry Electrodes for Electrophysiological Sensing

Amanda C. Myers, He Huang and Yong Zhu

*As published in RSC Advances

Wearable sensors for health, wellness, and activity monitoring that track physiological data and sync with smart recording devices are becoming increasingly popular [129]–[132]. In particular, long-term monitoring of electrophysiological (or bioelectronic) signals such as electrocardiograms (ECGs), electromyograms (EMGs), and electroencephalograms (EEGs) gives a wealth of physiological information that can be used to both monitor the body and diagnose and treat various ailments [133], [134]. However, conventional electrodes used to record these electrophysiological signals, while giving high-quality signals and suitable for short-term or clinical use, cannot be used in a long-term, wearable setting due to the addition of an electrolytic gel layer between the skin and electrode used to enhance the clarity of biopotential recordings; the gel eventually dries which irritates the skin and causes signal degradation [135]–[137].

Dry electrodes are a viable alternative due to the elimination of the electrolytic gel layer. However, solid metal dry electrodes are uncomfortable to wear, have high skin-electrode impedance, and have large motion artifacts that result from the electrode slipping on the skin and from hairs between the skin and electrode [136], [137].

The aforementioned problems with dry electrodes can be mitigated or eliminated if the electrode has intimate, conformal contact with the skin. Recent advances in flexible and stretchable electronics [131]–[134] have paved the way for dry electrodes. By creating a flexible/ stretchable dry electrode, the issue of maintaining intimate skin contact is mitigated while also allowing for comfortable wear that does not impede the day-to-day activities of the user. A number of flexible/stretchable dry electrodes have been reported [138]–[150]. Invasive electrodes, using microneedles, have good signal quality, but cannot be used long-term due to patient discomfort and high motion artifact. Among the variety of noninvasive (or surface) electrodes, some have costly fabrication methods [142], [143], [145], [147], [151] and/or run the risk of the conductive metal (e.g., Au) delaminating from the flexible substrate, while others show large motion artifacts that can be attributed to the lack of conformal contact with skin [142], [152]. Conductive textile electrodes [139], [150] have been demonstrated, but the electrophysiological signals acquired have poor signal-to-noise ratios due to the electrodes sliding on the skin. Additionally, the biocompatibility of multiple dry surface electrodes has not been evaluated [143], [148]–[150].

In this paper, we present a silver nanowire (AgNW) based dry electrode that is noninvasive and wearable for electrophysiological sensing. The AgNWs are inlaid below the surface of an elastomeric substrate made of polydimethylsiloxane (PDMS), which prevents the NWs from delamination while creating a highly conductive surface (with constant conductivity >5,000 S/cm) [153]. The electrode is flexible and stretchable, which can conform to the curvilinear surfaces of the body thus reducing skin-electrode impedance and eliminating most motion artifacts. The AgNW dry electrodes perform as well as, and in some cases better than, the

conventionally used Ag/AgCl wet electrodes in ECG and EMG measurements. Silver is widely used in biomedical applications due to its antibacterial properties, and reported studies on silver nanoparticles and NWs have shown that the antibacterial properties of bulk silver could translate to the nanoscale [154]–[156].

The AgNW electrodes were fabricated following the method reported previously [153], [157]–[159] with modifications. AgNWs with average diameter of 90 nm and length of 10 – 60 μm, synthesized by the polyol method [160], [161], were used (from Blue Nano). After liquid PDMS was poured over the AgNW network, a metal snap that is compatible with current ECG/EMG equipment was pressed into the AgNW/ PDMS mixture. After curing, the AgNW network was inlaid in PDMS and the snap is securely connected to the AgNW/PDMS network. The fabrication process is shown in **Figure 1a** along with a finished electrode, **Figure 1b**. Velcro straps (or tapes) were used to attach the electrodes to the wrist for ECG measurements, as shown in **Figure 1c**, or to the forearm for EMG measurements.

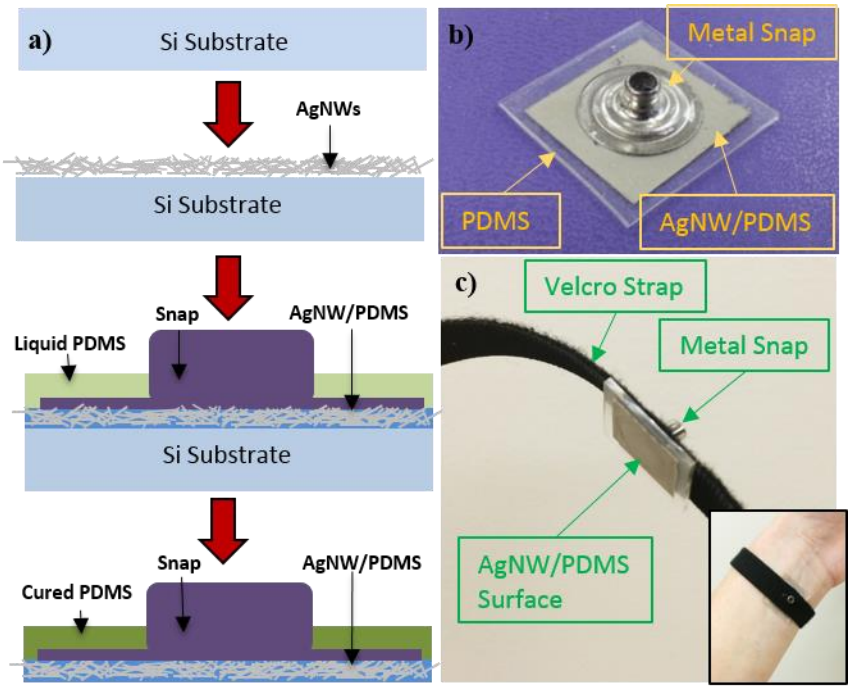


**Figure 1.** (a) Schematic of the fabrication process of the AgNW dry electrodes. (b) AgNW dry electrode with a metal snap. (c) AgNW dry electrode with Velcro strap for ECG measurements.

The topmost layer of skin, the *stratum corneum*, is considered a dielectric material with the most prominent effect on electrode-skin impedance; the drier the stratum corneum, the higher the impedance [140], [162], [163]. While the conventional Ag/AgCl electrodes use electrolytic gel to moisten the skin and improve electrode-skin contact, dry electrodes eliminate the use of this gel. Therefore, dry electrodes need a low electrode-skin impedance to attain electrophysiological signals of comparable quality to the Ag/AgCl electrodes [140], [162]. The electrode-skin impedance was measured by performing a frequency sweep from 40 Hz – 100 kHz over two skin-mounted electrodes (one electrode on the left wrist and one on the right) using an impedance analyzer (4294A Precision Impedance Analyzer, Agilent). The application pressure of the electrode has a significant effect on the quality of electrode-skin contact[135],

[140]. The electrode-skin impedance was recorded at various application pressure levels (light, medium, and heavy) to determine the proper electrode application pressure.

In addition to applying the electrolytic gel to the skin, two more steps are typically taken to treat the *stratum corneum* before taking an ECG with the Ag/AgCl wet electrodes to increase signal quality and improve electrode-skin contact – abrading the skin to remove dead skin cells and cleaning the electrode application area [135]. However, no skin preparation was performed before the AgNW/PDMS electrodes were applied for ECG testing. Three sets of ECG data were gathered with increasing intensity of movement to study the effects of motion artifact on the electrodes. The first set of data was taken the subject was seated and resting (no movement). The second set while the subject was standing and swinging their arms (one degree of movement). And the last test was performed while the subject was jogging (two degrees of movement).

Unlike the ECG measurements, the stratum corneum was only cleaned with 70% Isopropyl Alcohol before applying the wet or dry electrodes for the surface EMG measurement. The electrodes were placed on the right *extensor digitorum communis*. Two tests were performed where EMG signals were acquired: a settling trial and a wrist-extension trial. For the settling test, the subject was seated and relaxed. The right arm was placed on a flat table with a neutral/relaxed wrist position while the left arm was relaxed by the subject's side. EMG data was recorded with any muscle contractions. For the wrist-extension trial, the posture was kept the same as in the settling test. The subject performed ten wrist-extension contractions with consistent effort and approximately a 60-degree wrist extension. Each contraction lasted 3 seconds with a 10 second rest interval between each contraction. Frequency analysis was

performed on the acquired EMG signals, with DC offset removed, to interpret and compare the signals gathered from each type of electrode.

**Figure 2** shows how the electrode-skin impedance changes with the application pressure. As expected, the impedance decreases with increasing pressure. This trend is attributed to the increased electrode-skin contact area with increased pressure. The medium level of pressure (0.27 psi) is most similar to the pressure applied by a wristwatch. It was also noted that increase in pressure beyond the medium level did not have a correspondingly strong effect on the reduction of skin-electrode impedance. Therefore, the medium pressure (0.27 psi) was used as the application pressure in our electrophysiological measurements.

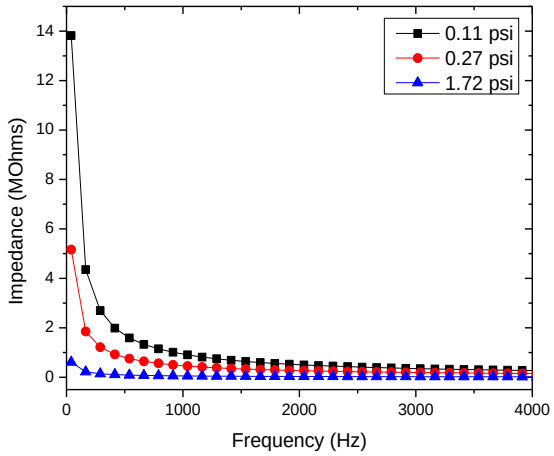


**Figure 2.** Electrode-skin impedance with increasing application pressure.

The ECGs taken with the AgNW electrode and with the Ag/AgCl electrode while the subject was resting are shown in **Figure 3a**. For comparison, the ECG signals are included on the same figure although they were recorded separately. No significant differences were noted between the two, zero-degree-of-movement ECG signals. Each wave of the ECG signal (P, QRS complex, and T) are clearly defined and the absence of a wandering baseline shows that the

dry electrode is well attached to the skin, as shown in **Figure 3b**. No filtering in addition to the predetermined settings on the ECG amplifier was used in plotting the ECG signals, so while the signal acquired with the AgNW electrode is slightly noisier, the noise can be reduced via post-process filtering.

The effect of motion artifact on signal quality was investigated by taking ECG measurements with increasing degrees of movement. The first test, shown in **Figure 3c**, consisted of localized movement near the sensing area, or one degree of movement: swinging the arms. The second test, shown in **Figure 3d**, added a second degree of movement, jogging while letting the arms swing naturally. As before, the signals acquired with the AgNW electrode were measured separately from the Ag/AgCl electrode. In both tests, the AgNW electrode outperformed the Ag/AgCl electrode in terms of signal quality. This is attributed to the conformal contact of the AgNW electrode with the skin whereas the wet electrode can slide on the skin due to the gel layer. In the first test (**Figure 3c**), the ECG waveform is clearly visible for both the wet and dry electrode; although the wet electrode signal has wandering baseline indicating that there is some minor slipping of the electrode on the skin. Additionally, the wet electrode shows slightly more noise in the signal than the dry electrode, making it difficult to distinguish minor nuances in the recording acquired with the wet electrode. This would pose a challenge in using the ECG signal for diagnostic purposes where clear signals are of the utmost importance. Both signals show significant degradation with the addition of a second degree of movement. For the Ag/AgCl electrode, the only discernible ECG waveform is the R peak, which could be used to determine heart rate but does not show the complete ECG spectrum. Therefore, it is unusable in applications that require a more detailed view of the heart's performance during activity.

For the AgNW electrode, the P wave, QRS complex, and T wave are still visible although the waveform has a significant amount of noise and wandering baseline.

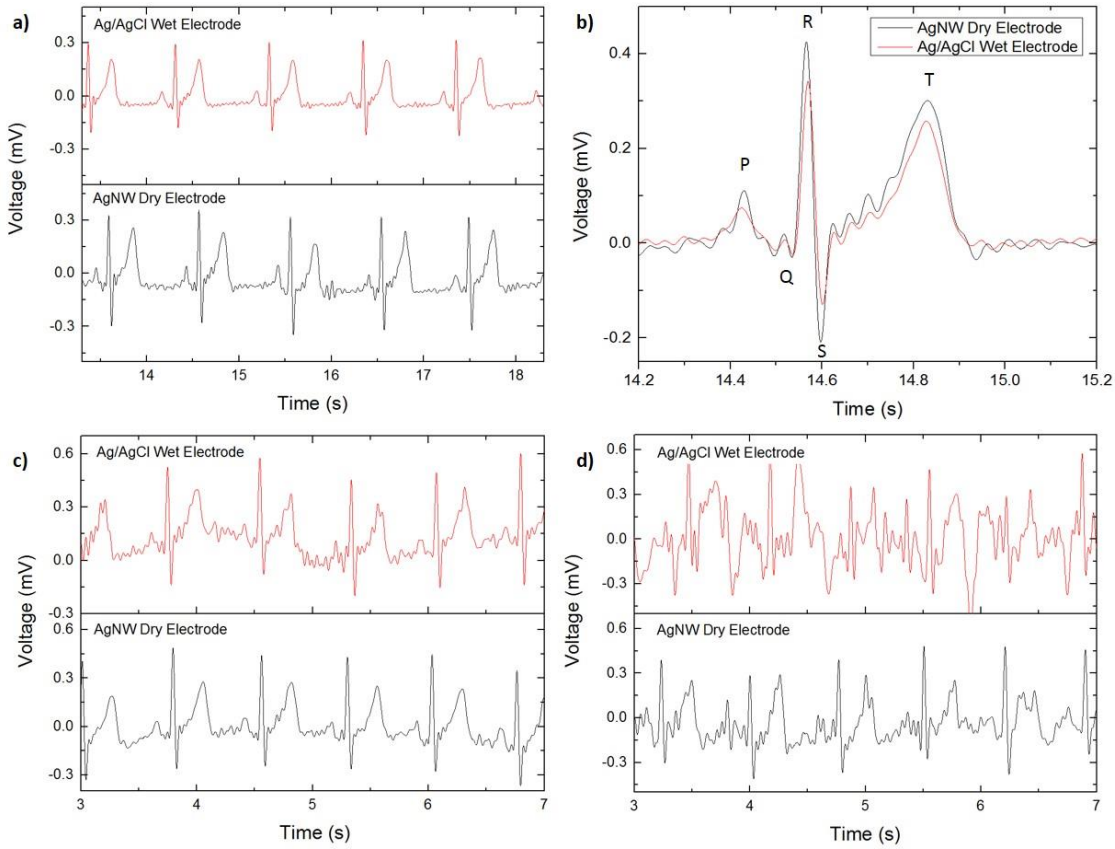


**Figure 3**. (a) ECG recording of Ag/AgCl wet electrode and AgNW dry electrode taken while subject was seated and resting. (b) ECG signal comparison of the P, Q, R, S, and T waves between the Ag/AgCl electrode and NW electrode. (c) ECG signal comparison of the subject swinging their arms, one degree of movement. (d) ECG signal comparison of the subject jogging, two degrees of movement.

The AgNW electrodes could be worn for 3 hours at a time and repeatedly for a week during a test with no noticeable discomfort or skin irritation. Degradation of AgNW electrodes over time due to oxidation could potentially compromise the device performance [164], [165]. Compared to unprotected AgNW electrodes (i.e., AgNWs on top), fully embedded AgNW

electrodes in PDMS were found to keep the same resistance for a much longer period of time [165]. In our case, the AgNW electrodes were re-used over the course of 4 months with no signal degradation.

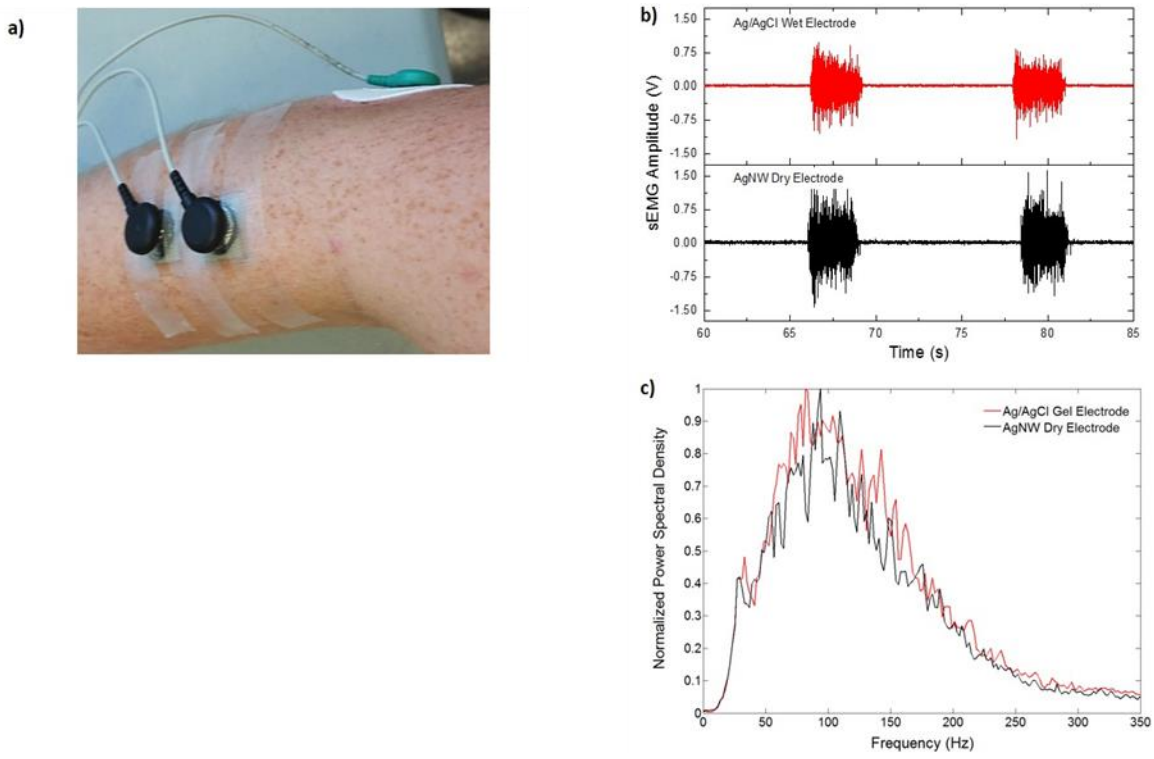


**Figure 4.** (a) AgNW electrodes on the forearm for EMG sensing (with black caps) and the ground/reference electrode (with green cap). (b) EMG signals from the Ag/AgCl wet electrode and AgNW dry electrode. (c) Normalized power spectral density of each electrode from the wrist extension trials.

**Figure 4a** shows the location of the electrodes used in the EMG measurements**. Figure 4b** shows the EMG data gathered from the Ag/AgCl electrode and from the AgNW electrode during the wrist-extension trials, respectively. Visual inspection of the EMG recordings shows almost no difference between the two electrodes other than the slight amplitude increase in the

AgNW recording. The EMG signal, where the subject flexed for 3 s and relaxed for 10 s, from the right *extensor digitorum communis* is clear in each electrode data set. While the EMG signal amplitude is higher when acquired with the AgNW electrode, the signal-to-noise ratio (SNR) of the wet Ag/AgCl electrode, 27.3 dB, is higher than that of the dry AgNW electrode, 24.7 dB. These results show that the wet and dry electrodes are comparable and that the dry AgNW electrode can be used to measure high-quality EMG recordings. The power spectral density of the each signal, shown in **Figure 4c,** displays comparable spectra with the dominant frequency components of each signal residing between 25 and 180 Hz. The AgNW electrodes have mean frequency (MNF) and median frequency (MDF) values of 115.2 Hz and 135.6 Hz, respectively, while Ag/AgCl electrodes have 119.1 Hz and 139.0 Hz, respectively. The AgNW frequency values are only slightly lower than the Ag/AgCl values, again showing nearly identical electrode performance. In particular, the AgNW electrodes show promise for use in prosthetic applications as they acquire high-quality EMG signals without compromising the comfort of the wearer due to drying of the electrolytic gel or Ag/AgCl plate pressing into the skin. The AgNW electrodes can also be integrated into gel liners used in artificial limb applications.

Compared to most other dry electrodes [139], [142], [150], [152], both the EMG and ECG signals acquired with the AgNW dry electrodes show much better quality. In addition, the AgNW electrodes generate a larger signal magnitude than the Ag/AgCl wet electrodes. Such an increase in signal magnitude can be attributed to the intimate contact between the NW electrode and the skin. The intimate contact of our AgNW electrodes is key to eliminating motion artifacts and enhancing the electrophysiological sensing capability.

In summary, wearable AgNW dry electrodes were fabricated and used to measure ECG and EMG signals with excellent performances. The electrodes are flexible and stretchable, which allows for high-quality electrophysiological measurement due to their intimate, conformal contact with the skin. When the subject was resting, ECG signals measured by the AgNW dry electrode are comparable to those by the conventional Ag/AgCl wet electrode. With increasing degrees of movement, AgNW electrodes showed less motion artifacts than the Ag/AgCl electrodes. The AgNW electrodes recorded strong, clear EMG signals with similar signal-to-noise ratio compared to the Ag/AgCl electrodes. The AgNW electrodes showed no signs of skin irritation or signal degradation after long-term wearing. In addition, the fabrication process of the AgNW electrodes is simple and cost-effective. The present study demonstrates that the AgNW dry electrodes can be an alternative to the wet electrodes in electrophysiological sensing, particularly for the long-term health monitoring.

**Experimental**

*ECG Measurements*: ECG signals were measured using an ECG amplifier (ADInstruments Powerlab with ECG attachments). All ECG signals were acquired with the electrodes in the lead 1 position (negative electrode placed on the right arm, positive electrode placed on the left arm, and ground electrode placed on the right leg). Pre-gelled Ag/AgCl electrodes (Red Dot$^{TM}$, 3M, St. Paul, MN) were used as the commercial electrodes in ECG measurements.

*Surface EMG Measurements:* For EMG measurement, the measurement electrodes were placed in a bipolar configuration with the electrodes 22 mm apart (center-to-center), parallel to the muscle fiber direction. The ground electrode was placed on the elbow. EMG signals

were sampled at 1000Hz using a 16-channel EMG system (MA300, Motion Lab System, LA) containing a preamplifier that filtered the signals between 10 and 2000Hz with an adjustable pass-band gain of 1000. Pre-gelled Ag/AgCl electrodes (Norotrode 20, Myotronics, Kent, WA) were used as the commercial electrodes in EMG measurements.

*Frequency Analysis of EMG Signals*: For both wet and dry electrodes, the SNR is defined as

$$\mathrm{SNR_{dB}} = 10\log_{10}(\frac{A_{signal}}{A_{noise}})^2 = 20\log_{10}(\frac{A_{signal}}{A_{noise}}), \quad (1)$$

where $A_{noise}$ was estimated from the data gathered in the settling trials and $A_{signal}$ from the muscle contraction data in the wrist-extension test. Note that *A* is the root mean square (RMS) of the signal.

Both MNF and MDF were used to compare the two types of EMG electrodes.[29] MNF is the sum of the product of the EMG power spectrum (*P*) and frequency ( *f*) divided by the sum of the power spectrum

$$MNF = \sum_{i=1}^{M} f_i P_i \Big/ \sum_{i=1}^{M} P_i, \quad (2)$$

where the subscript *i* denotes the variable value at the $i_{th}$ frequency bin and *M* denotes the total number of frequency bins. MDF is the power spectral density of the EMG signal divided into two segments with equivalent cumulated power

$$\sum_{i=1}^{MDF} P_i = \sum_{i=MDF}^{M} P_i = \frac{1}{2}\sum_{i=1}^{M} P_i \ , \quad (3)$$

The power spectral density (PSD) for each muscle contraction recorded in the EMG trials was approximated from the signals without DC offset using Welch's averaged modified periodogram. The PSD values across the ten contractions were normalized between 0 and 1

according to the maximum and minimum power recorded then averaged over the 10 contractions. The MNF and MDF were then calculated using the normalized PSD values.

# A Wearable Hydration Monitor with Conformal Nanowire Electrodes

Shanshan Yao[a], Amanda Myers[a], Abhishek Malhotra, Feiyan Lin, Alper Bozkurt, John F. Muth[*] and Yong Zhu[*]

[a] *Authors contributed equally to this work*

* As published in Advanced Healthcare Materials

A wearable skin hydration sensor in the form of a capacitor is demonstrated based on skin impedance measurement. The capacitor consists of two interdigitated or parallel electrodes that are made of silver nanowires (AgNWs) in a polydimethylsiloxane (PDMS) matrix. The flexible and stretchable nature of the AgNW/PDMS electrode allows conformal contact to the skin. The hydration sensor is insensitive to the external humidity change and is calibrated against a commercial skin hydration system on artificial skin over a wide hydration range. The hydration sensor is packaged into a flexible wristband, together with a network analyzer chip, a button cell battery and an ultralow power microprocessor with Bluetooth. In addition, a chest patch consisting of a strain sensor, three electrocardiography electrodes and a skin hydration sensor is developed for multimodal sensing. The wearable wristband and chest patch may be used for low-cost, wireless and continuous sensing of skin hydration and other health parameters.

## Introduction

Hydration of the body is an important physiological parameter to measure, but is challenging to measure accurately. For example, high performance athletes would like to know more about their hydration state since this can be directly linked to athletic performance. Such knowledge

is also of interest to workers such as first responders who may dehydrate when working in extreme conditions. It is a well-known problem that when coaches start training young athletes for American football in the summer, and when the military starts physically training recruits that dehydration and heat stroke pose serious risks.

Many methods to assess dehydration are qualitative, for example, by accessing how the person looks (e.g., sunken eyes and cracked lips), or by examining the volume and color of urine. More quantitative assessment relies on measuring change in hydration by weighing a naked person before and after exercise, or by using instruments that measure the physical properties of the skin such as conductance, capacitance, impedance, thermal conductivity, and reflectance of optical or electromagnetic radiation [166]–[169]. Almost all of these measurements are taken in clinical settings.

To replace the expensive, bulky instruments and achieve low-cost, long-term hydration monitoring, hydration sensors that are mechanically compliant and can form a conformal contact with the skin are a significant technological advance. The mechanical compliance can facilitate the long-term wearability of the sensors, and allows for spatially mapping the electronic properties of the skin by using an array of sensors [170]. Ultrathin "electronic tattoo" [107], [171] is a representative example, which adopts the top-down approach (i.e. patterning followed by transfer printing) to enable high-performance stretchable electronics.

In this paper, we report a low-cost and stretchable hydration sensor that is built up from bottom-up synthesized silver nanowires (AgNWs) inlaid in a polydimethylsiloxane (PDMS) matrix. The compliant, stretchable AgNW/PDMS electrode provides a conformal electrical/mechanical interface to the skin and can be worn continuously to monitor the skin

hydration based on the skin impedance method. The fabrication process is simple and scalable to large areas. By integrating the hydration sensor with other electronic components (e.g., for data acquisition and wireless communication), two wearable form factors, a wristband for skin hydration monitoring and a multifunctional chest patch for concurrent sensing of strain, electrocardiography (ECG) and hydration are demonstrated.

## Results and Discussion

### Sensor fabrication and sensing mechanism

The skin hydration sensors were developed based on our previously demonstrated highly stretchable and conductive AgNW conductors, in which AgNWs were embedded just below the surface of PDMS. Due to the superior conductivity of silver and the mechanical robustness of nanomaterials and polymers, stretchable conductors which can maintain good conductivity at highly strained state (conductivity of ~5000 S/cm at 50% tensile strain) were achieved [153], [172]. The AgNW-based skin hydration sensor was fabricated following the procedure reported previously [158], [173], as shown in **Figure 1**a. The AgNWs were cast in an interdigitated pattern with finger length of 20 mm and spacing of 2 mm and then embedded just below the surface of PDMS to form two stretchable, interdigitated electrodes. The two electrodes act as a capacitor that can be used to measure skin hydration. Interdigitated patterns were chosen to maximize the interaction between the two electrodes within a small area. The two contact pads are used to connect the hydration sensor to other circuit components. The resulting hydration sensor is stretchable and mechanically/electrically robust, which allows for

long-term use. In addition, the flexible and stretchable nature of the electrode enables conformal contact with the surface of the skin that is generally rough.

Skin impedance is a commonly used method to measure skin hydration [174] and is achieved by placing two electrodes on the surface of the skin. The fringing field between the two electrodes penetrates the upper layer of skin, as schematically shown in Figure 1b. The skin impedance measured by the two electrodes can be electrically modeled using a series of capacitors and resistors. The contact interface between electrode and the skin surface can be described by a resistor $R_I$ in parallel with a capacitor $C_I$, which is dependent on applied pressure and the humidity of the skin [175], [176] . The epidermis is modeled by a parallel circuit consisting of a capacitor $C_E$ and a resistor $R_E$. The dermis and underlying subcutaneous tissues, mainly composed of blood vessels, nerves, preparatory glands and hair follicles, exhibits a pure resistive behavior and can be modeled by a resistor $R_D$. Due to symmetry of the two electrodes, the equivalent circuit can be approximated as a parallelly connected resistor $R_e$ and capacitor $C_e$ arising from the electrode-skin contact interface and epidermis, in series with a resistor $R_d$ from the dermis and the underlying tissue [177]. Increasing the water content of the skin increases the conductivity and the dielectric constant of the skin by providing more conductive pathways [176], [177]. The decreased contact impedance and decreased impedance from the epidermis result in a decrease of the measured skin impedance as a function of skin hydration level. The working frequency range of the reported skin hydration sensors was chosen to be in the range of 10-100 kHz. This is comparable to the frequency range used in references [178], [179].

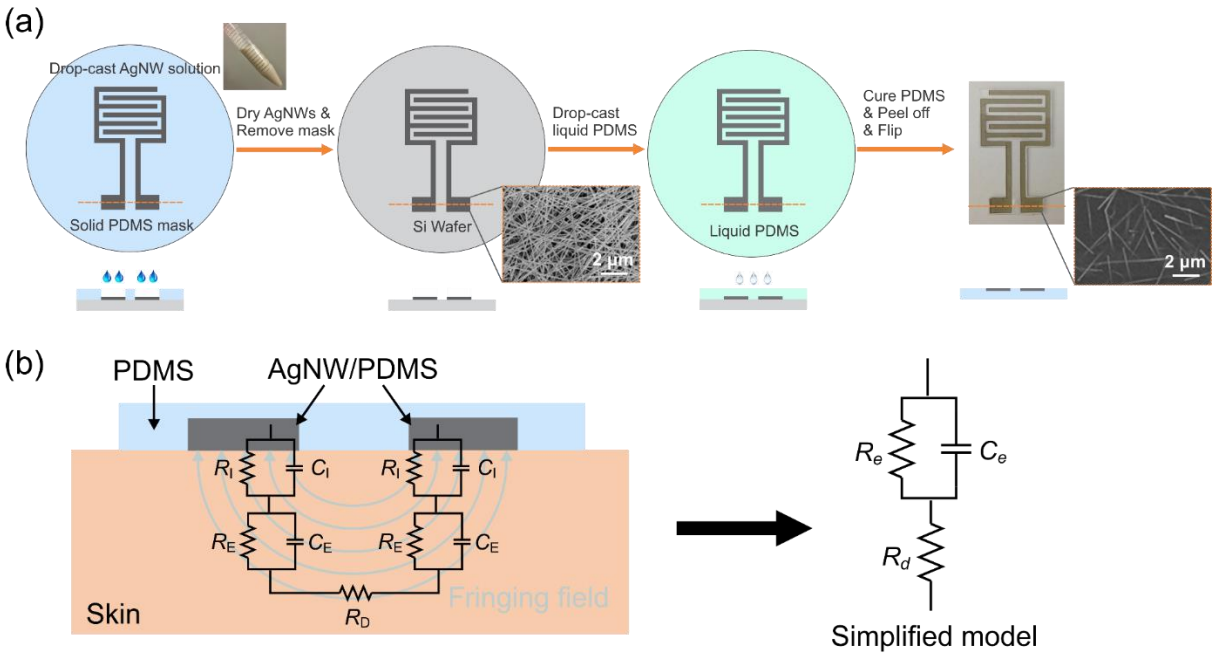


**Figure 1.** (a) Fabrication process of the AgNW sensor. The left SEM image shows the AgNW conductive network before being embedded into the PDMS matrix. The right SEM image shows the surface of the AgNW/PDMS electrode. The exposed nanowires provide surface conductivity while the remaining nanowires are embedded in the PDMS. Scale bars: 2 µm. (b) Schematic illustration of the AgNW sensor placed onto the skin with the fringing field penetrating the upper layer of skin, the equivalent electrode-skin model and the simplified model.

**Sensor characterization**

The skin hydration sensors were characterized by three different tests to evaluate the effect of the ambient hydration or humidity, and the skin hydration using both artificial skin and human skin. In other words, we investigated the sensor response to external (ambient) and internal (physiological) water content.

The first test investigated the effect of the ambient relative humidity on the skin impedance of the hydration sensor. Artificial skin with similar electrical properties to the upper layers of

human skin was fabricated according to Ito et al. [180] and optimized for low frequency sensing following the compound ratios outlined by Yamamoto et al. [181]. The artificial skin served as a control in the sense that its own water content remained constant throughout the test to ensure that any change in the measured impedance was a result of the varying external humidity. The hydration sensor was placed on the artificial skin and inserted into a humidity chamber. The humidity was lowered to 20% relative humidity by flooding the chamber with nitrogen gas. From there, the intake of nitrogen was adjusted to allow the humidity to slowly increase over a period of approximately 60 min, which allowed the humidity levels to stabilize at each interval while being fast enough to prevent any water evaporation from the artificial skin. An impedance measurement at 10 kHz was recorded at a 5% humidity increase interval. At approximately 45% relative humidity, a bubbler was used to continue increasing the humidity up to 100% relative humidity. During the test, the temperature of the humidity chamber was 20 ± 0.5 °C. The results, depicted in **Figure 2**a, show a 0.62% change in impedance readings with increasing relative humidity levels. This indicates that the skin hydration sensor can give stable readings regardless of the external environment of the wearer. Water vapor did not seep between the skin and sensor interface, causing abnormal impedance readings, which confirms the robust, conformal contact of the hydration sensor and skin.

The second test investigated the effect of the internal water content, or the skin hydration level, on the skin impedance using an artificial skin as a control. This test also served as a calibration of the AgNW skin hydration sensor against a commercially available hydration meter (DelfinTech MoistureMeterD) (Figure 2b). The MoistureMeterD (MMD) implemented rigid open-ended coaxial probes, as indicated in Figure 2b, to measure the dielectric constant of the

skin relative to that of the air; the hydration level is indicated using the relative dielectric constant [182]. The use of the artificial skin allows precise control of the skin hydration level over a wide range.

The artificial skin was prepared to be in a highly hydrated state. As the water inside the artificial skin evaporated with the help of a hair dryer, the hydration was measured using both the MMD and the AgNW hydration sensor. As expected, the impedance measured by the AgNW sensor increased as the water content of the artificial skin decreased, which was correlated with the decrease in the reading of the MMD (Figure 2c). The relationship between the impedance measured at 100 kHz and the MMD reading follows an exponential relationship, as shown in Figure 2d. Then Echem Analyst software (Gamry Instruments) was employed to extract the equivalent circuit model parameters of skin impedance. We found that with the current electrode design and sensing frequency, $R_e$ and $C_e$ play a major role while the value of $R_d$ does not change much in the resulting skin impedance. For this reason, only the fitted values of $R_e$ and $C_e$ were summarized, as shown in Figure 2e. $R_e$ decreases while $C_e$ increases with the increase in the hydration level as a result of improved electrode-skin contact and increased conductivity and dielectric constant of skin.

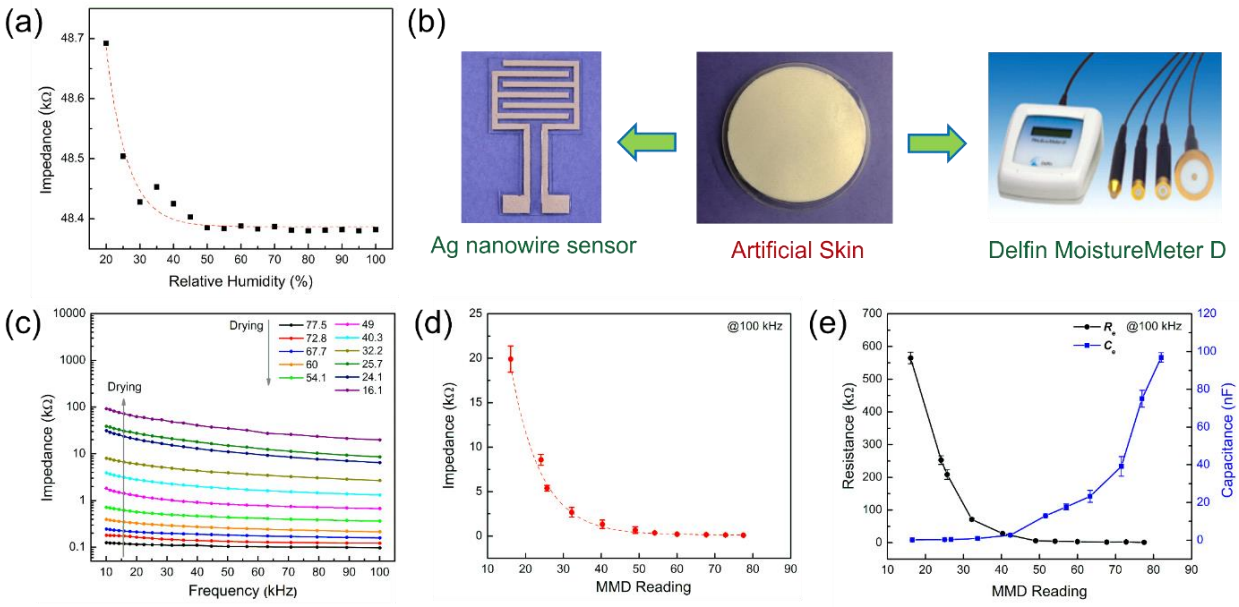


**Figure 2.** (a) Impedance values measured from AgNW sensor on artificial skin at 10 kHz as a function of increasing humidity. (b) The calibration was conducted on artificial skin between the AgNW sensor and a commercial moisture meter MoistureMeter D (MMD). (c) Skin impedance measured from AgNW sensor between 10-100 kHz and the corresponding MMD readings as the artificial skin dries. (d) Comparison of skin impedance measured from AgNW sensor at 100 kHz and MMD readings. (e) Extracted equivalent circuit model parameters ($R_e$, $C_e$) as a function of MMD readings. (d)-(e) Results presented were averaged from three experiments and expressed as the Mean ± SD.

Finally, the AgNW sensor was tested for human skin (**Figure 3**a). Skin lotion was applied on the skin of the forearm for 5 min to increase the skin hydration level and then the excess lotion on the skin was removed. Due to the moisturizing effect, a significant drop in skin impedance was observed in the initial reading after applying lotion (Figure 3b and 3c), corresponding to an increase in skin hydration. The skin impedance slowly recovered with time and fully recovered to the value before applying lotion after 20 min. Consistently, $R_e$ showed a similar trend with skin impedance and $C_e$ showed an opposite trend, which is consistent with the previous analysis (Figure 3d).

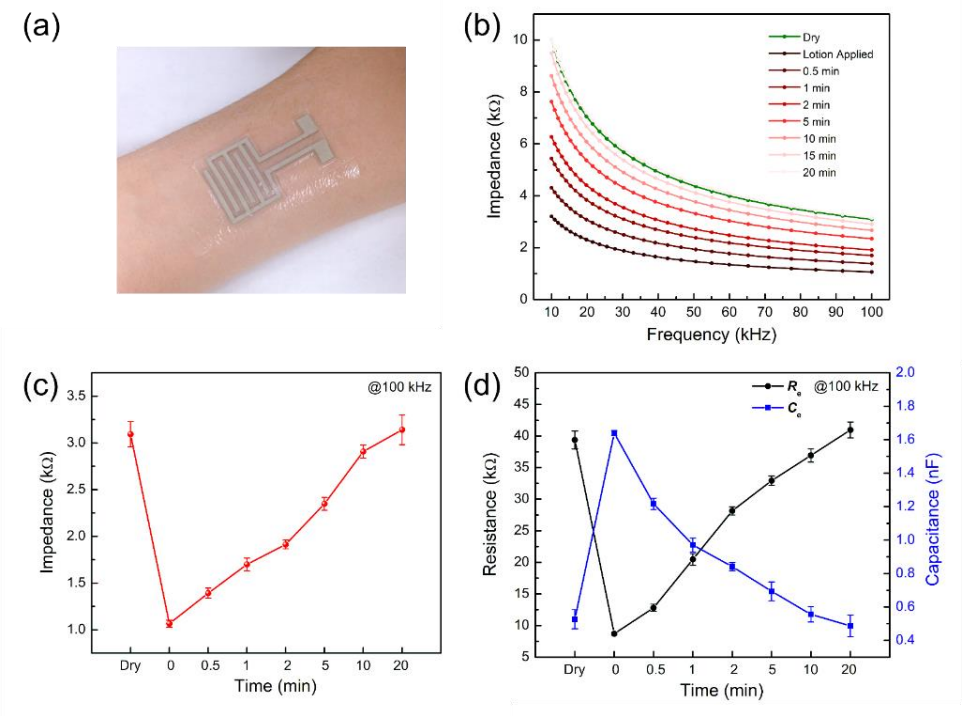


**Figure 3.** (a) Photograph showing the AgNW sensor placed on the inner side of forearm. (b) The measured impedance change between 10-100 kHz from human skin before (Dry) and after applying lotion. (c) Comparison of skin impedance measured from AgNW sensor at 100 kHz before (Dry), and after applying lotion. (d) Extracted equivalent circuit model parameters ($R_e$, $C_e$) before (Dry) and after applying lotion. (c)-(d) Results presented were averaged from three experiments and expressed as the Mean ± SD.

**Wristband for skin hydration monitoring**

The wristband was chosen as the first form factor due to the good user acceptance of wearing wristwatch like devices, although the sensor can also be integrated into an armband, a chest strap, or a headband. A small-scale, low power circuit was designed to acquire the signals and transmit the data wirelessly via Bluetooth communication. The printed circuit board (PCB) layout and block diagram of the personal hydration monitor is shown in **Figure 4**a. The principle components were chosen to realize the desired functions at low power. The

impedance was measured using a high precision impedance converter chip AD 5933 (Analog Devices) that combines an on-board frequency generator with an analog-to-digital converter (ADC). A microcontroller CC2541 (Texas Instruments) offers a power-optimized system on chip solution for low-power Bluetooth, with an industry standard 8051 microcontroller, 256 kilobytes in-system programmable flash memory, and 8 KB random access memory. Impedance measurements on the same AgNW interdigitated sensor were performed using both the AD5933 network analyzer and a desktop impedance analyzer (HP Agilent 4392A), sweeping the frequency from 10 to 100 kHz. The measured impedances using AD5933 controlled by the CC2541 microcontroller and the HP Agilent 4392A showed good agreement (Figure 4b). This indicates that the AD5933 impedance converter system is viable as a portable alternative to standard desktop impedance analyzers.

As shown in Figure 4c-4d, a PCB containing the network analyzer chip (AD5933), the ultra-low power microprocessor with Bluetooth radio (CC2541) and a button cell battery was connected to the AgNW sensor, using micro coaxial cables and rubber epoxy that allows the connection to remain secure while still retaining the stretchable nature of the electrode. A 3D printed spacer was used to enable secure contact between the AgNW sensor and the skin, and isolate the sensing component from the electrical circuit. The PCB, spacer, and electrode were secured and worn on the body using an iPod Nano wristband, as the dimensions of the personal hydration monitor and the iPod Nano are identical. Figure 4e shows the assembled system as worn on the wrist.

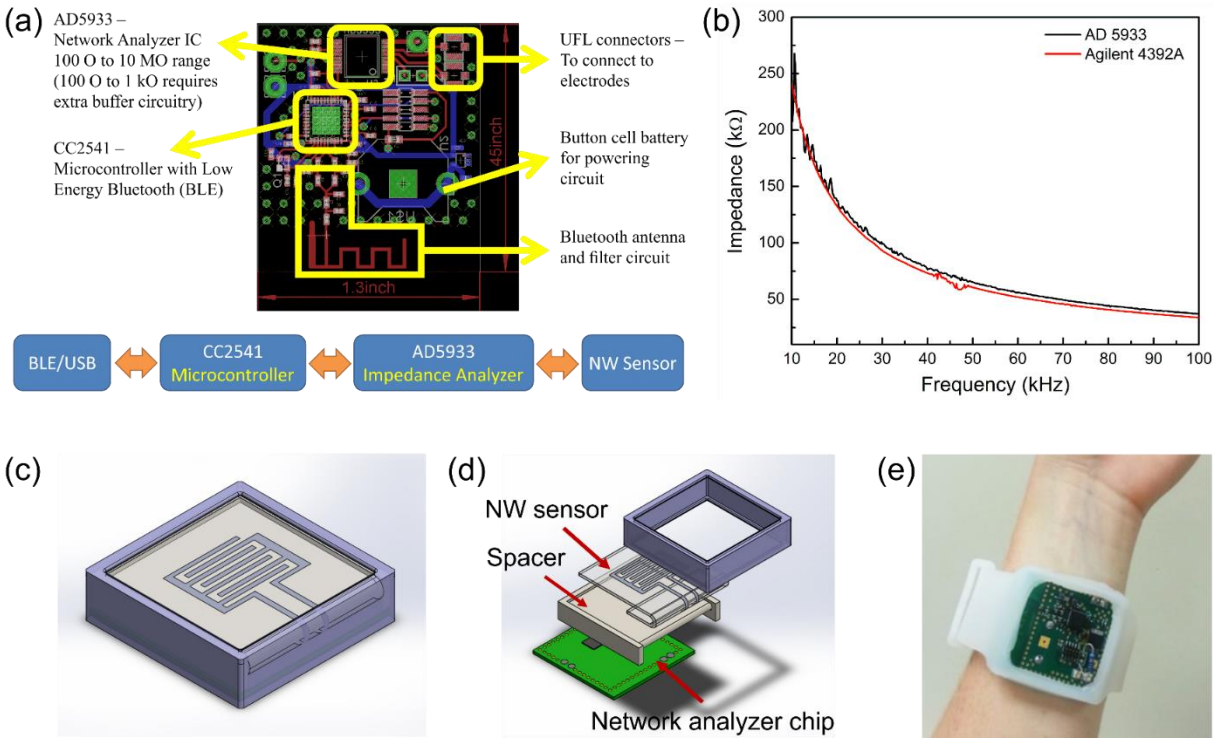


**Figure 4.** (a) PCB layout (top) and block diagram (bottom) of system. (b) Comparison of the impedance measurement from the AgNW sensor on the artificial skin between a desktop impedance analyzer (HP Agilent) and the portable evaluation board. (c) CAD rendering of the assembled portable hydration monitor. (d) Exploded view showing the PCB, 3D printed spacer, AgNW electrode, and encasing. Note that the flexible electrode allows the top surface contacts to be folded over to make contact with the printed circuit board contacts. (e) The hydration monitor as worn on the wrist like a watch.

### Chest patch for multimodal sensing

Dehydration can be a risk factor, the cause or symptoms of various diseases, such as kidney stone disease, skin disease, gastroenteritis, diabetes, respiratory infections and heart disease [183]–[185]. To better track the personal health parameters and monitor the related diseases, multimodal sensing in addition to the hydration sensing is needed. To demonstrate the application of the hydration sensor for multimodal sensing, a multifunctional sensor patch using the chest patch form factor was developed.

In view that ECG is a powerful tool in diagnosing and treatment of cardiovascular diseases, central nervous system disorders, electrolyte imbalances, lung diseases and other conditions [186] and the fact that cardiovascular disease is one of the main cause of death, ECG sensing is included to monitor the heart activity and access the heart rate during workout. Continuous ECG monitoring in a wearable form factor could significantly cut down the cost and personnel load on healthcare. The commonly used gel electrode, however, cannot be used in a long-term, continuous setting due to the skin irritation caused by the gel and signal degradation as the gel dehydrates. The highly conductive and stretchable AgNW/PDMS dry electrode eliminates the use of the conductive gel but maintains compliant contact with the skin, which allows for high signal quality and enables long-term, continuous ECG monitoring [187].

Dehydration often occurs during exercise and training. It would be beneficial to monitor the hydration level and track the activities simultaneously. A highly stretchable capacitive strain sensor [157] was also incorporated in the chest patch to track the skin strain, due to the following two reasons: (1) Together with the heart rate from ECG, the strain associated with human motions during workout can be used to analyze the intensity of the activities and prevent dehydration; (2) Since the ECG signals collected under motion are typically noisy, the strain signals may be correlated with the ECG signals and has the potential to mitigate the motion artifacts in ECG signals. In addition, while demonstrated for skin hydration sensing, the skin impedance measurement also has the potential to be used for the tracking of other health parameters. For example, excursions of glucose levels can change the electrolyte balance in blood, surrounding cells and interstitial fluids, resulting in a change in the dielectric spectrum [188], [189]. Emotional arousal levels affect the sweat gland activity, and hence change the

skin conductance response [190], [191]. Hence, various physiological parameters relevant to the wellness can be correlated to skin impedance.

The sensor layout and circuit diagram of the chest patch are given in **Figure 5**a and 5b. To achieve a compact layout and facilitate the connection, the configuration of two parallel strips was adopted as the hydration sensor instead of the interdigitated pattern as used previously. Three square-shaped AgNW/PDMS electrodes at the corners of the chest patch serve as the ECG electrodes, two adjacent parallel AgNW/PDMS strips around the top ECG electrode are used to record the skin impedance, and a three-layer capacitive structure comprising two strips of AgNW/Dragon Skin conductors with a dielectric layer (Ecoflex 0010) in between act as the strain sensor [157]. A self-adhesive substrate was used to attach the patch to skin [192]. The capacitive strain sensor was calibrated using a tensile stage to record the relative capacitive change as a function of tensile strain up to 100%. The demonstrated strain range is far beyond that of traditional thin film based strain gage (typically 5%) and sufficient for detecting the strain associated with human motions. The gage factor of the strain sensor, defined as the relative capacitive change divided by the mechanical stain is 1 (Figure 5c).

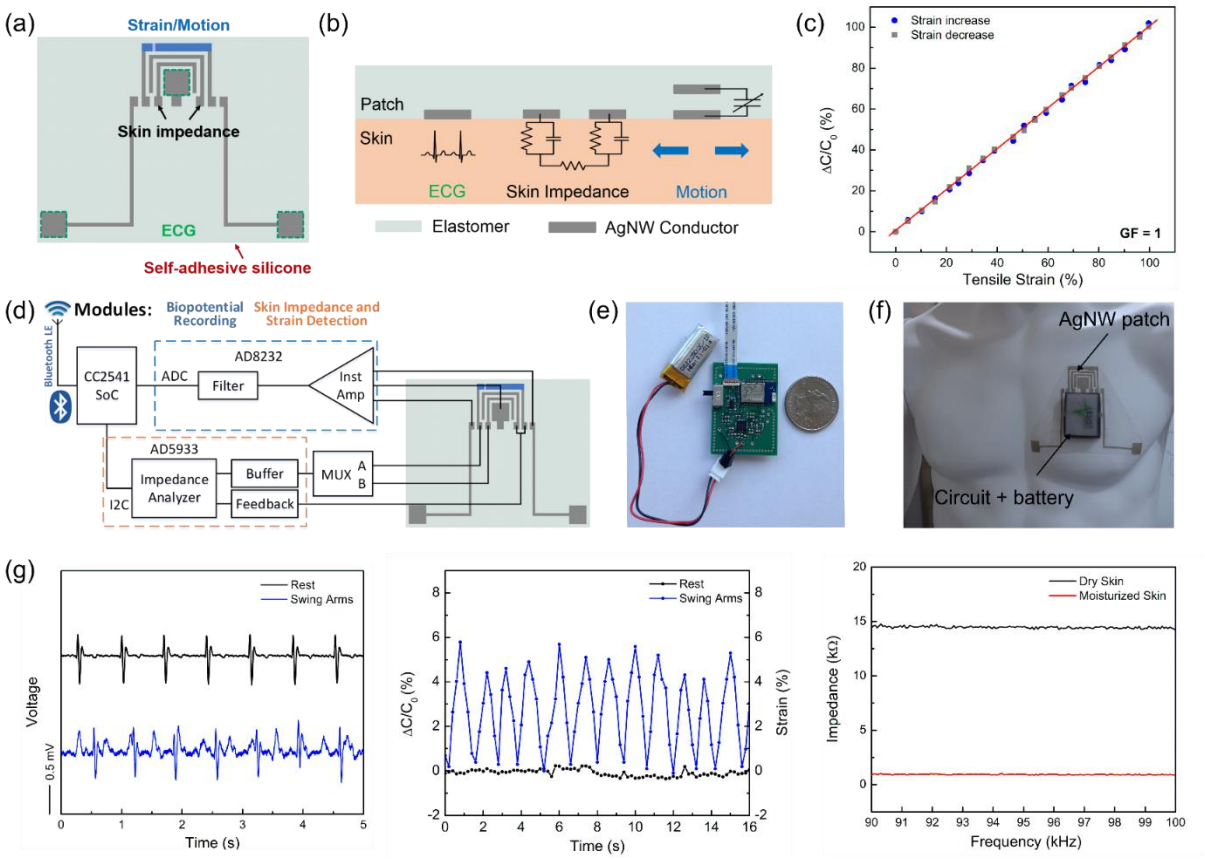


**Figure 5.** (a) Layout of the patch including three ECG electrodes (boxed), a strain sensor and an impedance sensor. (b) Schematic illustration of the sensing concepts. (c) Relative capacitance changes as a function of applied tensile strain. Block diagram of interface circuit (d) and actual populated printed circuit board (e). (f) Integrated chest patch with circuit board and battery enclosed in a 3D printed box self-adhering to the chest of a mannequin. (g) Multimodal data obtained from chest: ECG signals under rest and motion; skin strain associated with swinging arms and skin impedance before and after applying lotion.

ECG recording was achieved using Analog Devices AD8232 heart rate monitor front end with three-lead configuration for optimal signal detection. Since both skin impedance and strain can be detected and deduced from impedance spectroscopy, both sensing elements shared an Analog Devices AD5933 impedance converter in order to minimize overall size of the circuit. A circuit board with Texas Instruments Bluetooth Low Energy microcontroller CC2541 was used for wireless transmission to a nearby data aggregator (Figure 5d). The final size of the

PCB board was 2.5×3.5 $cm^2$ (Figure 5e). The PCB, sensor patch connected on the PCB using a flexible flat cable (FFC), and a rechargeable Li-ion polymer battery were packed in a 3D printed box that can be directly mounted on top of the sensor patch (Figure 5f). When the circuit is powered by a rechargeable 1.48 Wh Li-ion polymer battery, it can operate up to 37 hours with power consumption of 40 mW. The multifunctional chest patch was able to simultaneously detect the ECG under rest and under motion, the skin strain associated with body motion, and the skin hydration change. The initial testing results are shown in Figure 5g, which demonstrated the feasibility of recoding multiple health parameters using the multimodal sensors. The multimodal sensing and correlation of the data give a more comprehensive understanding of the body conditions and will greatly facilitate the tracking of wellness and the treatment of illness.

**Conclusions**

A wearable AgNW based skin hydration sensor was fabricated and calibrated with respect to external humidity change and internal skin water content change. Results showed that the sensor is insensitive to external humidity change and the skin impedance decreases with the increase in skin hydration level due to the increase in skin conductivity and dielectric constant. The wearable, low-cost hydration sensor compared well with the MMD commercial instrument. Two wearable form factors, a wristband for skin hydration sensing and a multifunctional chest patch composed of strain sensor, ECG electrode and skin hydration sensor, were demonstrated. While the present hydration sensor was designed to measure hydration in the epidermis, the spacing of the electrodes and the operating frequency can be

adjusted to measure hydration in other skin layers [174], [193]. This noninvasive, low-cost, wearable and wireless system has potentials to help detect dehydration among athletes, military personnel and the elderly, provide insight to athletic performance and other physiological parameters, assist the cosmetic scientists for the development of moisturizers, and benefit the diagnosis of skin diseases.

**Experimental Section**

*Fabrication process of AgNW/PDMS skin hydration sensor*: The fabrication process of the AgNW/PDMS skin hydration sensor is schematically illustrated in Figure 1a. Liquid PDMS ((Sylgard 184, Dow Corning) with the weight ratio of "base" to "curing agent" of 10 : 1 was cast onto a Si substrate, degassed in a vacuum chamber and cured at 60 °C for 2 hours. The cured PDMS was patterned into an interdigitated shape with finger length of 20 mm and spacing of 2 mm. AgNWs in ethanol (SLV-NW-90, Blue Nano) with average length and diameter of 10 μm and 90 nm were drop cast into the area defined by the mask. The solvent was then evaporated with a temperature of 50 °C. After removing the PDMS mask, AgNWs patterns were formed on the substrate. Next, liquid PDMS was cast on top of the AgNW pattern, degassed, and cured at 60 °C for 2 hours. The patterned AgNWs were embedded just below the PDMS surface when it was peeled off the Si substrate. Conducive paste was finally applied onto the two ends of the AgNW/PDMS sensor to interconnect with other components.

*Fabrication process of artificial skin*: The preparation of artificial skin follows the methods developed by Ito and Yamamoto et al.[17, 18] Briefly, 0.3267 g sodium chloride (Sigma-Aldrich)

and 1.743 g Agar (Sigma-Aldrich) were measured and mixed well in 56.25 g purified water, where purified water determines the water content, sodium chloride adjusts conductivity and Agar allows for self-shaping and prevents water from separating. The mixture was then heated on a hot plate while being slowly stirred to prevent burning the agar. When the increase in viscosity of the mixture was observed, the mixture was removed from hot plate. Following that, 5.625 g polyethylene powder (Sigma-Aldrich) (adjusts the dielectric constant) and 1.382 g TX-151 (Balmar, LLC) (allows agar and polyethylene powder to be mixed and increases the viscosity) were added into the mixture and thorough mixed. Transferring the mixture into a petri dish or other molds finished the preparation of skin phantom.

*Fabrication process of multifunctional chest patch*: Briefly, a thin layer of liquid PDMS (Sylgard 184, Dow Corning) with the base to curing agent weight ratio of 10:1 was coated on a PET sheet followed by degassing and curing at 60 $^{o}$C for 2 hours. The mask for sensors were prepared by cutting the cured PDMS using a cutting tool (Silhouette CAMEO). AgNWs in ethanol (SLV-NW-90, Blue Nano) were drop-cast into the area defined by the mask. After drying the AgNWs on a hotplate with a temperature of 50 $^{o}$C, the mask was removed. To render the AgNW into a stretchable manner, the AgNW area for the patch (except for the strain sensor electrodes) was encapsulated by PDMS with a base to curing agent weight ratio of 10:1. The AgNW area for strain sensor top and bottom electrodes were embedded by Dragon Skin FXO (Smooth-On, Inc.) with part A to part B ratio of 1:1. The area surrounding the AgNWs were covered by slacker (Smooth-On, Inc.) modified Dragon Skin FXO (Smooth-On, Inc.) to provide a self-adhesive and very compliant substrate. Curing at room temperature for 6 hours

was performed to crosslink the silicone. To finish the fabrication of strain sensors, liquid Ecoflex 0010 (Smooth-On, Inc.) serving as the dielectric for the capacitor was used to sandwich the AgNW/Dragon Skin FXO bottom electrode on the patch and the top electrode prepared separately beside the patch. The patch was cured at room temperature for another 6 hours. A line was cut between the connecting pads for the top and bottom electrodes to help the strain sensor top electrode connect to the connecting pad on the back (the side on the skin). The sensor patch was then peel off the PET substrate. The resulting self-adhesive patch can be readily placed onto the skin for the multifunctional sensing.

# APPENDIX B: IRB DOCUMENTATION

NORTH CAROLINA STATE UNIVERSITY
INSTITUTIONAL REVIEW BOARD FOR THE USE OF HUMAN SUBJECTS IN RESEARCH SUBMISSION FOR NEW STUDIES
Protocol Number 5527

*Project Title*

ASSIST - Mapping Energy Harvesting on the Human Body

*IRB File Number:*

*Original Approval Date:*

03/18/2015

*Approval Period*

03/06/2017 - 03/06/2018

*Source of funding (if externally funded, enter PINS or RADAR number of funding proposal via 'Add New Sponsored Project Record' button below):*

5-55706: ASSIST; NSF

*NCSU Faculty point of contact for this protocol:NB: only this person has authority to submit the protocol*

Myers, Amanda Caton: Textile Engineering, Chemistry & Science

*Does any investigator associated with this project have a significant financial interest in, or other conflict of interest involving, the sponsor of this project? (Answer No if this project is not sponsored)*

No

*Is this conflict managed with a written management plan, and is the management plan being properly followed?*

No

*Preliminary Review Determination*

*Category:*

Expedited 4, 7

*In lay language, provide a brief synopsis of the study (limit text to 1500 characters)*

The study will use wearable thermoelectric and piezoelectric energy harvesting devices to generate a map of ideal kinetic and thermal energy harvesting locations on the body. Participants will complete various activities (walking, jogging, and reading) to characterize the energy harvested in different scenarios.

*Briefly describe in lay language the purpose of the proposed research and why it is important.*

The proposed research investigates the use of commercial and research-based wearable electronic devices. This research is being conducted in conjunction with ASSIST, an NSF-funded engineering research center (ERC). The focus of the ASSIST center is explore low-power wearable systems that correlate a person's health and wellness to external environmental conditions. This study is similar to the ASSIST IRB study #3347: Evaluation of Wearable Electronics. The data collected during this study will be used to create associations both on an individual level as well as in a social context.

This study has two primary objectives. First, the creation of an energy harvesting, or electric power generation from temperature or movement, body map that shows optimal energy harvesting locations on the body. Second, the data collected will be analyzed to show correlations between user's activities and power generated from piezoelectric and thermoelectric energy harvesting devices. A piezoelectric energy-harvesting device is a noninvasive device that generates power from movement. A thermoelectric energy-harvesting device is a noninvasive device that generates power from a temperature difference, in this case the difference in temperature between the surface of the skin and ambient air. The collected data will be published in scientific research and education journals as well as be presented at conferences.

*My research qualifies for Exemption. Exempt research is minimal risk and must fit into the categories b.1 - b.6 found here: http://www.hhs.gov/ohrp/humansubjects/guidance/45cfr46.html*

*Is this research being conducted by a student?*

Yes

*Is this research for a thesis?*

No

*Is this research for a dissertatiion?*

Yes

*Is this independent research?*

No

*Is this research for a course?*

No

*Do you currently intend to use the data for any purpose beyond the fulfillment of the class assignment?*

No

*Please explain*

*If so, please explain*

*If you anticipate additional NCSU-affiliated investigators (other than those listed on the Title tab) may be involved in this research, list them here indicating their name and department.*

*Will the investigators be collaborating with researchers at any institutions or organizations outside of NC State?*

No

*List collaborating institutions and describe the nature of the collaboration*

*What is NCSU's role in this research?*

*Describe funding flow, if any (e.g. subcontractors)*

*Is this international research?*

No

*Identify the countries involved in this research*

*An IRB equivalent review for local and cultural context may be necessary for this study. Can you recommend consultants with cultural expertise who may be willing to provide this review?*

*Adults 18 - 64 in the general population?*

No

*NCSU students, faculty or staff?*

Yes

*Adults age 65 and older?*

No

*Minors (under age 18--be sure to include provision for parental consent and/or child assent)?*

No

*List ages or age range:*

*Could any of the children be "Wards of the State" (a child whose welfare is the responsibility of the state or other agency, institution, or entity)?*

No

*Please explain:*

*Prisoners (any individual involuntarily confined or detained in a penal institution -- can be detained pending arraignment, trial or sentencing)?*

No

*Pregnant women?*

No

*Are pregnant women the primary population or focus for this research?*

No

*Provide rationale for why they are the focus population and describe the risks associated with their involvment as participants*

*Fetuses?*

No

*Students?*

No

*Does the research involve normal educational practices?*

Yes

*Is the research being conducted in an accepted educational setting?*

Yes

*Are participants in a class taught by the principal investigator?*

No

*Are the research activities part of the required course requirements?*

No

*Will course credit be offered to participants?*

No

*Amount of credit?*

None

*If class credit will be given, list the amount and alternative ways to earn the same amount of credit. Note: the time it takes to gain the same amount of credit by the alternate means should be commensurate with the study task(s)*

*How will permission to conduct research be obtained from the school or district?*

*Will you utilize private academic records?*

No

*Explain the procedures and document permission for accessing these records.*

*Employees?*

No

*Describe where (in the workplace, out of the workplace) activities will be conducted.*
*From whom and how will permission to conduct research on the employees be obtained?*
*How will potential participants be approached and informed about the research so as to reduce any perceived coercion to participate?*
*Is the employer involved in the research activities in any way?*

No

*Please explain:*
*Will the employer receive any results from the research activities (i.e. reports, recommendations, etc.)?*

No

*Please explain. How will employee identities be protected in reports provided to employers?*
*Impaired decision making capacity/Legally incompetent?*

No

*How will competency be assessed and from whom will you obtain consent?*
*Mental/emotional/developmental/psychiatric challenges?*

No

*Identify the challenge and explain the unique risks for this population.*
*Describe any special provisions necessary for consent and other study activities (e.g., legal guardian for those unable to consent).*
*People with physical challenges?*

No

*Identify the challenge and explain the unique risks for this population.*
*Describe any special provisions necessary for working with this population (e.g., witnesses for the visually impaired).*
*Economically or educationally disadvantaged?*

No

*Racial, ethnic, religious and/or other minorities?*

No

*Non-English speakers?*

No

*Describe the procedures used to overcome any language barrier.*
*Will a translator be used?*

No

*Provide information about the translator (who they are, relation to the community, why you have selected them for use, confidentiality measures being utilized).*
*Explain the necessity for the use of the vulnerable populations listed.*

Participants will be selected on a first come first serve basis. While existing teacher/student or employer/employee relationships may exist between participants, each study will be conducted individually so participants are not aware of other individuals participating in the study. Due to minimal risks and benefits to participation in the study, no conflict of interest is foreseen between vulnerable populations. No

teacher/student or employer/employee relationships between researcher and participants will be included in the study.

*State how, where, when, and by whom consent will be obtained from each participant group. Identify the type of consent (e.g., written, verbal, electronic, etc.). Label and submit all consent forms.*

Consent will be obtained from the participant group before the research begins. Participants will be given a consent form with a description of research procedures and any risks associated with the research that must be signed and returned before continuing with the research.

In regard to comments on 3/17/15 the consent form was updated to account for some data security edits according to a comment received. All other forms are repeats and were mistakenly uploaded.

*If any participants are minors, describe the process for obtaining parental consent and minor's assent (minor's agreement to participate).*

Minors will not be allowed to participate in the study.

*Are you applying for a waiver of the requirement for consent (no consent information of any kind provided to participants) for any participant group(s) in your study?*

No

*Describe the procedures and/or participant group for which you are applying for a waiver, and justify why this waiver is needed and consent is not feasible.*

*Are you applying for an alteration (exclusion of one or more of the specific required elements) of consent for any participant group(s) in your study?*

No

*Identify which required elements of consent you are altering, describe the participant group(s) for which this waiver will apply, and justify why this waiver is needed.*

*Are you applying for a waiver of signed consent (consent information is provided, but participant signatures are not collected)? A waiver of signed consent may be granted only if: The research involves no more than minimal risk. The research involves no procedures for which consent is normally required outside of the research context.*

No

*Would a signed consent document be the only document or record linking the participant to the research?*

No

*Is there any deception of the human subjects involved in this study?*

No

*Describe why deception is necessary and describe the debriefing procedures. Does the deception require a waiver or alteration of informed consent information? Describe debriefing and/or disclosure procedures and submit materials for review. Are participants given the option to destroy their data if they do not want to be a part the study after disclosure?*

*For each participant group please indicate how many individuals from that group will be involved in the research. Estimates or ranges of the numbers of participants are acceptable. Please be aware that participant numbers may affect study risk. If your participation totals differ by 10% from what was originally approved, notify the IRB.*

College students, faculty, and associated NCSU User ID holders of age greater than or equal to 18. Although these groups have no particular vulnerability related to the study, they are chosen because of their anticipated ease of availability on the campus where we are conducting the study. An interested participant is included in the study if he or she is willing to use a device (e.g., smart phone, wearable electronic) we provide. 5 to 10 participants are sought for this study.

*How will potential participants be be found and selected for inclusion in the study?*

An email seeking active participants will be sent to a group of undergraduate student, graduate student, and faculty. The email will include introductory description of the study. Participants will be chosen on the first-come-first-serve basis.

*For each participant group, how will potential participants be approached about the research and invited to participate? Please upload necessary scripts, templates, talking points, flyers, blurbs, and announcements.*

Each participant is provided with an informed-consent form the purpose of the study and describing the data being collected. Each consenting participant will return the signed informed-consent form before participation.

*Describe any inclusion and exclusion criteria for your participants and describe why those criteria are necessary (If your study concentrates on a particular population, you do not need to repeat your description of that population here.)*

No specific populations are identified.

*Is there any relationship between researcher and participants - such as teacher/student; employer/employee?*

Yes

*What is the justification for using this participant group instead of an unrelated participant group? Please outline the steps taken to mitigate this relationship.*

Depending on the subjects participating, there may be existing teacher/student and employer/employee relationships between faculty and the students.

*Describe any risks associated with conducting your research with a related participant group.*

As the research is collection of individual data, no risk is associated with a related participant group for this study.

*Describe how this relationship will be managed to reduce risk during the research.*

Participants will be given a numerical ID so that individual data is anonymous.

*How will risks to confidentiality be managed?*

Participants will be given a numerical ID so that individual data is anonymous.

*Address any concerns regarding data quality (e.g. non-candid responses) that could result from this relationship.*

None.

*In the following questions describe in lay terms all study procedures that will be experienced by each group of participants in this study. For each group of participants in your study, provide a step-by-step description of what they will experience from beginning to end of the study activities.*

Participants are required to use a wearable electronic device that consists of an energy harvesting sub-system (EHSS) and energy harvesters, and a Droid-based operating

device that will be provided by the ASSIST ERC and/or through the Computer Science department for the duration of the study. The EHSS is a device that records the amount of power the energy harvesters produce. The energy harvesters (thermoelectric generators or piezoelectric generators) are embedded in a non-invasive, wearable platform (headband, wristband, or collar) so that they touch the surface of the skin and connect to the EHSS. This allows the participant to wear the devices as one would a normal piece of clothing, while generating power to be monitored by the EHSS. The EHSS sends the collected data to the Droid-based tablet or cellphone where it is saved in a secure file. The participants are required to accept the terms and conditions enforced by the inventory system. The following is a brief description of the terms and conditions of the inventory system.

Each device used in the study will be assigned a part number that will be associated with the user's assigned ID number.

Participants will be required to return all loaned devices at the end of the study.

If participants choose to leave the study before completion, they will be asked to immediately return all loaned devices.

Moderated activity:

Participants will meet with the investigator at the participant's convenience determined by the introductory email correspondence. They will be given one of the wearable devices mentioned above, a questionnaire and instructions on how to wear and operate the personal devices. Before participating in the following activities the participant will complete the survey. The following is provided as structured activities to be monitored by the investigators:

1) Walking: The participant will be required to walk for 15 min on NCSUâ€™s Centennial Campus and/or on a treadmill located in the ASSIST Physiological lab located in the MRC building on Centennial Campus.

2) Activity: The participants will be required to run/jog or play basketball for 10-15 min on NCSU's Centennial Campus and/or on a treadmill located in the ASSIST Physiological lab located in the MRC building on Centennial Campus.

3) Idle Time: Participant will be required to watch a movie, read a book, or work at a computer for a period of 30 min at the Hunt Library on NCSU's Centennial Campus.

At the end of the activity, the moderator will collect the devices and download the data to a restricted access folder. Should any physical distress occur to the participant during the study, all activity will immediately cease. The moderator will be on hand to attend to the distressed participant and seek the necessary actions, i.e. allowing the participant to rest, calling NCSU emergency services, or acquiring any necessary first aid. The following is a brief description of each type of data collected on participant's personal device and the wearable device.

Accelerometer readings: A device's acceleration measured by an accelerometer that that EHSS is equipped with. The readings are made every few seconds. The purpose of collecting this information is to learn from a user's movements.

Exposure Temperature: Ambient air temperature is measured by a thermocouple installed on the EHSS. The readings are made every few seconds. The purpose of

collecting this information is to determine the ambient air temperature that the participant is exposed to during the duration of the activities. This information will be used for TEG calculations.

Humidity: Humidity is measured by a sensor if the device is equipped with one. The readings are made every few seconds. The purpose of collecting this information is to learn from a user's environment.

Ozone: Ozone is measured by a sensor if the device is equipped with one. The readings are made every few seconds. The purpose of collecting this information is to learn from a user's environment.

Skin Temperature: Skin Temperature is measured by a thermocouple installed on the EHSS. The readings are made every few seconds. The purpose of collecting this information is to gather localized skin temperature data for TEG calculations.

The following is a brief description of each type of generator used in this study.

Thermoelectric Generator: A thermoelectric generator is a non-invasive device that generates power from a temperature difference. In this study, the temperature difference will be that of the skin temperature and the ambient air temperature.

Piezoelectric Generator: A piezoelectric generator is a non-invasive device that generates power from movement. In this study, participants will perform a variety of movements, as described previously, to generate power.

The data uploaded by users is analyzed using statistical learning techniques to 1) determine associations between a user's activities and power generated from the energy harvesting devices; 2) create a map of optimal energy harvesting locations on the body for both piezoelectric energy harvesting and thermoelectric energy harvesting.

*Describe how, where, when, and by whom data will be collected.*

The data will be collected by the graduate student conducting the study. Data is gathered by downloading individual, anonymous data gathered using software on a smart phone or tablet. The research will be performed at the participants' convenience during the day on Centennial Campus in either the College of Textiles building or Monteith Research Center building.

*Social?*

No

*Psychological?*

No

*Financial/Employability?*

No

*Legal?*

No

*Physical?*

Yes

*Academic?*

No

*Employment?*

No

*Financial?*

No

*Medical?*

No

*Private Behavior?*

No

*Economic Status?*

No

*Sexual Issues?*

No

*Religious Issues/Beliefs?*

No

*Describe the nature and degree of risk that this study poses. Describe the steps taken to minimize these risks. You CANNOT leave this blank, say 'N/A', none' or 'no risks'. You can say, "There is minimal risk associated with this research."*

Some activities designed may include some active participation (walking, running, basketball, etc). The subjects will be guided ahead of time that if at any time they feel any form of discomfort, that they should stop their activity. Should an emergency occur, campus police will be notified and corresponding action will be taken according to the wishes of the participant.

Bottled water will be provided for all activity. It will be freely available, on nearby tables, to participants at any point in the study.

*If you are accessing private records, describe how you are gaining access to these records, what information you need from the records, and how you will receive/record data.*

N/A

*Are you asking participants to disclose information about other individuals (e.g., friends, family, co-workers, etc.)?*

No

*You have indicated that you will ask participants to disclose information about other individuals (see Populations tab). Describe the data you will collect and discuss how you will protect confidentiality and the privacy of these third-party individuals. If you are collecting information that participants might consider personal or sensitive or that if revealed might cause embarrassment, harm to reputation or could reasonably place the subjects at risk of criminal or civil liability, what measures will you take to protect participants from those risks?*

N/A

*If any of the study procedures could be considered risky in and of themselves (e.g. study procedures involving upsetting questions, stressful situations, physical risks, etc.) what measures will you take to protect participants from those risks?*

The subjects will be guided ahead of time that if at any time they feel any form of discomfort, that they should stop their activity.

*Describe the anticipated direct benefits to be gained by each group of participants in this study (compensation is not a direct benefit).*

The subjects will be directly involved in acquisition and analysis of their own data which will promotes active/involved learning.

*If no direct benefit is expected for participants describe any indirect benefits that may be expected, such as to the scientific community or to society.*

The data collected will be utilized by future researchers to identify new methods for wearable energy harvesting.

*Will you be receiving already existing data without identifiers for this study?*

No

*Will you be receiving already existing data which includes identifiers for this study?*

No

*Describe how the benefits balance out the risks of this study.*

There are few risks to this study. Participants will be involved in learning without any threat to their safety. Should the participant feel any discomfort, then they are encouraged to cease the activity.

*Will data be collected anonymously (meaning that you do not ever collect data in a way that would allow you to link any identifying information to a participant)?*

Yes

*Will any identifying information be recorded with the data (ex: name, phone number, IDs, e-mails, etc.)?*

No

*Will you use a master list, crosswalk, or other means of linking a participant's identity to the data?*

No

*Will it be possible to identify a participant indirectly from the data collected (i.e. indirect identification from demographic information)?*

No

*Audio recordings?*

No

*Video recordings?*

No

*Images?*

No

*Digital/electronic files?*

Yes

*Paper documents (including notes and journals)?*

Yes

*Physiological Responses?*

No

*Online survey?*

No

*Restricted Computer?*

Yes

*Password Protected files?*

Yes

*Firewall System?*

No

*Locked Private Office?*

No

*Locked Filing Cabinets?*

No

*Encrypted Files?*

No

*Describe all participant identifiers that will be collected (whether they will be retained or not) and explain why they are necessary.*

Each participant will be provided a user ID that not will not be associated with the any real identity of the participant. All data uploaded by the participant will be linked his (or her) user ID. The image taken will be a thermal image with very limited physical identifiers that could be linked back to the participant. A sample thermal image is uploaded in Supporting Documentation.

*If any links between data and participants are to be retained, how will you protect the confidentiality of the data?*

*If you are collecting data electronically, what (if any) identifiable information will be collected by the host site (such as email and/or IP address) and will this information be reported to you?*

The data is collected with an app developed by the investigators. No data is shared with a host site.

*Describe any ways that participants themselves or third parties discussed by participants could be identified indirectly from the data collected, and describe measures taken to protect identities.*

None.

*For all recordings of any type: Describe the type of recording(s) to be made Describe the safe storage of recordings Who will have access to the recordings? Will recordings be used in publications or data reporting? Will images be altered to de-identify? Will recordings be transcribed and by whom?*

The data will be stored on a secure server with access restricted to the principal investigator and the supporting investigators. Before beginning the study, participants will be asked if the data they reported can be shared for use by other researchers. If participants consent to future use of the data they provided, the data will be retained in a folder noting the consent of participants, but any identifiers associated with the participant will be deleted. If not, all the data reported by a user will be stored in a separate folder for use only in this study and to be deleted permanently from the server when the study is completed. If a participant used a device we provided for the study, all data in the device is deleted when the device is returned at the end of the study.

Participant emails will only be associated with the participant name for correspondence through the duration of the study. Correspondence will be limited to the researcher and participant for the duration of the study so only the researcher is familiar with any identification of the participant for the duration of communications about and

completion of the study. As the researcher is actively involved in moderating study activities, this will not create a conflict of interest as previously addressed. After the study is completed, the researcher will delete any participant email addresses and names and data will be identified by anonymous user IDs.

*Describe how data will be reported (aggregate, individual responses, use of direct quotes) and describe how identities will be protected in study reports.*

Reports will include data related to a respective User ID or a collective group participating in an activity.

*Will anyone besides the PI or the research team have access to the data (including completed surveys) from the moment they are collected until they are destroyed?*

Before beginning the study, participants will be asked if the data they reported can be shared for use by other researchers. If participants consent to future use of the data they provided, the data will be retained in a folder noting the consent of participants, but any identifiers associated with the participant will be deleted. If not, all the data reported by a user will be stored in a separate folder for use only in this study and to be deleted permanently from the server when the study is completed. If a participant used a device we provided for the study, all data in the device is deleted when the device is returned at the end of the study.

*Describe any compensation that participants will be eligible to receive, including what the compensation is, any eligibility requirements, and how it will be delivered.*

No compensation will be provided.

*Explain compensation provisions if the participant withdraws prior to completion of the study.*

# APPENDIX C: LIST OF PRESENTATIONS AND PAPERS

## PUBLICATIONS

- A Myers, R Hodges, J Jur "Human and environmental analysis of wearable thermal energy harvesting" *Energy Conversion and Management* 2017, 143, pp. 218 – 226.
- S Yao, A Myers, A Malhotra, F Lin, A Bozkurt, J Muth, Y Zhu "A Wearable Hydration Sensor with Conformal Nanowire Electrodes" *Advanced Healthcare Materials* 2017, 1601159.
- J. S. Jur, M Yokus, R Foote, A Myers, R Bhakta "Flexible Interconnects, Systems, and Uses Thereof" US Patent App. 15/174,677, 2016.
- A Myers, R Hodges, J Jur "Human and Environment Influences on Thermoelectric Energy Harvesting Toward Self-Powered Textile-Integrated Wearable Devices" *MRS Advances* 2016.
- A Myers, A Malhotra, J Muth, Y Zhu, S Yao "Personal hydration monitor" US Patent App. 15/160,594, 2016.
- A Myers, H Huang, and Y Zhu "Wearable silver nanowire dry electrodes for electrophysiological sensing" *RSC Advances* 2015, 5, 15, pp. 11627 – 11632.
- Y Zhu, S Yao, L Song, A Myers "Electrodes and sensors having nanowires" US Patent App 15/127,455, 2016.
- A Myers and Y Zhu "Soft Dry Electrodes for Electrocardiogram with Conductive Silver Nanowires" *MRS Symposium Proceedings* 2014. 1685.
- L Song, A Myers, J Adams, Y Zhu "Stretchable and reversibly deformable radio frequency antennas based on silver nanowires" *ACS Applied Materials and Interfaces* 2014, 6, pp. 4248 – 4253.
- A Myers, L Du, H Huang, Y Zhu, "Novel Wearable EMG Sensors Based on Nanowire Technology" *Proceedings of IEEE EMBS Conference* 2014, pp. 1674 – 1677.

## ORAL PRESENTATIONS

- J. S. Jur, R. Bhakta, H. Shahariar, A. Myers, L. Yin, A. Bowles, and J. Twiddy "Textile Electronics for the Connected Body" International Conference on Flexible and Printed Electronics 2017, Sept. 4-7 2017, Jeju Island South Korea
- A. Myers and J. S. Jur "Effects of thermal energy harvesting on the human – clothing – environment microsystem" Autex World Textile Conference 2017, May 29-31, 2017, Corfu, Greece.
- A. Myers and J. S. Jur "Knit Textiles for Thermal Energy Harvesting" MAE Graduate Student Symposium 2017, Raleigh, NC, March 24, 2017.
- A. Myers and J. S. Jur "Strategies for Human-based Energy Harvesting in Textiles" Textile Summit 2017, Raleigh, NC, March 21 – 22, 2017.

- A. Myers, R. Hodges, and J. S. Jur "Human and Environment Influences on Thermoelectric Energy Harvesting Toward Self-Powered Textile-Integrated Wearable Devices" MRS Spring Meeting & Exhibit 2016, March 28 – April 1, 2016, Phoenix, Arizona.
- A. Myers, L. Du, H. Huang, Y. Zhu "Novel Wearable EMG Sensors Based on Nanowire Technology" 36th Annual International IEEE EMBS Conference, Chicago, IL, August 26 – 30, 2014.
- A. Myers and Y. Zhu "Soft Dry Electrodes for Electrocardiogram with Conductive Silver Nanowires" MRS Spring Meeting 2014, San Francisco, CA, April 21 – 25, 2014.
- A. Myers and Y. Zhu "Nanowire Electrodes for Bioelectronic Sensing" SEM Graduate Student Symposium, Raleigh, NC, March 8 – 9, 2013.

POSTER PRESENTATIONS

- A. Myers and J. S. Jur "Passive thermal management to improve energy harvesting using textiles" ASSIST Industry Meeting 2017, Raleigh, NC, January 26 – 27, 2017.
- A. Myers, R. Bhakta, and J. S. Jur "Enabling Electronic Textiles" Biomedical Science & Technology for Special Operations Forces (SOF) – Human Performance and Portable Lab Diagnostics, June 9, 2016, Durham, NC.
- A. Pilli, A. Myers, A. Malhotra, D. Eidson, S. Sankar "H2O" PDMA Conference, Charlotte, NC, April 24, 2015.
    - Winner of Innovate Carolina Competition
- A. Pilli, A. Myers, A. Malhotra, D. Eidson, S. Sankar "H2O" Poole Management Contest, Raleigh, NC, April 16, 2015.
- A. Myers and Y. Zhu "Skin-Mountable Dry Electrodes with Conductive Nanowires" REC Symposium, Raleigh, NC, March 28, 2014.
- A. Myers and Y. Zhu "Skin-Mountable Dry Electrodes with Conductive Nanowires" Sigma Xi Student Research Conference, Research Triangle Park, NC, November 8 – 9, 2013.